THE SEPARATION OF SOURCE, PATH AND SITE EFFECTS

ON HIGH FREQUENCY SEISMIC WAVES:

AN ANALYSIS USING CODA WAVE TECHNIQUES

by

William Scott Phillips

B.A., University of California at Berkeley
Geophysics (1979)

Submitted to the Department of
Earth, Atmospheric, and Planetary Science
in Partial Fulfillment of the Requirements
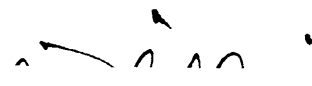for the Degree of

DOCTORATE OF PHILOSOPHY

in

GEOPHYSICS

at the

MASSACHUSETTS INSTITUTE OF TECHNOLOGY

February, 1985

©Massachusetts Institute of Technology 1985

Signature of author:_____
      Department of Earth, Atmospheric, and Planetary Sciences

Certified by:_____
                                       Keiiti Aki
                                  Thesis Advisor

Accepted by:_____
                              Theodore R. Madden
                Chairman, Departmental Committee

THE SEPARATION OF SOURCE, SITE, AND PATH EFFECTS

ON HIGH FREQUENCY SEISMIC WAVES:

AN ANALYSIS USING CODA WAVE TECHNIQUES

by

William Scott Phillips

Submitted to the

Department of Earth, Atmospheric, and Planetary Sciences

on 22 February, 1985, in partial fulfillment of the

requirements for the degree of Doctor of Philosophy

ABSTRACT

This work represents an intensive study of coda waves from local earthquakes in California. The goals of this study are to evaluate the ability of coda wave analysis to further our understanding of the earth, and to augment our knowledge concerning the generation of the coda itself.

The methods used here are the simple extensions of single station coda wave techniques used by many workers (e.g. Aki and Chouet, 1975). Under non-restrictive assumptions of coda stability, a method is constructed to isolate source or site effects on high frequency waves (1.5-24 Hz). These techniques allow incorporation of data from earthquakes of many sizes, and from stations lying great distances apart. Digital data are drawn from the U.S.G.S. California Network (CALNET) archives; over 1200 records are used from over 90 earthquakes in the Coast Ranges of California between San Francisco and San Luis Obispo. Application of our techniques yields a variance reduction of 75-90% depending on data processing details. The methods of Aki (1980a) and Aki and Chouet (1975) are also used in order to evaluate the path effect (Q) of both coda and direct shear waves.

The site effect on coda waves is calculated for the data set which was especially collected for this purpose. In spite of a bias toward hard rock sites in the CALNET, a tremendous variation in site response is found. At low frequencies the results spread over a range that is too large to be explained solely by the impedence effect. Other

processes such as inefficiently damped trapped modes must exist in extreme cases. The model of coda waves as backscattered waves from randomly-situated heterogeneities in the earth must be extended to include this possibility. At high frequencies attenuation controls the site effect, although strange variations, especially at granite sites, remain unexplained.

The source effect is calculated for the data set in much the same manner as for the site study. Results are expected to be sensitive to details of the rupture process and anelastic properties of the near source medium. Variations attributable to near source attenuation exist, but are not as strong as the attenuation induced site response variations seen in Chapter 3. The results are compared to simple ω-squared and ω-cubed source models. The ω-squared model fits the best, except for the group of Coyote Lake earthquakes that exhibit a constant corner frequency independent of size. This indicates that a source-controlled limiting corner frequency, or f_{max}, exists in the Coyote Lake data. The result is not strong and should be investigated further with a more appropriate distribution of data.

An exhaustive search is carried out to determine the factors upon which the quality factor of coda waves (Q_c) depends. The most interesting result is a dramatic change in crustal Q_c (by a factor of 2) at high frequencies between the high Q Salinian and the low Q Franciscan regions. This could be due to scattering loss at high frequencies in the highly-deformed Franciscan, or to low intrinsic Q. Except for this crustal effect Q_c is shown to be independent of source-reciever path. The quality factor of shear waves (Q_β) is found to agree with crustal Q_c within error bars. Temporal variations in $\overline{Q_c}$ and M_L-M_{coda} are also investigated. M_L-M_{coda} is observed to decrease after the magnitude 5.0 Bear Valley Earthquake.

I have demonstrated that coda analysis can effectively deal with an extensive data set. The results of this thesis encourage further work on many fronts.

Thesis Supervisor: K. Aki

Title: Professor of Geophysics

ACKNOWLEDGMENTS

people readily responded to frequent cries for help; special recognition goes to Carol Blackway who single-handedly taught me UNIX and to Gilles Garcia who helped with matrix manipulations.

Francis Doughty typed three chapters with speed and accuracy. His help came when I needed it most. Sharon Feldstein kept me afloat financially which has been especially tricky during these last few months. Sharon will be missed by all when she moves on to the Treasury Dept. position that should be offered her soon.

MIT students occasionally get a bad rap from outsiders, but I found the course 12 group to be multitalented and composed of people of many different backgrounds which made daily life stimulating and fun. I looked up to and tried to emulate advanced grad students and postdocs; Cliff Thurber and Arthur Cheng were particularly helpful in the early years while John Nabelek, Ru-Shan Wu, Steve Roecker, Rob McCaffery, and Miguel Herraiz also served as role models. I also thank the younger grad students who, through asking advice, have made me feel sage and accomplished these last few years. Particular thanks and best wishes to Mark Murray, Stephen Pierce, Jose and Joao Rosa, Lind Gee, Beth Robinson and Peter Roberts. Mark also reviewed my thesis; all of the commas are his. I owe the most to my immediate contemporaries, with whom I sat through courses and hurdled all the obstacles that make MIT such an interesting place to study. Darby Dyar, Steve Bratt, Dave (MVP) Olgaard, Roger Buck, Kaye Shedlock

and Steve Park form the core of a great group of friends and have provided excuses for many activities, from distance running and softball, to notoriously wild parties --most of them legal. Tom Wissler was my office mate and good friend for the duration; I wish him luck with his micro-rocks. Thanks also to Tianqing Cao, Kiyoshi Yomogida, Bob Nowack, Paul Okubo, Lynn Hall, Steve Hickman, Paul Huang, Fico Pardo, Craig Jones, Stuart Stevens, and Rafael Benites.

Others who do not fit into any of the above catagories, yet befriended me along the way include Anne Vaughan, Rufus Catchings, Amy Sterling-Bratt, Karen Garrison y mi amigo Héctor Vargas.

Miscellaneous thanks to the FFT Diner [sic] and to the Thai population of Boston for unparalleled cuisine. Also to the Boston Red Sox and the Grateful Dead for keeping me entertained during late night computer binges (to Paul Huang too, for the same reason). And to old friends from the UC Berkeley (Cal) nordic ski team, some of whom, lacking quality door stops, have requested copies of my masterpiece.

Darby helped .... I will never be able to thank her enough.

Most importantly, I am grateful to my family for their support. I am sure they wonder how I could write over 100 pages of text during these final stages, without writing one letter home.

TABLE OF CONTENTS

Chapter 1: <u>INTRODUCTION</u>

The word "coda" comes from the Latin word meaning "tail" or "end." Seismologists use this word to denote the energy trailing direct waves on both teleseismic and local records. This thesis is concerned with the "S-coda," which follows the direct S and surface waves from <u>local</u> earthquakes recorded at distances up to 100 km (Figure 1.1). In the following, "coda" will refer to the S-coda of local earthquakes unless otherwise noted. A useful measure of time in the coda is the "lapse time," which is the time elapsed from the earthquake's origin time.

The S-coda from local earthquakes has proven to be quite useful to seismologists, and, as will be shown in this thesis, promises great potential for future work. Its usefulness stems from the now widely-held idea that coda waves are a superposition of secondary waves backscattered from randomly-situated heterogeneities in the lithosphere. If the earth can be thought of as a stationary random medium (i.e., statistical parameters describing the medium do not change with position), at least for a given region, the coda should reflect such stability. This is generally observed, as the coda is found to be independent of the path from source to receiver. The region of stability is the region of "common coda path" which grows with lapse time as illustrated in Figure 1.2.

The highly heterogeneous outer portions of the earth,

while responsible for the generation of the coda, severely complicate the measurement and interpretation of high frequency direct waves which are quite sensitive to lateral changes of elastic parameters. This has led seismologists to make use of the coda. The duration of a seismic disturbance has long been recognized as a useful indication of magnitude (Bisztricsany, 1958); further spectral characterization of the seismic source using coda has been carried out by Tsujiura (1978), Rautian and Khalturin (1978) and Chouet et al. (1978).

Coda waves have also been used to characterize the earth medium through measurements of the path effect, summarized by the quality factor, Q (e.g. Aki and Chouet, 1975; Aki, 1980), and through inferences as to the degree of heterogeneity needed for its generation (Sato, 1978; Aki, 1980). The coda can also be used to determine the site effect, as will be shown in Chapter 3. Other interesting observations have included temporal changes in the coda shape (Chouet, 1979) which, if reflecting changes in the earth medium, should be considered as earthquake (or volcanic) precursory information. This possibility alone justifies the extensive examination of coda behavior presented here.

1.1 The Composition of the Coda of Local Earthquakes

It is important to emphasize that the coda of local earthquakes is thought to be composed of backscattered shear

waves. Early models of coda generation assumed that backscattered surface waves, rather than body waves, made up the coda (Aki, 1969). Later, the application to band passed data of specific coda models, such as the single scattering model, led to the measurement of a highly frequency dependent quality factor (Q_c) of coda waves. This resulted in the hypothesis that low frequencies (~1.5 Hz) in the coda are predominantly surface waves that are confined to the low Q near surface, while high frequencies (up to 24 Hz) are body waves that have travelled throughout the high Q lower crust and upper mantle (Aki and Chouet, 1975).

Several recent observations indicate that the coda is instead made entirely of body (shear) waves in the band 1.5-24 Hz, and that the Q of the lithosphere is simply frequency dependent. For example, the Q of shear waves (Q_β) was found to exhibit the same frequency dependence as Q_c in the Kanto region, Japan (Aki, 1980a). Subsequent work in other regions has supported this observation and will be reviewed in Chapter 5. Other evidence includes the observation that the site effect of coda waves (relative spectral amplification between stations for a given earthquake) agrees with the average site effect determined from shear waves and is quite different from the average site effect of P waves (Tsujiura, 1978). Similarly, Chouet et al. (1978) showed that source parameters such as corner frequency measured from coda waves matched those measured from direct S waves in Bear Valley, California. Finally, coda measured

in a borehole at a depth of 3 km at the Iwatsuki observatory,
Japan, are qualitatively similar to surface measurements,
thus reducing the probability that surface modes dominate the
coda at lower frequencies (Sato and Matsumura, 1980).

1.2 Topics to be Covered

This thesis represents a contribution to observational
seismology. Improvements over previous work include the use
of methods relying on less restrictive assumptions, and the
utilization of a digital data base embracing a very large
number of stations. The analysis is subdivided by topic into
several chapters as follows:

Chapter 2: METHODS AND DATA. Past techniques of coda
measurement are reviewed in order to place current advances
in perspective. The data reduction procedure is described,
followed by a simple method for isolating source and site
effects based on the general model of coda waves as
backscattered shear waves. Details are left to the Appendix.
Particulars of the U.S.G.S. California Network (CALNET) data
set are also included.

Chapter 3: THE SITE EFFECT. Methods developed in
Chapter 2 are applied to the California data set in order to
delineate the site response. Since the CALNET has been set
up to study microearthquakes, sediment sites of interest to
strong motion seismologists are under-sampled. The study is
highly useful to workers seeking ideal reference sites. The

results are examined with an eye to local geology, in order to determine the controlling factors.

Chapter 4: <u>THE SOURCE EFFECT</u>. Much energy has been expended by other workers to develop methods for measurement of source spectra from "saturated" recordings. Pulse width techniques have been demonstrated by O'Neill and Healy (1973) and O'Neill (1984). In this chapter, a coda method is employed to calculate source spectra. This method, which is a variation of the method used in Chapter 3, is also useful for application to saturated recordings, which gives it great potential. Although the data set is not ideal for a source study, interesting results are obtained. An attempt is made to address the "f_{max}" controversy.

Chapter 5: <u>THE PATH EFFECT</u>. Previous observations of the path effect of shear and coda waves (Q_β, Q_c) are reviewed. Chouet's (1976) method is applied to the CALNET data in order to search for the factors that control coda decay.

Chapter 6: <u>SUMMARY</u>. Findings are summarized and suggestions for future work are given.

Figure 1.1:

a) Microearthquake record from the Alfacar station, Spain, from Herraiz (1981). Ticks are minutes.

b) Microearthquake record from the Iwatsuki Observatory, Japan, from Sato (1977b).

Figure 1.2:

Schematic 2-D map view illustrating the concept of the "coda path." The star denotes a source and triangles denote receivers, although the reverse is also valid for the following. Assuming that the coda energy travels its entire path as a shear wave, the energy arriving at a given time in the coda must have been confined to an ellipsoidal volume which grows with time. At long enough lapse times, the volumes travelled by waves arriving at two different stations are almost coincident.
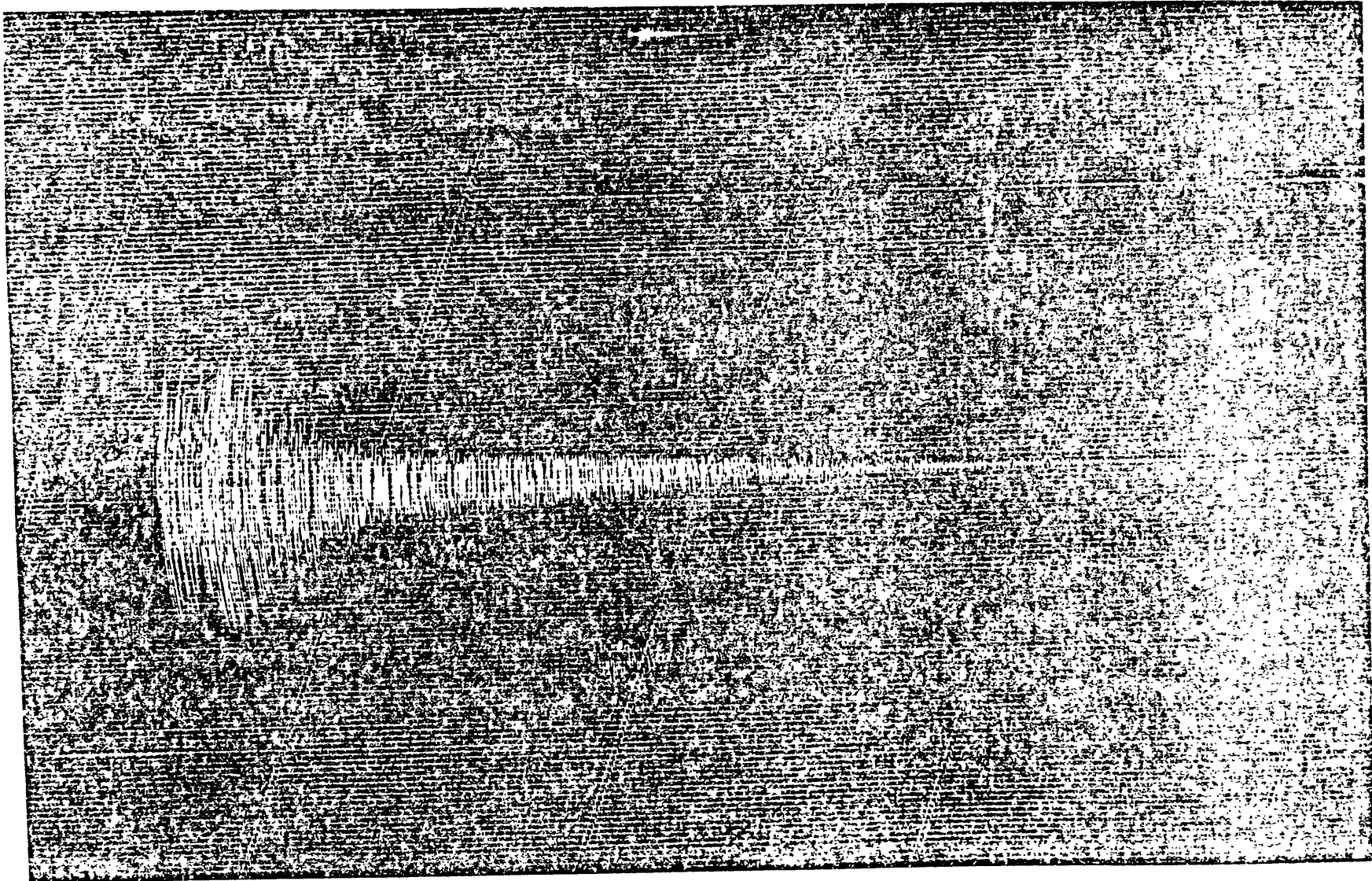
Figure 1.1a
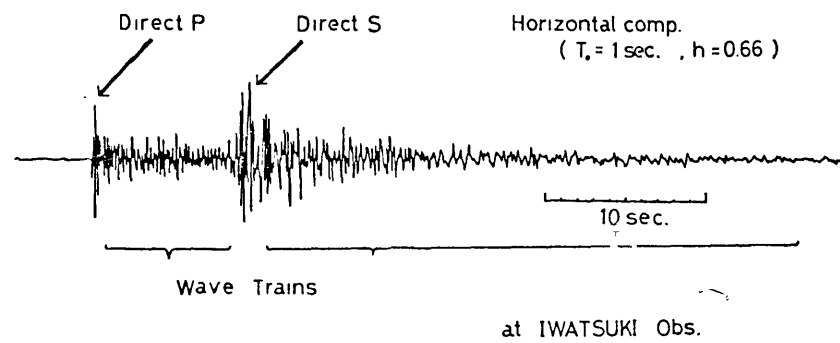
Figure 1.1b
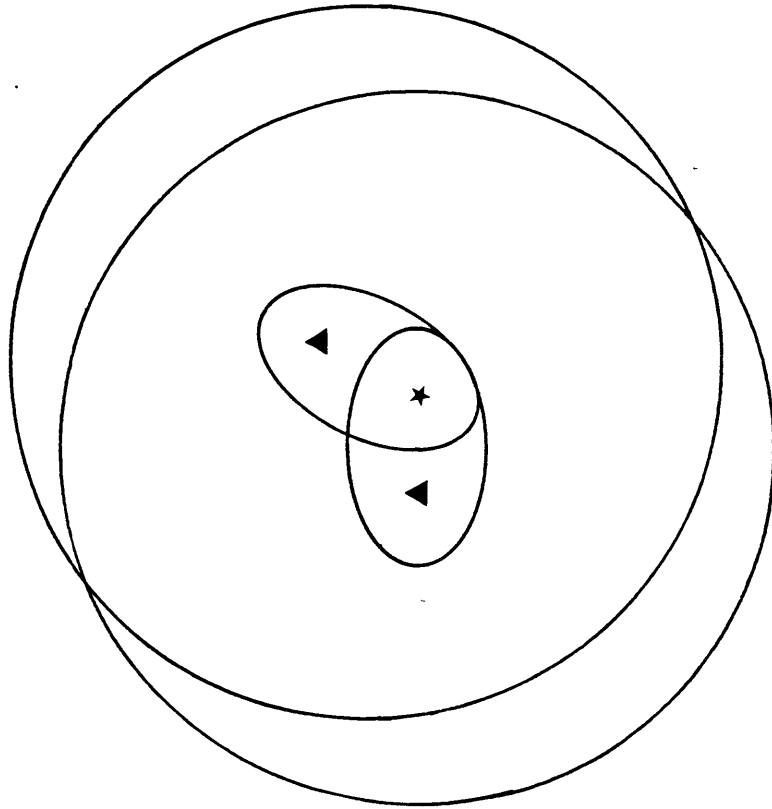
Figure 1.2

Chapter 2: METHODS AND DATA

My study of coda waves in Central California is based
on a large amount of digital microearthquake data. Assuming
a rate of 100 samples per second, the measureable portion of
one coda wave train of duration 100 seconds for a magnitude
3 event is represented by 10,000 data points.
Multiplication by 80, representing the number of stations
within 100 km of any given source, will show how many coda
wave data can be generated by one earthquake.

Reduction of these data to a few relevant parameters is
accomplished in two steps. First, a moving window FFT is
applied to the raw data in order to obtain a set of power
spectral decay curves, each corresponding to a specific
frequency band. Then for each frequency band of interest,
coda wave parameters describing the source and site effects
and temporal decay can be solved by using regression or more
general inverse techniques. In this chapter these data
reduction methods will be discussed, along with reviews of
past techniques. The U.S.G.S. CALNET data used in this
study will also be described.

2.1 Coda Measurement

2.1.1 Review of Methods

The study of seismic waves has advanced in parallel
with the availability of good quality data. This is
especially true for coda waves. Early coda analysis was

done with analog data, forcing workers to devise clever
techniques in order to make their measurements. Aki (1956)
used a sign bit method, employing the rudimentary computers
of the time in order to approximate the autocorrelation. In
that study he noticed the independence of the spectral
character of the coda on the path, as opposed to the
character of direct waves which is heavily path dependent.
Later techniques employed measurements of dispersion in the
coda (Aki, 1969), and have been further refined by Herrmann
(1980) and Singh and Herrmann (1983). These techniques are
still in use today in regions where digital data are not
available (Herraiz and Mezcua, 1984). Advances in coda
research were made with the advent of spectral analyzers
which consisted of a series of narrow band pass filters
that could be attached to the seismometer output (Tsujiura,
1978; Rautian and Khalturin, 1978). Recent studies using
digital data, including this one, have employed brute force
filtering or moving window techniques that mimic the
spectral analyzers with the advantages of speed and
automation. Future digital data techniques should attempt
to improve spectral resolution of the coda estimates,
especially for source and site studies. In the following, I
will discuss these methods in more detail, in order to place
current methods in perspective.

A) Raw Analog Data

Aki (1969) developed a technique for measuring the coda using analog data in order to calculate seismic moments. A quantity known as the reduced coda spectrum is calculated:

$$X(f_p) = t^{1/2} \left(\frac{1}{Q} \frac{dt}{df_p}\right)^{1/4} \langle y^2(t)\rangle^{1/2} \exp(\pi f_p t/Q) \quad (2.1)$$

where f_p is the peak frequency observable in the coda at time t, Q is the quality factor of the backscattered waves that comprise the coda, and $\langle y^2(t)\rangle^{1/2}$ is the rms signal. The rms signal is related to the measured average peak to peak amplitude (A) by:

$$\langle y^2(t)\rangle^{1/2} = A(t)\cdot 8^{-1/2}\cdot |I(f_p(t))|^{-1}$$

where I is the instrument correction. Assuming that the coda is composed of single scattered surface waves, and that the frequencies measured are less than the corner frequency of the source spectrum, the reduced coda spectrum is a product of source moment and regional scattering terms. In this case the source is determined by its low frequency asymptote or moment, and the combined effect of source, medium, and instrument filters is constant for all codas, which makes dt/df_p stable. Equation 2.1 was used to estimate the regional scattering term using an earthquake of known moment; subsequent moment calculations could then be

performed using this parameter. This technique is still in common usage when only analog data are available (Herraiz, 1982; Herraiz and Mezcua, 1984).

A disadvantage to the above technique is that Q must be chosen a priori instead of being determined by the data. Herrmann (1980) extended these techniques to include a variable Q by simply transforming from t to t* = t/Q. Since the dispersion in the coda for frequencies less than the source corner frequency is simply due to the combined instrument and earth medium (expressed by Q) filters, $f_p(t*)$ can be calculated numerically. Master curves representing $df_p/dt*$ and coda shape as a function of f_p and t* can be compared to data to determine an average Q over the bandwidth in use. Herrmann (1980) found that Q's measured from coda in this way are consistent with the Q's measured using the Lg phase. The $f_p(t*)$ technique could conceivably be used to estimate Q using clipped data if the phase is not affected in the oversaturated portions, as is the case for USGS CALNET data (Ellis and Lindh, 1976).

In addition, recent observations of the Q of coda and shear waves suggests that Q is frequency dependent in the range 1-20 Hz. Herrmann's master curve method can be modified to include this possibility by setting $Q = Q_0(f/f_0)^N$ and deriving new sets of master curves to be fit to data. This was done by Singh and Herrmann (1983), who used WWSSN and LRSM data to study variations in Q_0 and N throughout the United States. The factor N is

constrained by using data from instruments with different peak responses.

B) Spectral Analyzers

Analog filters have played an important part in the study of coda waves. These devices consist of a set of narrow band pass filters that can be plugged into seismometer or playback outputs, yielding multi-channel chart recordings written in ink. The spectral analyzer used by Tsujiura (1978), Chouet (1976) and Aki (1980a) contained octave-width filters with center frequencies from 0.75 to 96 Hz. The ChISS instrument used in the Soviet Union (Rautian and Khalturin, 1978) is similar, except center frequencies extended lower, running from 0.27 to 40 Hz.

The most common method of measuring these filtered codas is to read hand-smoothed envelopes from the chart for each channel recorded. Power spectra $P(\omega,t)$ can then be estimated directly. Since by definition, the power spectrum is the Fourier transform of the autocorrelation function, at zero lag:

$$\langle y^2(t) \rangle = \frac{1}{2\pi} \int_{-\infty}^{\infty} P(\omega,t)d\omega$$

After modification by a narrow band pass filter, the coda power can be approximated by:

$$P(\omega,t) = \begin{matrix} 0 & \omega < \omega_1 \\ P_t & \omega_1 \le \omega \le \omega_2 \\ 0 & \omega > \omega_2 \end{matrix}$$

where ω_1 and ω_2 define the band pass bounds. In this case:

$$\langle y^2(t) \rangle = \frac{1}{\pi} P_t (\omega_2 - \omega_1)$$

The rms signal is equated to the amplitudes measured from the charts to obtain the power spectral estimate. The coda measurement is much more direct with this type of data as compared to techniques used to analyze raw analog data. In addition, no restrictions are placed on the use of high frequencies. Data can be compared to the power spectral decay predicted by various coda wave models in order to estimate Q_c. Broad-band source characterization also becomes possible (e.g. Chouet et al., 1978).

These techniques have also been applied to raw analog data (e.g. Sato, 1978). There are disadvantages to this approach, but if ease of measurement and speed are important, these may be overlooked. The search for fluctuations in temporal decay parameters of coda waves may be dependent on this technique since spectral and digital data are not often routinely collected. Of course, discoveries of changes in coda decay using this approach

must not be confused with changes in source character.

C) <u>Digital Data</u>

Digital data are becoming more common these days, making things easier for seismologists. Coda wave students have not yet taken full advantage of the data available, preferring to use filtering and moving-window techniques to mimic the spectral analyzers of the past decade in a brute force way. Of course, the considerable savings of time are important.

The most commonly applied technique is the use of narrow band-pass digital filters; subsequent analysis is the same as that shown in the previous section (Roecker <u>et al</u>., 1982; Pulli, 1984; Del Pezzo <u>et al</u>., 1984). The method I use employs a moving window, smoothed periodogram estimate of the power spectrum. Del Pezzo <u>et al</u>. (1984) compared the two methods, calculating a $Q = Q_0(f/f_0)^N$ law for the Ancona region of Italy. Parameters measured using each method were slightly different but not significantly so. Certainly no difference should be expected. The moving window method used here will be described in more detail in a following section.

In the future, techniques should be experimented with that will result in a higher resolution in the frequency domain. This will be especially important for source and site studies where precise measurements in the frequency domain are crucial. Spectral estimation techniques

developed by Thomson (1982) merit consideration.

2.1.2 Moving Window Method

Starting with raw digital data, our goal is to produce
an estimate of the power spectrum, or signal energy per unit
time. Power spectra estimation techniques are usually
applied to stationary time series. The coda has been called
"quasi-stationary"; the power spectrum can be estimated for
small time windows in the coda, during which the signal is
essentially stationary. A smoothed periodogram power
spectral estimate is used here. Smoothing increases the
stability of the estimate (see Aki and Richards, 1980), and
allows us to mimic the spectral analyzer band pass
measurements made by previous workers.

The starting point in the coda for the moving window is
governed by the onset of unclipped data, and should not be
much less than twice the shear wave travel time,
(Figure 2.1). A reference noise window is also chosen,
usually falling before the first arrival or towards the coda
tail. Data are thrown out if the signal to noise amplitude
ratio falls below 2. A Hanning (cosine bell shaped) window
has been used throughout this study; however, any reasonable
window should work quite well.

The FFT of the windowed signal is corrected for
instrument response and averaged over bandwidth. The power
spectrum is estimated via:

$$P(\omega_0, t_0) = \langle |D(\omega)|^2 |I(\omega)|^2 \rangle \omega_0 / \Delta t$$

where:

$$D(\omega) = FFT([d(t) - \overline{d}(t_0)] \cdot w(t - t_0))$$

Here, D is the FFT of the product of the data d less the mean signal at t_0 and the window w, I is the instrument correction and Δt is the window length. The $\langle \rangle \omega_0$ represents an arithmetic average over an octave width frequency band centered at ω_0. The instrument correction is not extremely important since our final results will be expressed relative to their mean. To first order, relative values of displacement, velocity or acceleration are equivalent. Second order effects may be introduced by the smoothing operation, but this should not affect later interpretations.

Experience has taught us that window length and increment should vary with the frequency band being measured. Window length must be long enough to allow a sufficient number of oscillations of the frequency in question, but short enough that a number of measurements of the coda can be made without overlapping too many windows. The increment itself must be long enough to produce uncorrelated residuals, which will be a basic assumption used in calculating standard errors in later analysis. The

shortest possible time increment should depend most strongly
on window length and shape. Using the Durbin-Watson test
(see Montgomery and Peck, 1982) on real data, it was found
that increments of greater than or equal to 0.4 times the
window length would produce uncorrelated residuals under
simple regression analysis for the Hanning window. Window
lengths and increments used in this study which worked well
for a variety of earthquakes (magnitudes 1.5 - 3.3) are
listed in Table 2.1.

A program was written to run the moving window FFT and
perform peripheral tasks such as correcting erroneous first
arrival picks, choosing the noise window, removing glitches
and assigning "qualities." Preliminary work has shown that
careful examination of the data during routine processing is
very important. A subjective quality judgment was made for
each frequency band of every record as follows:

1 = good quality coda decay curve

2 = fair quality; not enough data to constrain the
decay, yet useful for amplitude studies.

3 = poor quality; many glitches, low signal to noise,
spurious events in the coda, etc.

Later analysis screens the data by quality, generally using
only types 1 and 2, and sometimes only type 1.

Glitches were identified using a home-grown
second-derivative threshold method which worked with
variable success. A median filter method should be more
effective. A program outline is included in the Appendix

for those who may wish to duplicate or improve on my scheme.
An example of the graphic screen output used during
processing is given in Figure 2.2. This example represents
good data, typically obtained from station JAL sited on
Franciscan terraine to the west of Gilroy.

2.2 Separation of Source, Path and Site Effects Using Coda

The second of our two step data reduction procedure is
to distill the coda spectral decay into a small number of
parameters using various assumptions or models. The
simplest coda model states that the time rate of decay of
the energy (or power) in the coda is independent of
source-receiver location, whereas the amplitude of the coda
is dependent on the characteristics of the source and site:

$$P(\omega,t) = |site(\omega)|^2 \cdot |source(\omega)|^2 \cdot C(\omega,t) \qquad (2.2)$$

where C represents the regional coda decay term. This type
of model is predicted by the assumption that coda waves are
backscattered from randomly distributed inhomogeneities in
the earth. Observational support for this model is given by
Aki (1969), Rautian and Khalturin (1978) and Tsujiura
(1978). As will be seen, this law does not always hold (see
Chapter 3), but if care is taken, estimates of the source
and site terms as well as the quality factor of S waves (Q_β)
can be calculated using Equation 2.2.

The assumption of a specific coda generation model

permits the calculation of the quality factor of coda waves Q_c. The most commonly used model is the simple single backscattering model (Aki and Chouet, 1975).

$$C(\omega,t) \sim t^{-\alpha} \exp \left(\frac{-\omega t}{Q_c}\right) \qquad (2.3)$$

where α is a geometrical spreading term. Experiments have shown that $Q_c \cong Q_\beta$ for many regions of the world (Aki, 1980a; Herrmann, 1978; Roecker et al., 1982), which supports the idea that coda is composed of backscattered shear wave energy, and that Q_c indeed represents an average Q of shear waves. In any case Q_c is a valuable parameter to measure, whether or not one believes that Q_c represents Q_β.

By way of review, single station separation techniques will be briefly described, followed by the extension of these techniques to an array of stations upon which the present work is based.

2.2.1 Single Station Techniques (a Review)

Many coda wave studies employ only one or two stations equipped with spectral analyzers. Under simple assumptions of constant coda shape (Equation 2.2) earthquake source character can be compared. Rautian and Khalturin (1978) did this by measuring coda amplitudes at a constant lapse time of 100 s. This is very simple in principle, but more difficult in practice since the signal has to be well above the noise level at the given lapse time for a wide range of

earthquake sizes. This problem can be alleviated by recording at more than one gain setting, or by making a number of measurements for each record in the hope that sufficient overlap will occur and direct comparison(s) can be made somewhere in the coda. The latter method will be described in the next section, and will be used to study site and source effects in Chapters 3 and 4.

The source effect has also been estimated using a specific single scattering model (Aki and Chouet, 1975; Chouet et al., 1978; Tsujiura, 1978). Coda source factors were determined by fitting decay curve data to the combination of Equations 2.2 and 2.3, coupled with a direct determination of the smallest and closest events. Although it is effective, this method does have problems resulting from the assumption of constant Q_c in the single scattering model. Q_c has not been observed to be constant, but instead to increase with lapse time (Tsujiura, 1978; Roecker et al., 1982; Pulli, 1984; this study, Figure 5.1); this will bias the results since the lapse time range over which the coda is measured depends on the source size. It should be possible to include a lapse time dependent Q_c in the calculation, but it is probably best to ignore the specific single scattering model and make relative source measurements by direct comparison of the codas at certain lapse times.

A technique has been developed to estimate Q based on Equation 2.2 (Aki, 1980a). Briefly, the S-to-coda ratio is

formed:

$$R = \frac{t_S A_S(\omega,\theta)}{A_c(\omega,t_0)}$$

where t_S is the S wave travel time, the S wave amplitude A_S is a function of frequency and azimuth θ, while the coda amplitude A_c is measured at a fixed lapse time t_0. If a sufficient amount of data is used, the azimuthal dependence of R (due to source radiation and azimuthal site effects on the direct wave) will be averaged out. Regional Q_β can then be obtained by plotting average ln(R) vs. distance. Q_β calculated in this manner should be viewed with great confidence since few restrictive assumptions have been made. Results of a Q_β study based on a relatively small amount of California array data will be discussed in Chapter 5.

A method for calculating Q_c and coda source factors using the single scattering coda model has been mentioned. While perhaps not the best way to estimate relative source effects, the specific coda model approach is necessary in order to obtain estimates of the coda decay parameter Q_c. Aki and Chouet (1975) applied Equation 2.3 to a large body of data. It was found that a poor determination could be made of the spreading factor α, while the Q_c was fairly well constrained. Their method involved the simultaneous determination of Q_c, α and the coda source factors; the matrix of normal equations is very sparse and is given in

Chouet et al. (1978). A practical solution of such a matrix is given in the Appendix for α = constant. This solution enables the use of a very large amount of data; the size of the data base is limited only by machine precision, and not by the capacity of a linear inversion routine. The study of Q_c will be the subject of Chapter 5.

2.2.2 Array Techniques

There are obvious advantages to using data from an extensive array of stations. Most importantly, the extra freedom allows the observation of regional changes in source, path and site effects. Singh and Herrmann (1983) used a large array of stations to delineate Q_c throughout the United States. Similar, yet simpler, techniques will be used to study the regional variation of Q_c in California in Chapter 5.

A) Source and Site terms

Our coda wave power spectra estimates carry information about both source and site effects. To separate out these effects we use a restatement of 2.2:

$$\frac{1}{2} \ln P_{ij}(\omega_1, t_k) = d_{ijkl} = r_i(\omega_1) + s_j(\omega_1) + c(\omega_1, t_k)$$

$$(2.4)$$

where the r_i are the site terms, s_j the source terms and c is independent of source-receiver location. Indices i, j,

k, and l represent site, source, time, and frequency band, respectively. A factor of one half is introduced so that later results can be expressed in terms of relative amplitude. Under the assumption that the coda shape is common to all records, for a given earthquake, as expected from the backscattering model of coda waves, (2.4) can be reformulated as follows:

$$d_{ijk} - \overline{d_{ijk}}^{(jk)} = r_i - \overline{r_i}^{(jk)} \qquad (2.5)$$

Here, an average represented by the bar is taken holding source and time indices constant; the frequency index is omitted since each band will be analyzed separately. Similarly, if the coda shape is common for all sources at a given station:

$$d_{ijk} - \overline{d_{ijk}}^{(ik)} = s_j - \overline{s_j}^{(ik)} \qquad (2.6)$$

Under the usual least squares criterion, equations 2.5 and 2.6 can be used to find the relative site amplifications, and source terms, respectively. These equations are similar to those obtained after the removal of origin time error terms for the three-dimensional velocity inversion method using teleseismic data (Aki and Richards, 1980). Note that it will be necessary to group data into time "bins." The normal equations will be shown in the Appendix, along with

a general discussion of the inversion technique.

If, for every source, the coda power spectrum is measured at all stations and for all lapse time bins under consideration, then the least squares solution reduces to a simple average. Since this special case does not hold for an array of large extent, or a broad range of source sizes, the full inversion must be done. We have used singular value decomposition and generalized inverse techniques in order to remove the expected zero-eigenvalue corresponding to the non-uniqueness. The solution is then the minimum of all possible solutions. In the site effect case, this means that the array mean is thought of as a reference station. Similarly, the source effect results will be expressed relative to an average source.

It is conceivable that more than one zero-eigenvalue will be found. This indicates an additional level of non-uniqueness, due to a lack of data that, in the site effect case, results in the isolation of a subset of stations and sources. The problem is similar to the non-uniqueness introduced when adjoining blocks are each sampled by the same set of rays in the 3-D velocity inverse analog (Aki and Richards, 1980). The solution to this problem is either to remove the uncoupled stations, or to add more data, placed to bridge the gap between independent subsets of stations (see illustration, Figure 2.3). In this study we simply retain the largest subset of stations. This decision only has to be made for frequency bands for which

the data are most sparse, in our case at 18 - 24 Hz.
Similar decisions must be made if a subset of sources
becomes uncoupled while solving for source terms.

In the past we have noted variations in coda and noise
amplitudes that can only be attributed to poorly recorded
instrument gain settings. These data must be identified and
removed or corrected at this stage. Routine identification
is based on summing residuals for each source-station pair.
These occurrences are uncommon, but can affect the results
and error estimates.

B) Errors

Analyses of the residual variance after applying
Equations 2.5 and 2.6 and of the standard errors of the
estimates will be found in the appropriate chapters. A more
general discussion follows.

The residual variance reflects the degree to which the
data fit our assumptions or model. An estimate of the
residual variance is obtained via:

$$\sigma_r^2 = \frac{1}{N-n_r+1} \sum_{ijk} [d_{ijk} - \overline{d_{ijk}}^{(jk)} - (r_i - \overline{r_i}^{(jk)})]^2 \tag{2.7}$$

$$\sigma_s^2 = \frac{1}{N-n_s+1} \sum_{ijk} [d_{ijk} - \overline{d_{ijk}}^{(ik)} - (s_j - \overline{s_j}^{(ij)})]^2 \tag{2.8}$$

Where N is the total number of data points used, n is the number of stations, or sources, and r and s refer to site and source terms, respectively. The residual variance can be compared to an estimate of the data variance:

$$\sigma_d{}^2 = \frac{1}{N-m} \sum_{ijk} [d_{ijk} - \overline{d_{ijk}}^{(jk)}]^2 \qquad (2.9)$$

where m is the number of combinations of j and k. Equation 2.9 is written for the site study case, but a similar expression is obtained by a permutation of indices for the source case.

For the site effect study the residual variance estimates are satisfactory, representing between 15 to 24% of the data variance, depending on frequency band, but are large enough to cause concern (Table 2.2). A series of experiments using small groups of stations were undertaken to understand the sources of these errors. The site amplification results and residual variance were found to be independent of the lapse time of the measurement (or earthquake size), the subset of stations (groups were chosen to lie in geologically dissimilar areas), and a subjective quality judgement made at the moving window stage (good and fair quality data were used, poor were not). However, the residual variance improved dramatically when the data were replaced by a "smoothed" data set. When all stations were used, the residual variance estimate was found to represent

less than 10% of the data variance for all bands.

Every method of measuring the power spectral decay of coda waves inherently employs a different degree of smoothing in the frequency and lapse time domains. By visual inspection, our method yields data that are less smooth in the time domain than data gathered from a spectral analyzing seismometer (e.g., Aki and Chouet, 1975). Our "smoothed" data set was obtained by interpolation from the best fit to a single scattering coda decay model (Equation 2.3) where the coda quality factor (Q_c) was fixed for each frequency band and was allowed to be different for short (10 - 30 s) and long (30 - 100 s) lapse times (Figure 5.1). These values were obtained by a simultaneous fit of Equation 2.3 to a large amount of data grouped by lapse time. An increase in Q_c with frequency and lapse time is commonly observed (Rautian and Khalturin, 1978; Roecker et al., 1982; Pulli, 1984); the lapse time effect may be due to the importance of multiple scattering, depth dependent Q and varying modal composition of the coda. The smoothing procedure allows us to separate the portion of the residual variance that results from the deviation of the data from a smooth curve, which is dependent on the data reduction method used, from the portion that represents a real deviation from our model assumptions, which should be independent of method. It is comforting to find that the original residual variance estimate is reduced considerably by removing its method dependent portion. This procedure

did not change the site amplification results themselves.

Similar experimentation was not carried out during the source study, however no change in these findings should be anticipated.

Standard errors of the results were calculated in the usual way (for the site case):

$$s_i = (\sigma_r{}^2 a_{ii}{}^{-1})^{1/2}$$

where $a_{ii}{}^{-1}$ is a diagonal element of the inverse matrix and i is the station, source or time bin index. The distribution of standard errors will be discussed in the appropriate chapters.

2.3 Data

This study relies on over 150 stations representing only a portion of the USGS-operated California network (see Figure 2.4, Table 2.3). The instruments are short period (1 Hz) vertical seismometers that are buried in the ground at depths up to 1 m, except for a site at Ravenswood (JRW) near the south end of the San Francisco Bay which lies on Franciscan basement in a borehole at -180 m. Data are transmitted over telephone lines as frequency modulated multiplexed signals to Menlo Park where they are recorded on magnetic tape. The system and its response is described by Eaton (1977, 1980) and Stewart and O'Neill, (1980); a response curve is shown in Figure 2.5. Digital

data are extracted from tape using the USGS ECLIPSE system. We use a data rate of 100 samples per second, which has been deemed sufficient to circumvent aliasing problems (Eaton, 1977). An outline of the data collection procedure is given in Figure 2.6.

Over 90 local earthquakes scattered throughout the array were used in this study (Figure 2.7, Table 2.4). These events were chosen for array coverage, as it was originally desired to study regional changes in the coda and the site effect. Our plans called for use of only 15 earthquakes of magnitude 2.5 to 3.3. Codas from earthquakes of these sizes can be measured at stations up to 80 km from the source thus providing ample coverage and redundancy over our array which measures 100 by 300 km. This proved to be sufficient only for the lower frequency measurements (bands 1.5 - 6 Hz). At higher frequencies, the measurements were difficult to make due to the high amplification of lower frequencies and subsequent instrument saturation especially at sediment sites. To remedy this situation, over 70 earthquakes of magnitude 1.5 to 2 were added to the data set. These events were chosen to lie along the length of the San Andreas through our array and in the Coyote Lake region along the Calaveras fault. Codas from earthquakes of these sizes can only be measured up to 30 km from the source, thus a larger number were needed for geographical coverage.

Table 2.1

Control Parameters for Moving Window FFT

center frequency (Hz)	window length (s)	increment (s)
1.5	10.24	4
3	5.12	2
6-24	2.56	1

Table 2.2

Data and Residual Variance
(For Site Effect Study)

(Napiers^2)

frequency (Hz)	raw data:			smooth data:		
	σ_d^2	σ_r^2	σ_r^2/σ_d^2	σ_d^2	σ_r^2	σ_r^2/σ_d^2
1.5	1.2	0.20	17%	1.1	0.09	9%
3	1.1	0.21	20%	0.9	0.08	9%
6	0.8	0.19	24%	0.7	0.06	9%
12	0.7	0.13	20%	0.6	0.05	9%
24	0.6	0.08	15%	0.5	0.04	8%

Table 2.3

CALNET Stations Used in the Coda Study

Station	Latitude (deg, sec)		Longitude (deg, sec)		Elevation (m)
BAVV	36	38.75	121	1.79	604
BBGV	36	35.48	121	1.52	1216
BBNV	36	30.60	121	4.53	448
BCGV	36	42.55	121	20.60	305
BEHV	36	39.88	121	10.45	342
BEMV	36	39.68	121	5.76	488
BHSV	36	21.35	121	32.39	646
BJCV	36	32.82	121	23.53	207
BJOV	36	36.65	121	18.81	1052
BLRV	36	39.96	121	16.36	232
BMCV	36	39.40	121	21.92	1022
RMHV	36	41.17	121	24.80	808
BMSV	36	39.78	120	47.51	811
BPCV	36	33.90	121	38.15	268
BPFV	36	13.80	121	46.30	349
BPIV	36	29.40	121	10.11	329
BPPV	36	10.12	121	22.68	1591
BRMV	36	50.70	120	49.42	372
BRVV	36	25.49	121	1.10	541
BSCV	36	38.50	121	15.59	323
RSGV	36	24.83	121	15.22	192
BSLV	36	46.53	121	20.96	155
BSRV	36	39.99	121	31.12	395
BVLV	36	34.51	121	11.34	510
BVYV	36	44.96	121	24.80	585
CACV	37	58.57	121	45.62	74
CADV	37	9.77	121	37.45	244
CAIV	37	51.68	122	25.77	223
CALV	37	27.07	121	47.95	265
CAOV	37	20.96	121	31.96	628
CBRV	37	48.97	122	3.72	610
CBSV	37	47.81	121	38.77	279
CBWV	37	55.45	122	6.40	221
CCOV	37	15.46	121	40.35	366
CCYV	37	33.10	122	5.45	67
CDAV	37	43.80	121	43.70	190
CDOV	37	43.80	121	50.12	198
CDSV	37	57.98	122	15.17	109
CDUV	38	1.78	122	.05	168
CDVV	37	33.98	121	40.81	250

CLCV	37	44.28	122	3.83	312
CMCV	37	46.88	122	10.55	90
CMHV	37	21.57	121	45.38	518
CMJV	37	31.25	121	52.23	498
CMLV	37	28.64	121	39.09	1076
CMMV	37	27.34	121	29.62	1117
CMOV	37	48.68	121	48.15	792
CMPV	37	21.46	121	18.51	799
CMRV	37	35.68	121	38.22	500
COSV	37	30.51	121	22.44	1020
CPLV	37	38.25	121	57.64	317
CPNV	37	39.01	121	51.70	200
CRAV	37	46.03	121	56.25	171
CRPV	37	54.75	121	54.33	331
CSAV	37	40.42	121	42.25	215
CSCV	37	17.11	121	46.35	128
CSHV	37	38.88	122	2.57	170
CTLV	37	39.44	121	38.63	458
CVLV	37	37.58	121	50.14	245
HAZV	36	53.08	121	35.45	122
HBTV	36	51.01	121	33.04	98
HCAV	37	1.52	121	29.02	332
HCBV	36	55.88	121	39.63	219
HCOV	36	53.31	121	42.34	129
HCPV	37	11.67	121	11.08	513
HCRV	36	57.46	121	35.01	241
HCZV	36	54.54	121	48.02	30
HDLV	36	50.12	121	38.64	204
HFEV	36	59.00	121	24.09	323
HFHV	36	53.29	121	28.13	101
HFPV	36	45.22	121	29.43	705
HGSV	37	5.75	121	26.83	778
HGWV	37	1.02	121	39.20	133
HJGV	36	47.88	121	34.43	171
HJSV	36	48.99	121	17.92	215
HKRV	36	54.10	121	25.56	66
HLTV	36	53.07	121	18.49	183
HMOV	36	36.03	121	55.06	192
HORV	36	55.03	121	30.46	98
HPHV	36	51.38	121	24.37	122
HPLV	37	3.13	121	17.40	152
HPRV	36	57.19	121	41.70	94
HQRV	36	50.02	121	12.76	536
HSFV	36	48.72	121	29.97	340
HSLV	37	1.16	121	5.13	520

HSPV	37	6.91	121	30.94	850
JALV	37	9.50	121	50.82	244
JBCV	37	9.62	122	1.57	660
JBGV	37	20.52	122	20.34	158
JBLV	37	7.69	122	10.08	792
JBMV	37	19.09	122	9.16	820
JBZV	37	1.07	121	49.15	213
JCBV	37	6.71	121	41.33	192
JECV	37	3.04	121	48.56	438
JEGV	37	30.84	122	27.74	202
JHLV	37	6.56	121	49.95	908
JHPV	37	26.65	122	18.09	347
JLTV	37	21.22	122	12.25	270
JLXV	37	12.11	121	59.17	244
JMGV	37	38.22	122	28.43	201
JPLV	36	58.62	121	49.93	158
JPPV	37	15.87	122	12.78	186
JPRV	37	47.70	122	28.43	107
JPSV	37	11.94	122	20.90	84
JRGV	37	2.22	121	57.86	213
JRRV	37	3.27	121	43.61	408
JRWV	37	29.24	122	7.75	-180
JSAV	37	34.95	122	25.03	207
JSCV	37	17.07	122	7.42	357
JSFV	37	24.31	122	10.55	143
JSGV	37	16.96	122	3.00	198
JSJV	37	20.03	122	5.48	122
JSMV	37	12.74	122	10.06	262
JSSV	37	10.17	121	55.84	946
JSTV	37	12.41	121	47.84	149
JTGV	37	1.71	121	52.58	253
JUCV	37	.07	122	2.91	177
NFIV	37	41.90	123	.00	107
NGVV	38	16.84	122	12.89	257
NHMV	38	9.28	121	48.02	65
NLHV	38	7.19	122	8.87	177
NOLV	38	2.50	122	47.62	37
NPRV	37	59.79	123	.98	165
NTBV	38	14.87	121	55.86	128
NTPV	37	55.22	122	33.78	274
PADV	35	38.36	120	51.86	471
PAGV	35	43.92	120	14.96	482
PANV	35	46.78	120	54.44	451
PAPV	35	54.77	121	21.70	1015
PARV	36	14.95	120	20.52	485

PBRV	35	32.91	121	.54	85
PBWV	36	18.90	120	55.75	381
PBYV	35	48.90	121	4.89	335
PCAV	35	55.90	120	20.22	1189
PCGV	35	25.52	120	44.34	314
PCRV	36	5.63	120	26.08	296
PGHV	35	49.86	120	21.17	433
PHAV	35	50.16	120	23.91	455
PHCV	35	40.93	121	9.15	514
PHGV	35	52.56	120	29.01	792
PHRV	36	22.38	120	49.10	732
PIVV	35	54.39	120	40.94	497
PJLV	36	5.39	121	9.33	290
PLOV	36	14.79	121	2.55	308
PMCV	35	43.48	120	22.23	488
PMGV	35	25.79	120	31.22	529
PMPV	36	12.91	120	47.69	784
PMRV	35	47.09	120	14.14	512
PPFV	35	52.91	120	24.81	469
PPRV	35	38.86	120	42.04	279
PPTV	36	6.50	120	43.27	506
PRCV	36	15.37	120	37.20	623
PSAV	36	1.52	120	53.30	184
PSEV	35	14.71	120	45.88	201
PSHV	35	35.45	120	24.92	390
PSMV	36	4.18	120	35.68	988
PSRV	35	51.47	120	16.81	552
PTRV	35	39.28	120	12.67	643
PTYV	35	56.73	120	28.45	552
PWKV	35	48.87	120	30.67	503

Table 2.4
Earthquakes Used in the Coda Study

Origin Time		Latitude (deg)	Longitude (deg)	Depth (km)	Magnitude
01/29/78	14:44:20.41	36.995	121.457	5	1.51
05/24/78	03:52:57.15	37.018	121.463	4	1.37
06/15/78	12:48:31.29	36.986	121.465	3	1.70
07/26/78	18:12:26.58	37.161	121.479	12	1.62
09/21/78	03:18:56.70	36.988	121.689	8	2.69
11/24/78	23:23:18.26	36.997	121.453	3	1.46
11/25/78	02:25:43.65	36.999	121.454	4	1.46
01/06/79	00:04:36.76	37.053	121.477	6	1.78
01/09/79	22:13:16.94	36.992	121.453	5	1.68
01/09/79	22:45:43.59	36.988	121.451	4	1.61
01/11/79	19:57:26.04	37.020	121.728	12	2.78
01/11/79	20:39:23.37	37.374	121.768	1	3.35
01/14/79	02:35:50.13	37.119	121.504	9	1.79
02/05/79	07:22:40.67	37.326	121.680	10	2.60
02/15/79	11:14:45.67	37.019	121.472	4	0.00
04/04/79	07:49:16.20	36.745	121.488	3	2.75
05/10/79	09:21:43.03	37.022	121.472	5	1.57
06/01/79	19:04:32.52	37.066	121.499	9	1.56
06/12/79	01:45:20.84	37.070	121.491	7	1.72
08/06/79	18:03:21.41	37.044	121.482	7	1.51
08/06/79	18:15:56.27	37.066	121.482	6	1.55
08/06/79	18:21:10.69	37.055	121.475	6	1.71
08/06/79	19:19:26.63	37.055	121.476	6	1.79
08/06/79	20:11:54.83	37.063	121.471	10	1.66
08/06/79	21:25:24.59	37.052	121.463	5	1.67
08/06/79	22:50:08.25	37.048	121.469	11	1.43
08/06/79	23:25:27.63	37.085	121.488	5	1.60
08/06/79	23:34:08.55	37.022	121.461	5	1.59
08/06/79	23:48:50.39	37.037	121.472	11	1.80
08/07/79	02:51:11.13	36.990	121.451	5	1.58
08/07/79	04:38:43.12	37.080	121.483	10	1.63
08/07/79	04:44:29.06	37.099	121.515	4	1.70
08/07/79	14:57:50.88	37.108	121.532	2	1.99
08/09/79	05:28:48.17	36.996	121.441	10	2.67
08/09/79	12:49:11.59	36.982	121.451	3	1.29
12/22/79	18:54:15.43	36.689	121.368	3	3.05
02/04/80	01:22:55.82	37.305	121.648	4	2.71
10/25/80	20:32:34.85	36.988	122.215	5	2.86
01/05/81	12:07:09.07	36.772	121.535	7	1.94
02/01/81	09:31:27.68	36.579	121.182	5	1.60

02/11/81	08:47:28.11	37.856	121.793	13	2.69
02/22/81	17:06:31.15	35.926	120.484	9	1.65
03/10/81	08:41:11.89	36.059	120.601	9	1.94
03/25/81	02:41:12.61	35.877	120.441	9	1.65
03/28/81	20:28:36.14	36.770	121.379	4	3.95
04/01/81	06:47:54.94	35.859	120.400	4	1.72
04/18/81	01:15:38.55	35.592	120.252	4	1.60
04/18/81	01:53:22.59	35.616	120.255	7	1.68
04/24/81	22:37:33.34	35.799	120.337	3	1.83
04/25/81	14:35:14.70	35.776	121.121	7	2.93
04/30/81	12:19:20.21	35.793	120.344	8	1.68
05/17/81	09:22:26.18	36.655	121.320	4	1.94
05/24/81	14:00:25.67	35.856	120.398	4	1.39
05/28/81	03:49:23.56	36.743	121.416	11	1.78
05/28/81	03:50:02.64	36.752	121.414	8	1.43
05/28/81	04:09:00.95	36.745	121.401	5	2.09
05/30/81	18:28:31.30	36.237	120.795	5	1.63
06/03/81	15:04:03.33	36.977	121.665	5	2.15
06/04/81	08:01:40.93	37.366	122.220	6	1.54
06/04/81	09:09:36.08	37.367	122.227	6	1.77
06/07/81	18:11:43.37	36.011	120.582	3	1.83
06/12/81	07:30:00.29	37.014	121.676	2	1.50
06/13/81	23:20:45.92	36.804	121.549	6	2.14
06/19/81	09:47:35.57	36.586	121.216	11	2.36
06/19/81	21:49:48.32	35.897	120.448	5	1.98
06/25/81	00:01:21.03	36.497	120.630	4	2.94
06/25/81	22:44:09.91	36.106	120.619	10	1.68
07/05/81	05:44:20.19	36.700	121.384	3	2.09
07/05/81	22:08:52.35	36.471	121.125	4	1.48
07/12/81	13:08:33.67	35.949	120.517	7	1.66
07/17/81	07:12:16.59	36.194	120.765	4	1.74
07/17/81	08:06:57.60	36.613	121.261	10	1.88
07/18/81	17:12:52.22	36.329	120.892	7	1.85
07/19/81	22:09:47.61	36.145	120.740	4	1.52
07/25/81	21:48:13.36	36.557	121.038	9	2.92
08/06/81	07:13:39.34	36.595	121.214	11	1.70
08/15/81	15:09:26.55	35.864	120.407	3	1.68
09/14/81	20:49:01.59	37.257	122.155	7	1.74
10/05/81	21:36:13.69	36.724	121.504	3	1.64
10/06/81	04:02:29.02	37.621	122.477	10	1.75
10/09/81	01:10:14.77	36.776	121.459	10	1.61
10/09/81	13:55:13.29	36.327	120.911	8	1.97
11/16/81	12:27:23.05	37.125	121.899	12	1.58
12/12/81	15:11:08.98	37.352	122.359	7	3.03

Figure Captions

Figure 2.1

Illustration of the moving window method used to reduce coda wave data. A reference noise sample can be taken before the first arrival, or after the coda has died away. Hanning (cosine shaped) windows are used. Note the instrument saturation that occurs well into the coda.

Figure 2.2

Graphic output of the moving window FFT program.

Figure 2.3

Schematic illustration of two sets of uncoupled sources and recording stations. Coda are measured for each event (stars) at any number of stations (triangles) at a given lapse time. Each measurement is represented by a solid line. In the depiction here, the two sets are isolated from each other. If this pattern continues for all lapse times the two groups can not be compared. The problem will disappear if measurements represented by the dashed lines can be made, or additional data can be added to overlap the two groups. In practice we have simply discarded any small uncoupled sets of sources and stations.

Figure 2.4a-e

CALNET high gain vertical instruments used in the study.

Figure 2.5

Amplitude response of the CALNET system. Except for
borehole station JRW, all instruments have the same
response, but may have different gains; this curve
corresponds to an amplifier attenuation setting of 30. High
gain stations are set between 6 and 24. There are 512
counts/2.5 volts.

Figure 2.6

Outline of the data collection procedure.

Figure 2.7

Epicenters of the earthquakes that were used in our
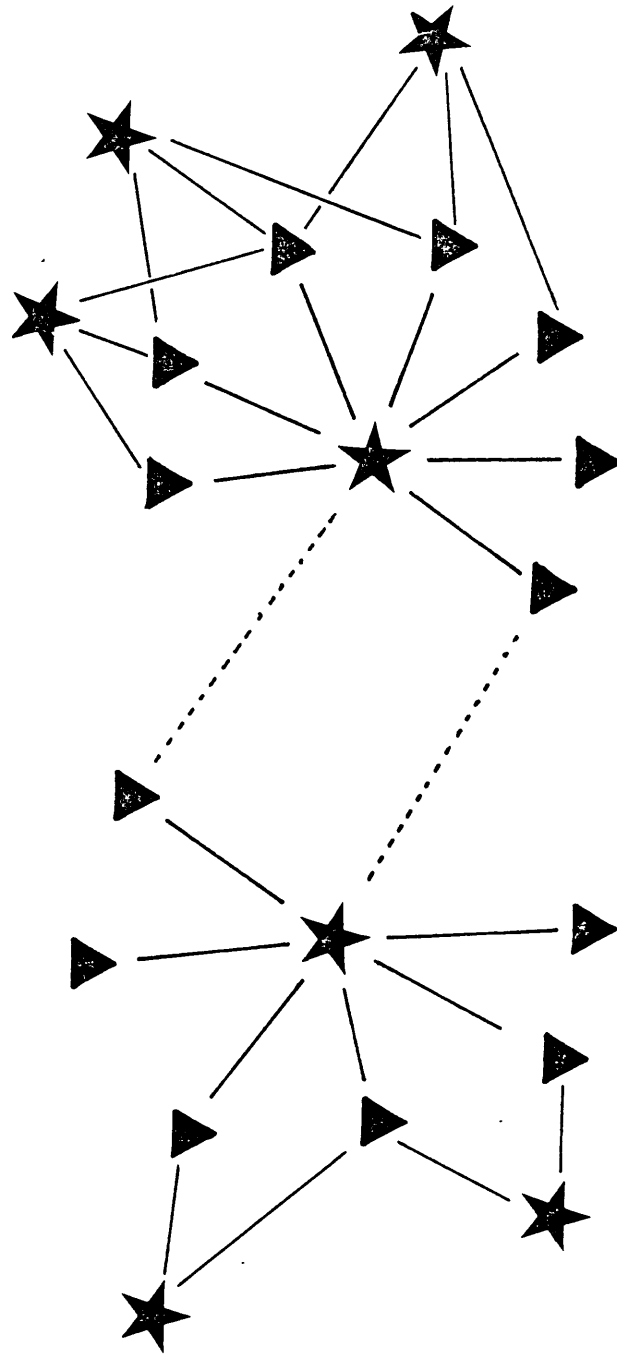study. Over 85 events are shown, including 30 in the Coyote
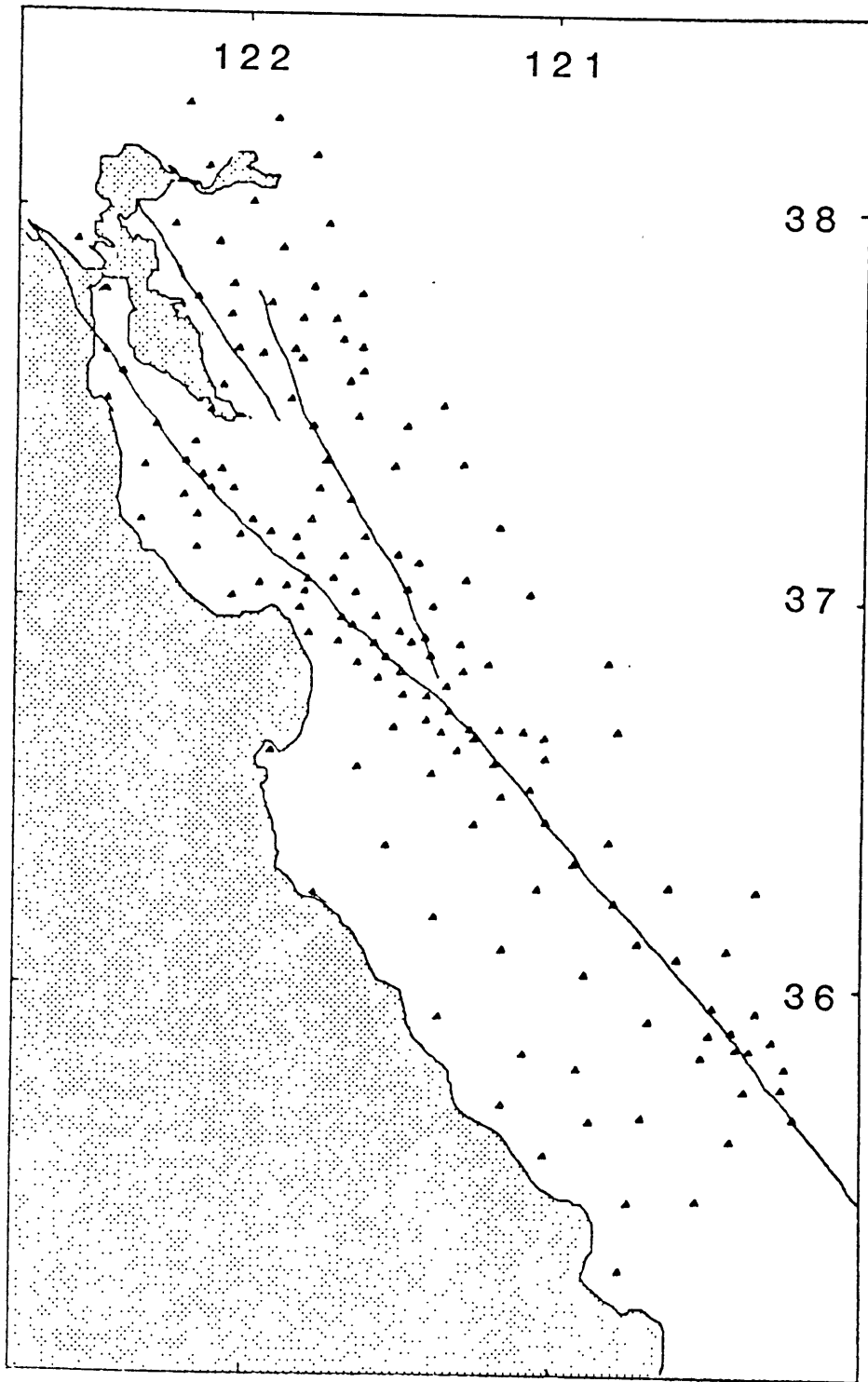Lake area (37°N, 121° 30'W).
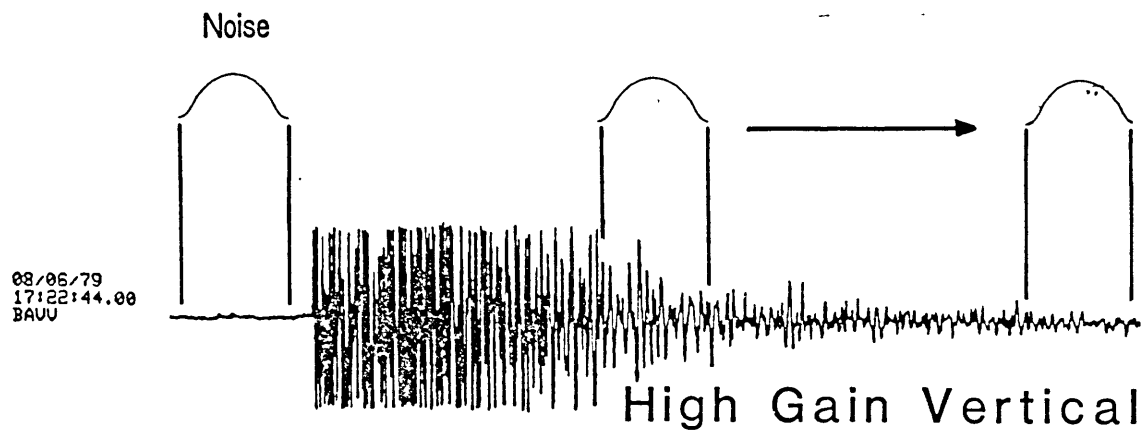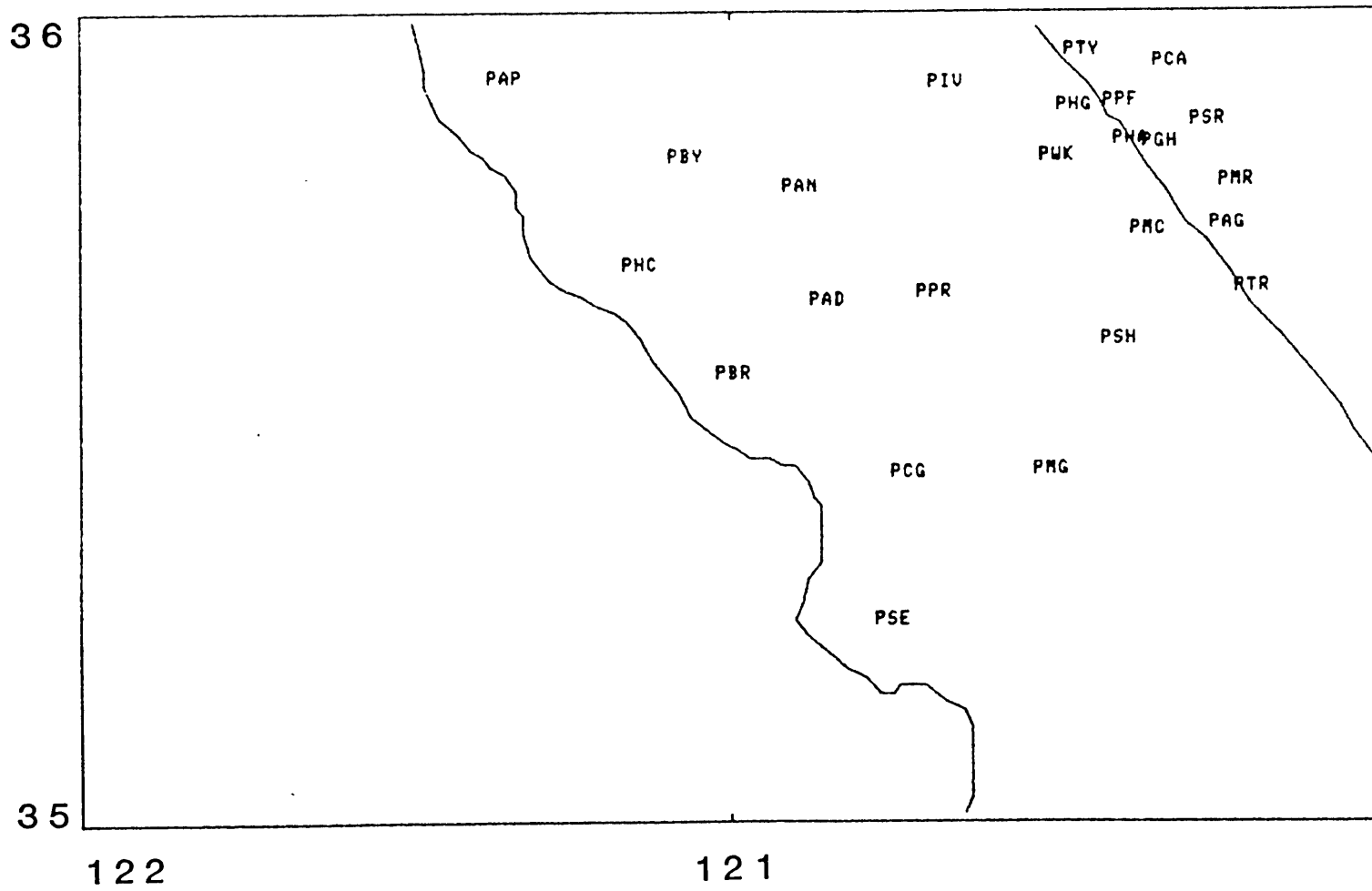
Figure 2.1
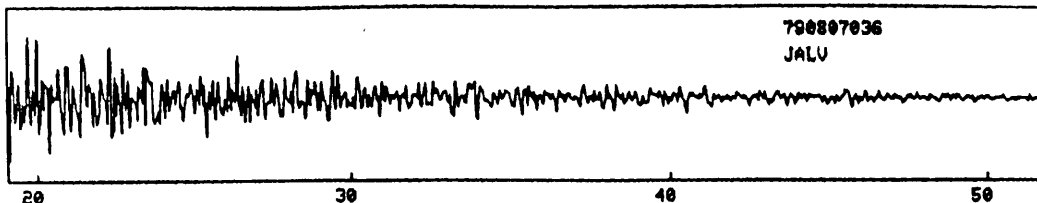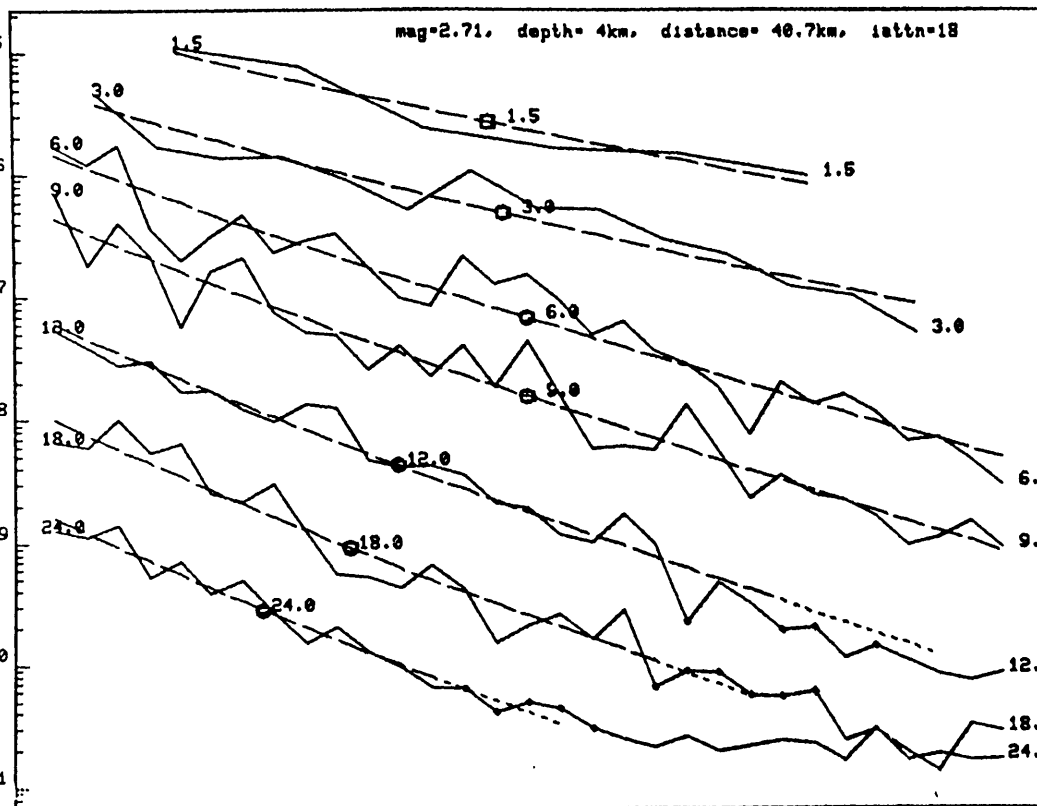
Figure 2.2

Figure 2.3

Figure 2.4a

Figure 2.4b

Figure 2.4c
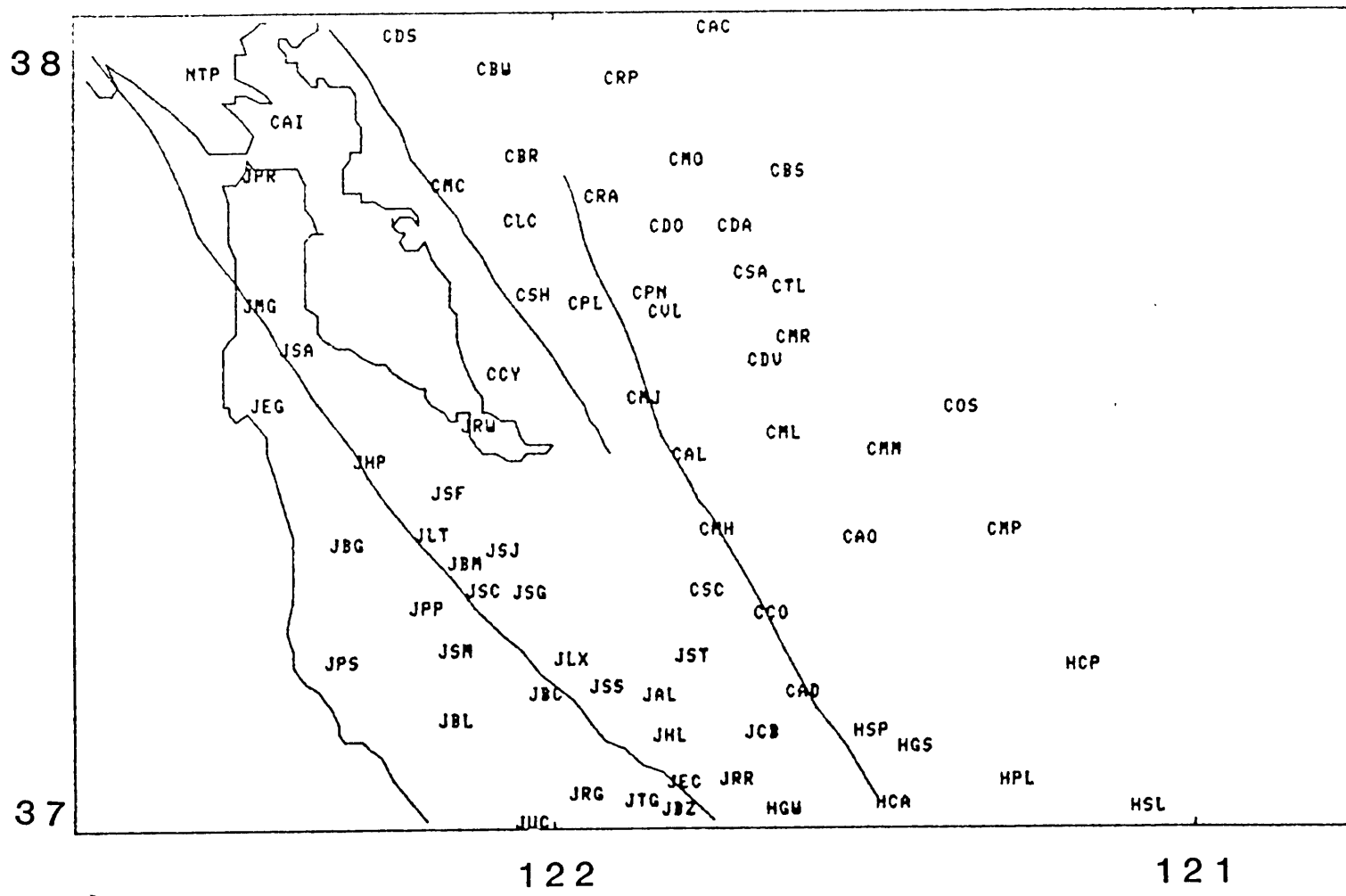
Figure 2.4d
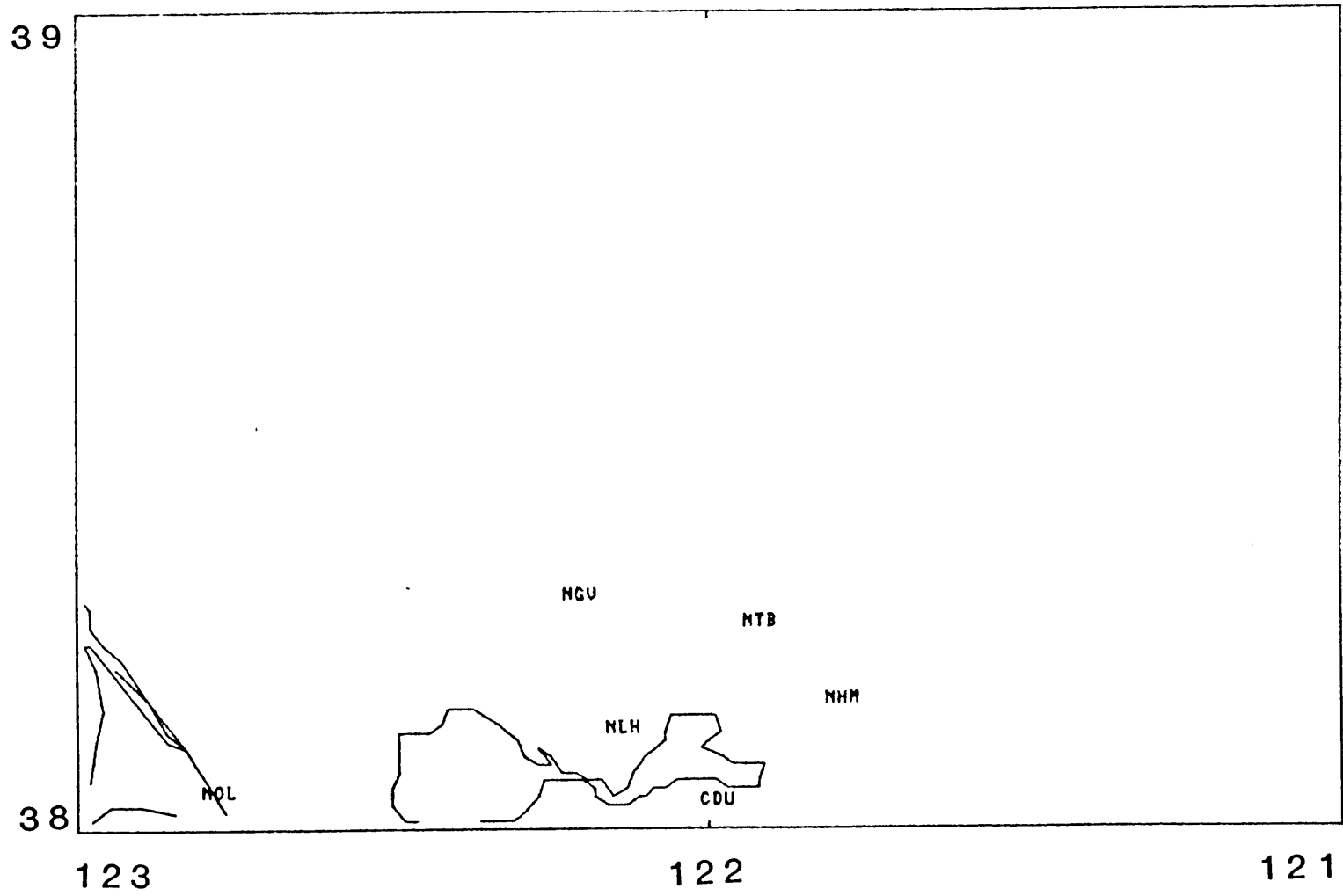
Figure 2.4e

Figure 2.5

PROCEDURE

```
┌─────────────────────────────────┐
│  Search USGS summary cards      │
└─────────────────────────────────┘
                 ▽
        ┌──────────────────┐
        │ Calnet dub tapes │
        │  12/77 - present │
        └──────────────────┘
                 ▽
   ┌────────────────────────────────┐
   │          Eclipse               │
   │ digitizing, picking, location  │
   └────────────────────────────────┘
                 ▽
          ┌──────────────┐
          │ BTRANS tapes │
          └──────────────┘
                 ▽
 ┌─────────────────────────────────────┐
 │ Convert to "gram" file format - Unix│
 │        (program B. Julian)          │
 └─────────────────────────────────────┘
                 ▽
        ┌──────────────────┐
        │ Data reduction   │
        │ moving window FFT│
        └──────────────────┘
```
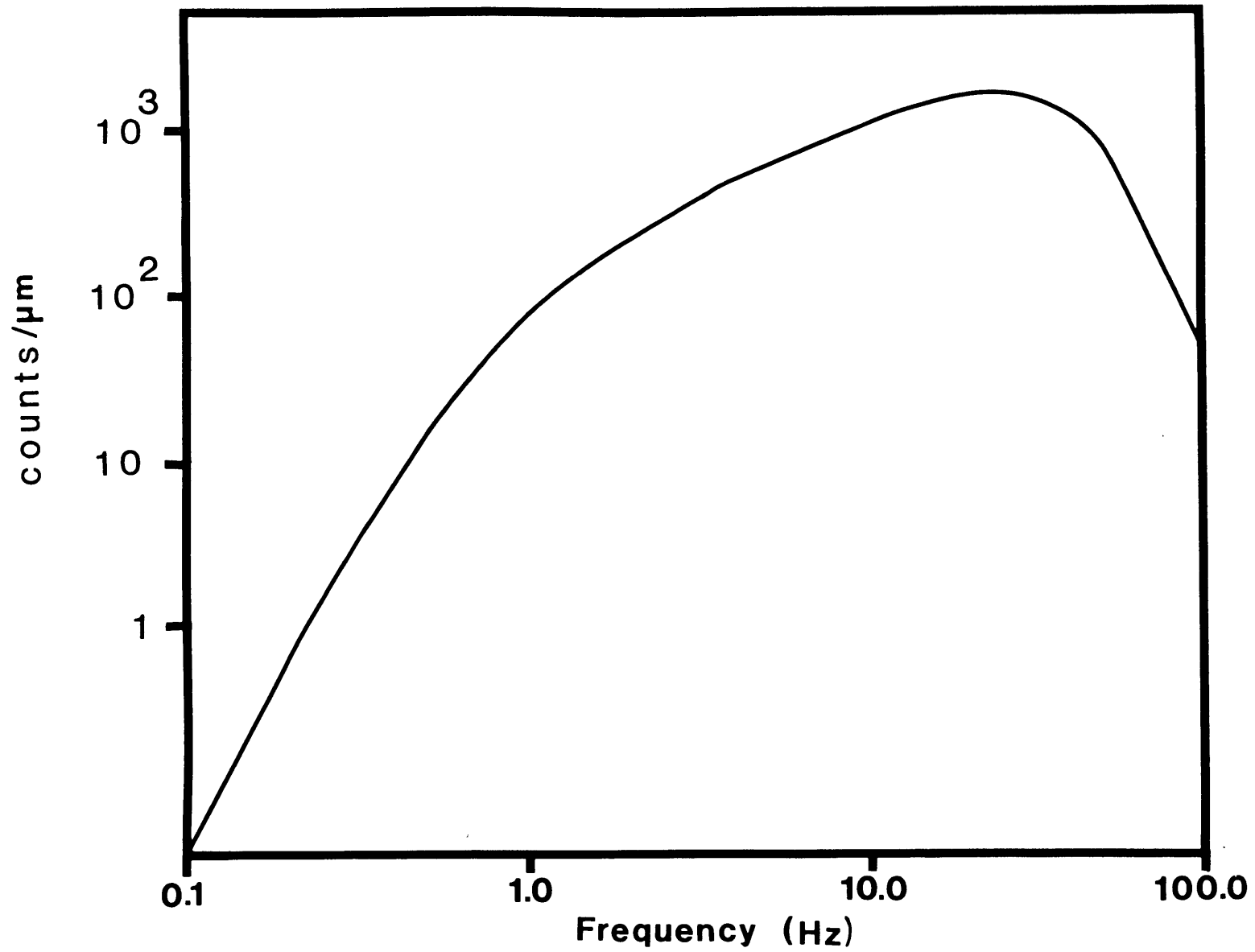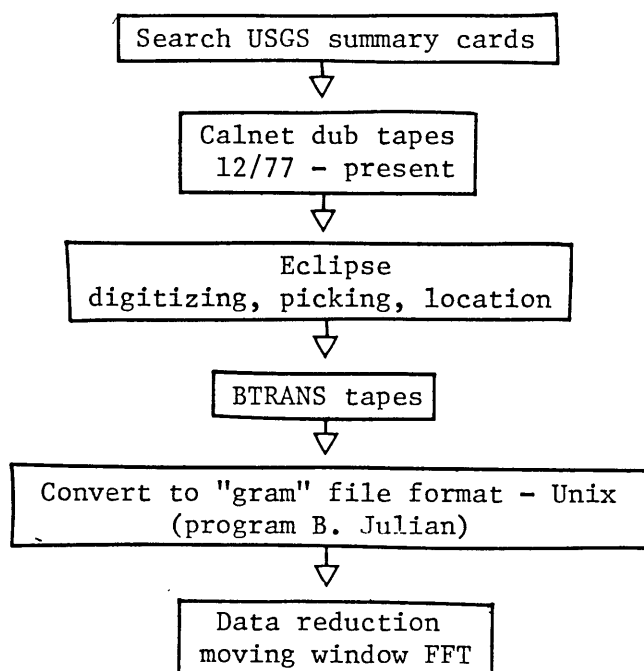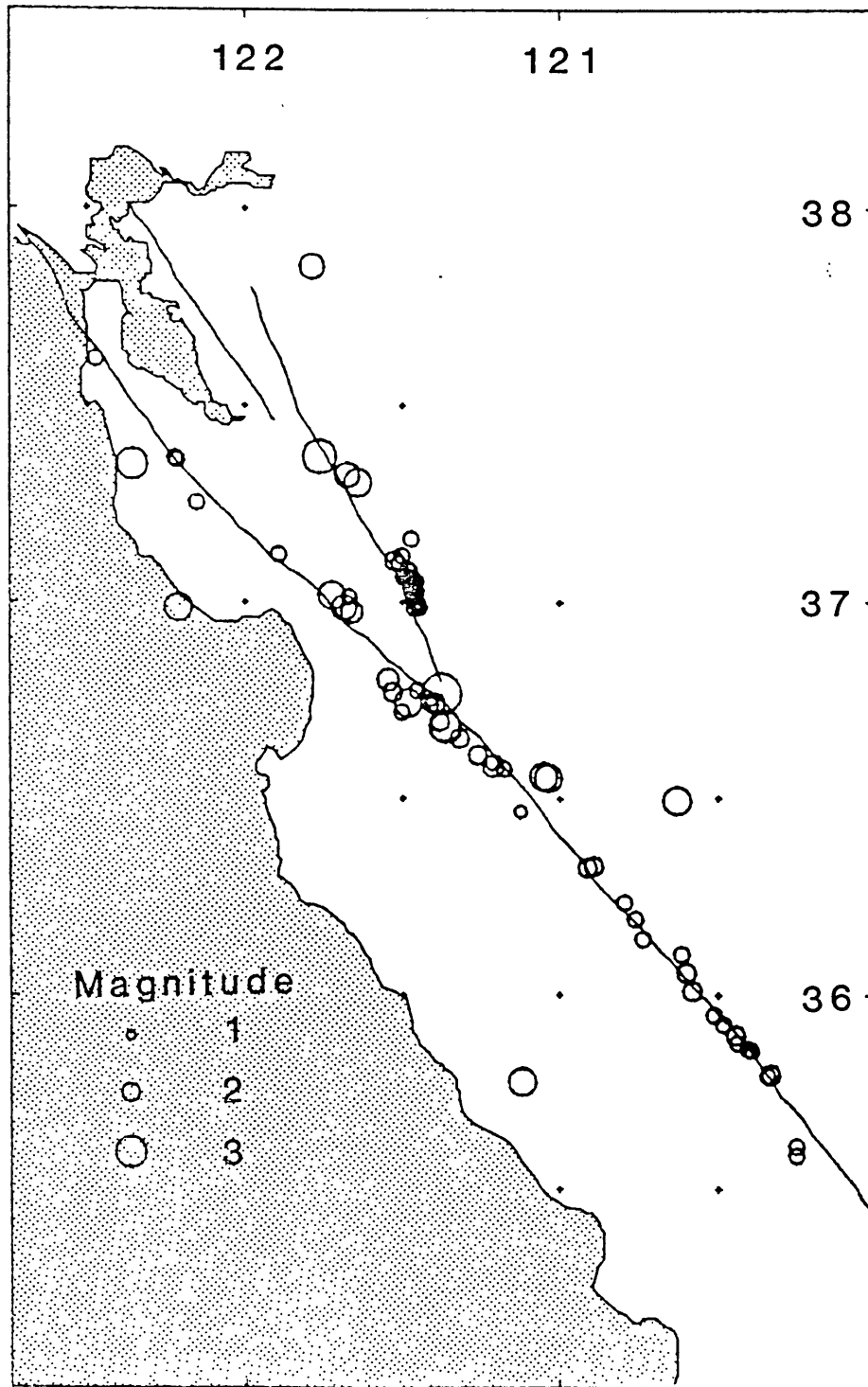
Figure 2.6

Figure 2.7

Chapter 3: THE SITE EFFECT

The goals of this study are threefold: 1) to examine the site effect of coda waves, believed to be the average site effect of shear waves, in order to understand its spatial and frequency dependent behavior, 2) to aquire the ability to extend single station coda wave techniques for source measurement to a large array of stations by applying a site correction, and 3) to learn what we can about the processes that generate the coda itself.

Understanding the site amplification effect of low strain seismic waves is a fundamental problem facing a broad range of seismologists. Strong motion seismologists and engineers must start with low strain information in their effort to predict accelerations due to a large, nearby earthquake. Direct waves have traditionally been used for this purpose. Most recently, Tucker et al. (1984), King and Tucker (1984), and Tucker and King (1984) studied hard rock and valley sediment site effects, and found no significant variation in relative site amplification from 10^{-5} to 0.2 g. Results from the low frequency end of our band should be especially important to workers in this area since man-made structures normally exhibit resonant frequencies between 0.1 and 5 Hz.

Other seismologists attempt to glean information about source and medium characteristics by using microearthquakes that radiate energy throughout our 1.5 - 24 Hz band. Site effects can influence these observations profoundly. For

example, Frankel (1982) discovered that corner frequencies of compressional and shear waves varied more strongly with station location than with moment in the N. E. Caribbean. This was attributed to an anomalous site effect rather than to a violation of the similarity assumption. In addition, Hanks (1982) argued that the site effect cannot be ruled out as controlling the f_{max} measured from shear wave acceleration spectra at distances < 10 km. If f_{max} can be assigned instead to source processes, interesting interpretations can be made (Papageorgiou and Aki, 1983a, b). Since site amplification will also affect moment calculations (Aki, 1969), results from our entire 1 - 24 Hz band should be useful to seismologists studying source characteristics of microearthquakes.

Clearly, both stable and easily applied techniques of measuring the low strain site effect must be investigated. The use of coda waves from local earthquake records is promising. Tsujiura (1978) showed that the coda exhibited a stable site effect which was very close to the average site effect of shear waves arriving from various directions for a small array at Mt. Dodaira, Japan. Similar agreement between the coda and S-wave site effects has been observed by Tucker and King (1984) for sedimentary basins in the Garm region, USSR. We have devised a simple method for estimating the site effect of coda, which we believe to be the average site effect of shear waves. Techniques described in Chapter 2 were applied to more than 1200 digital records from over 150

U.S.G.S. California network stations located in the Coast
Ranges between San Francisco and San Luis Obispo. Simple
linear regression will yield the site effect relative to the
"average" station for each of seven frequency bands, centered
at 1.5, 3, 6, 9, 12, 18, and 24 Hz. The final result is
effectively a calibration of this portion of the U.S.G.S.
network. The relationship between site effect and surface
geology will be discussed.

3.1 Geology of the Coast Ranges

As it is expected that surface geology will control the
site response, a brief review is justified. In order to
interpret our results, CDMG 1:250,000 scale geology maps were
used (Jennings, 1958; Jennings and Burnett, 1961; Jennings
and Strand, 1958). A simplified geology map is shown in
Figure 3.1. Place names referred to can be found in Figure
3.2. A listing of CALNET stations and associated surface
geology is given in Table 3.1.

Our study area spans the Coast Ranges of California,
between San Francisco and San Luis Obispo. This area is
dominated by northwest trending mountain ranges and
intervening valleys. To the west of the San Andreas fault
lie the Gabilan, Santa Lucia, and Santa Cruz ranges, to the
east the Diablo range. Long sediment filled valleys include
the Santa Clara, stretching south to Hollister, the Salinas,
the east-west trending Livermore, and the San Joaquin to the
east. Major active faults also trending northwest are the

San Andreas, Calaveras and Hayward faults.

The San Andreas and the Sur-Nacimiento faults divide the region geologically. To the east of the San Andreas (and Pilarcitos) and west of the Sur-Nacimiento faults lie rocks of the Franciscan complex. Containing some of the oldest rocks found in the area (pre-Cretaceous), the Franciscan consists of an assemblage of greywackes, cherts, altered volcanics and ultramafics. High pressure minerals such as glaucophane are found, supporting the idea that the highly deformed Franciscan originated as abyssal and trench deposits that were eventually thrust under the shelf and slope deposits that later became the Great Valley Sequence. No crystalline basement has been found associated with the Franciscan. For more details see Bailey et al. (1970). Between the Sur-Nacimiento and the San Andreas lie the Mesozoic granite-metamorphic basement rocks of the Salinian block. These rocks are thought to have origins similar to the Sierran plutonic block and have been displaced north-east to their present position (Ernst, 1981). Other rock units include Cretaceous shelf and slope deposits, Tertiary marine sediments and volcanics (such as the Quien Sabe field) and Cenozoic non-marine sediments.

This area has been heavily investigated seismically by both active and passive methods. P_n time terms have been calculated by Kind (1972) and Oppenheimer (1985), who find crustal thickening landward. Wesson et al. (1973) studied the P_g (g = granite or basement) arrivals and noted an

interesting trend towards smaller time terms going from the
Diablo anticline towards the Sargent fault, all in Franciscan
terrane. Their result is supported by work of Mooney and
Luetgert (1982) who interpreted refraction lines in the area
and postulated that a large body of greenstone, or altered
volcanics, lie at shallow depth between the Calaveras and
Sargent faults. Other refraction work includes that of
Stewart (1968) who noted high attenuation at depth in the
Gabilan range and ascribed it to a crustal low velocity
layer, Walter and Mooney (1982) who reinterpreted Stewart's
data, and Blümling and Prodehl (1983) who noted a crustal low
velocity zone in Diablo range data. Zandt (1978) also found
low velocities in the Diablo area, but at much greater
depths.

3.2 Results

As shown in Figures 3.3 a, d and Table 3.2, a
considerable variation in site response is observed
throughout the California Coast Ranges. These results were
obtained using the method outlined in Chapter 2 under the
assumption that coda decay is the same at all stations for a
given source. Variations in coda decay from site to site
constitute violations of the assumptions; their existance
will be discussed later.

3.2.1 Low Frequency (1.5 - 3 Hz)

At low frequencies site amplification is found to depend
on surface geology; high amplification is strongly associated

with young, usually upper Tertiary or Quaternary sediments. Prominent highs are located (north to south): 1) directly east of the San Francisco Bay Area (upper Tertiary marine sediments), 2) in the Santa Clara valley near Hollister (Plio-Pleistocene sediments), 3) in the Santa Cruz Mountains (Pliocene marine sediments), 4) near Watsonville (Quaternary sediments), and 5) between the Salinas river valley and the San Andreas fault zone, south of the Gabilan range (Pliocene marine and Plio-Pleistocene sediments). Low site amplification is found where stations are located on one of the two basement core complexes found in the area. These are the Franciscan formation, composed of Jurassic and Cretaceous meta-sediments, including greywackes, cherts and greenstones, and the granite-metamorphic basement of the Salinian block. The most prominent low is found over the Gabilan range granites. The Franciscan is responsible for almost all low measurements to the northeast of the San Andreas, and to the southwest of the Nacimiento faults. This includes two stations at the southern end of the San Francisco Bay, one of which is situated in a borehole at -180 m. Moderate site amplification is usually associated with Miocene or older marine sediments, including Cretaceous shelf deposits; amplification generally varies inversely with age.

3.2.2 High Frequency (6 - 24 Hz)

At higher frequencies, the site amplification pattern changes. The most obvious change can be seen throughout the Gabilan region where a well defined low gradually turns

moderate to high as frequency increases. This is reminiscent of observations made by Hudson (1972) and Tsujiura (1978) at granite and sediment sites in Pasadena and Japan, respectively. Lower near site attenuation in the granites is most likely responsible for this effect, which is also reflected in the scarcity of high frequency observations at most sediment sites.

Some elements of the site amplification pattern remain the same at high frequencies. Salinian block sediment measurements are moderate to high. In contrast to the Salinian granites most sites located on Franciscan basement remain low. The general pattern at high frequencies is that highs are measured on the Salinian block granites and sediments, while lows are measured elsewhere.

The highly frequency dependent nature of the site amplification effect can be seen in Figure 3.4, for the selected stations shown in Figure 3.5. It must be kept in mind that these results are expressed with respect to a reference mean. Thinking of the granite stations as having the flattest response is helpful. With respect to the granites, most sites exhibit amplification that decreases with frequency.

3.3 Discussion

The results of our study demonstrate that there are significant variations in the site effect with respect to surface geology and frequency. Surprisingly, variations also can be found within geologic units, such as the suite of

granite sites on the Salinian block. These results may be examined in light of mechanisms that have been proposed to explain the site effect. These include the effects of impedance, focusing, attenuation, topography and structures which can trap energy near the surface.

3.3.1 Low Frequency

A) Impedance

Elastic properties will influence the site effect. In the absence of resonance and absorption, amplitudes depend on the product of impedance and spreading factors. Strong focusing or de-focusing effects should be weakened by the natural averaging over incidence angle of the coda. Specializing to the 1-D case of impedance and velocity increasing with depth, the amplitude ratio predicted for a sediment with respect to a hard rock site will be an upper bound if the spreading effect is ignored in the calculation. Since coda wave energy may be incident from any direction, in this case:

$$\frac{A_s}{A_r} < \left(\frac{\rho_r v_r}{\rho_s v_s}\right)^{1/2} \tag{6}$$

where r and s represent hard rock and sediment sites respectively, A is coda amplitude, ρ is density and v is velocity (see Joyner et al., 1981). This relation will be used to assess the importance of the impedance effect on our results.

Aki (1969) interpreted 2.5 Hz coda site effect results from a small array near Parkfield as due to lateral variations in near surface impedance. The maximum amplitude ratio he observed was 8. Joyner et al. (1981) found that impedance variations were sufficient to explain a sediment to Franciscan peak velocity ratio of 3 in the Gilroy area. Our low frequency results qualitatively support the importance of impedance to the site effect since highest amplification is observed at young sediment sites, and lowest at basement sites. But in our case, an amplitude ratio of 20 is observed between the highest measurements (sediment sites near Hollister) and granites at 1.5 Hz. Figure 3.6 shows a histogram of measured site terms for the 1.5 Hz band; a bar indicates an upper bound on the range of amplifications expected from the difference in impedance between granite and very soft sediment. The fact that a substantial number of our measurements, including the Hollister sediment sites, lie above the predicted range means that other phenomena must be considered in order to explain these observations.

The USGS stations for microearthquake observation are usually sited on the most competent rock in a given region which means that soft sediment sites are under-represented in this study. At sites where the impedance governs the low frequency response our measurements represent a regional lower bound.

B) Trapped Modes

The near site structure must be responsible for the high amplifications observed at the Hollister sediment sites at low frequencies. Haskell (1960) showed that SH resonance in a plane layer of high Q sediment over bedrock can produce a peak response equal to the basement to upper layer impedance ratio, which for extreme cases could be greater than 20. A more reasonable, yet large estimate of the impedance ratio is 8.25 which is commonly used in modelling sediment effects. In any case, the effect of these peaks should be reduced since smoothing over octave width frequency bands has been employed in our measurement. In addition, coda energy is thought to be incident from many different directions. The natural smoothing over incidence angle will also reduce the influence of any flat layer resonance extrema on our measurements. Thus, contributions to the site measurement may be significant, but will not reflect the expected peak value.

Local 2 or 3-D structures can influence the site effect. Bard and Bouchon (1980a, b) showed that amplification is induced by 2-D structures such as sediment filled valleys of various shapes. Excitation of normal modes can take place in a deep valley, while surface waves can be generated and trapped by a shallow valley. The more general problem of a low velocity layer with surface roughness has been examined by Hill and Levander (1984). The gross structure of the Hollister sediment trough is approximately 2-D, measuring 20

km across and over 2 km deep, (Smith, 1964). The valley
filling sediments range from competent Cretaceous sediments
to the alluvium found over much of the surface. Since the
structure is so complicated, 2-D sediment filled valley
effects may occur on many scales in the Hollister area.

Wave energy that is trapped by the local structure may
remain for a long time. Dissipation of this energy will
depend on local attenuation, the radiated energy loss at
boundaries, and the spreading mode which depends on the wave
type (surface or body) and the geometry of the resonating
area or volume. If dissipation of excited modes or trapped
surface waves in a 2 or 3-D structure is inefficient, direct
and coda energy will generate a ringing phenomenon that
should be observable in the coda. The coda will increase in
duration and exhibit a higher Q_c (slower rate of decay with
time). This has been noted in observations of local
earthquake codas (Tsujiura, 1978) and Lg codas (Der et al.,
1984). Our results suggest that this is also occurring near
Hollister. Low frequency ringing is seen at short lapse
times (10 - 30 s) in the seismograms at station HOR
(O'Connell Ranch, Figure 3.7). Very high coda Q have been
measured at these stations. Increased signal duration has
also been noticed. Bakun (1984) calculated station
corrections to the usual magnitude-duration law (Lee, 1972).
After adjusting for instrument gain it was found that
duration magnitudes are overestimated by .50 on the average
at stations HOR and HFH near Hollister. These stations

exhibit the longest durations by far of the 42 CALNET stations Bakun examined. A correlation between duration and high site effect has also been found in Italy (Del Pezzo et al., 1984).

The observed change in the coda shape at Hollister sites is anomalous with respect to earlier observations of coda waves that lead to the assumptions we have used to calculate the site effect. Since the codas decay more slowly, the amplitude at Hollister relative to hard rock sites increases with lapse time. This produces a large site effect measurement which may not be expected to correspond to the average site effect of shear waves. If modes or surface waves in the valley sediments dissipate slowly, the coda power at a given lapse time will have been generated by waves incident at earlier times as well as those arriving currently. Thus the site effect of coda will overestimate the average site effect of shear waves. Fortunately, this situation can be detected by checking the coda decay or duration. If dissipation is rapid compared to the coda decay rate, or if there are no resonance effects, Q_c should be equal to the regional value, and the coda can be used to estimate the average shear wave site effect. Observations of valley sediment sites in Garm (Tucker and King, 1984) are consistent with this. Coda durations were found to be the same at hard rock and sediment sites, which lead to the conclusion that any sediment modes that had been generated were severely damped. Accordingly, coda and shear wave site

ratios were found to agree.

Our results also aid in understanding the results of
Poupinet et al. (1984) who detected phase differences that
increased progressively with lapse time between codas of
similar (doublet) earthquakes in central California. This
was attributed to a velocity change of 0.2% in the upper
crust. The inferred velocity change was strongest at the
same Hollister sites that exhibit high coda wave site
effects: HOR, HFH, HPH, and HKR. There is a possibility
that this change may be due to near site velocity changes
(i.e., water level fluctuation in the sediments) since our
results indicate that trapped energy dominates the coda at
short lapse times at these sites. A problem with this claim
is that high amplification is only observed at low
frequencies, while up to 24 Hz are included in the doublet
measurement. However, lower frequencies probably control the
doublet measurement since the high frequency signal quickly
falls below the noise level at these sites.

High site amplification measurements are also associated
with sediments in other areas such as the region of low
Bouguer gravity between the San Andreas and the
Zayante-Vergeles faults near Watsonville, and the upper
reaches of the Salinas River drainage between the Santa Lucia
range and the Cholame Hills west of Parkfield. These
measurements are not as large as those found near Hollister;
the largest corresponds to an amplification factor of 8
relative to the granites. These sediment bodies are possibly

too deep, broad, or leaky to support the processes that may be occurring at low frequencies near Hollister.

C) Attenuation

The variation of near site attenuation should be most obvious in the response at high frequencies, but at low frequencies, most site responses continue to rise with respect to granite sites (Figure 3.4). This can be attributed to a combination of the presence of low frequency trapped modes and a difference in near site attenuation relative to the granites, depending on the station location. Since the granite sites are the most likely to be the closest to the ideal flat site response, source spectra measured at the remaining stations in our array will rise towards low frequencies, making moment calculations difficult at non-granite sites. Fletcher et al. (1984) noted this problem while studying aftershocks of the Oroville earthquake, but ruled out the site effect as its cause. Our results conclusively show that the site effect is responsible.

D) Topographic Effects

It is expected from theory (e.g., Bard, 1982) and via observation (Davis and West, 1973; Griffiths and Bollinger, 1979) that topography will affect the amplification patterns of seismic wavelengths comparable to mountain dimensions. Amplification has been noted to occur on mountain tops with respect to nearby mountain base and slope sites. Numerical

results predict that an SV amplification of 30% will occur on top of a 2-D cosine shaped mountain with a height to half-width ratio of .375. Observations have indicated that numerical calculations underestimate the mountain top amplification.

If we are to encounter this low frequency effect, extraneous influences must be separated out as much as possible. To do this only granite sites are considered in order that minimal variation be due to surface geology. A summary of stations, topography and site effect at 1.5 Hz can be found in Table 3.3. Three stations are located on the peaks of broad mountains. Two of these are in the Gabilan range: BJO (Mt. Johnson) and BMC (McPhail's Peak). Their height to half-width ratios are about 0.15. The third is JBL (Ben Lomond Mtn.) located north of Santa Cruz, with a ratio of 0.25. Two other stations are located on top of smaller but steeper features in the Gabilans: BSR (Salinas radio site) on a subsidiary peak with a ratio of 0.3, and BMH (near Mt. Harlan) on a mountain pass with a ratio of 0.2. With the largest height to half-width ratios, the measurements at JBL and BSR are slightly amplified with respect to the majority of measurements. It is also apparent that topography is not a dominating factor as the remaining three mountain top measurements are no different from the valley and mountain slope measurements. This is not unexpected; since amplification at mountain tops decreases with incidence angle (Bard, 1982), the natural averaging property of the coda

waves should reduce this effect. In addition, numerical and experimental studies indicate that the mountain top effect should be less pronounced in the vertical direction of motion which we have measured.

3.3.2 High Frequency

A) Attenuation

At high frequencies, the effect of near site attenuation should dominate the site effect variations. The increasing differences between granite and other site responses with frequency is most likely due to higher Q in the granite, complicated by the possibilities of low frequency trapped modes in sediments and high frequency resonances in the granites. Attenuation is probably the only factor which can explain the difference in site effect between the granites and the Franciscan. This is supported independently by pulse width measurements of Reiter and Monfort (1977), who assigned a compressional wave Q of 19-28 to the upper crust associated with the Franciscan, assuming Q of 40-250 for granite as a reference. Low coda Q is also measured at Franciscan sites at lapse times 10 - 30 s, but this represents a crustal average (see Chapter 5). At 24 Hz, coda Q is 500 in the Franciscan, compared to 1000 in the Gabilan range (Figure 5.4, Chapter 5). While their coda Q are similar, site measurements made in the Franciscan along the Sargent Fault, and to the east of the Calaveras in the Diablo anticline are quite different. Sites in the Diablo anticline are depleted

in high frequencies (Figure 3.4) which may be related to the greater depth of the P_g refractor in that area (Wesson et al., 1973). The above independence of coda Q, and near site Q in the Franciscan, is further evidence that the coda is composed of backscattered body rather than surface waves. An attempt was made to measure the near surface Q in the Franciscan by comparing high frequency site response to the P_g time terms calculated by Wesson et al. Amplification was generally found to decrease with the size of the time terms, but Q could not be constrained well.

It also is neccessary to invoke a Q difference in order to explain differences in the site effect at high frequencies between the "fault zone" sites and the "sediment" sites (near Watsonville and west of Parkfield). The "fault zone" sites, whether granite or sediment, exhibit a response that falls off rapidly as frequency increases, whereas the "sediment" sites near Watsonville and to the west of Parkfield the site effect remains high at all frequencies (Figure 3.4). A higher Q for sediment sites near Watsonville and west of Parkfield could be the result of the presence of more competent and undisturbed sediments compared to the Hollister area which lies astride the junction of the San Andreas, and Calaveras faults. Some of the "fault zone" sites when compared to the granites exhibit a fairly rapid high frequency roll-off which could affect the measurement of source parameters such as f_{max}.

The spread in amplification at all frequencies is very

large, variations of at least a factor of 8 are observed. At 12 Hz this translates to a δx^* of 0.1 where:

$$\delta x^* = x_1{}^* - x_2{}^* = \frac{x_1}{Q_1} - \frac{x_2}{Q_2}$$

The x_i are thicknesses of near site low Q "layers", indices 1 and 2 represent sites at which low and high responses are measured, respectively. The assumed near surface low Q model is justified by the results of Reiter and Monfort who found that pulse widths, which are related to total path Q_α, are very site dependent. If $x_1{}^* >> x_2{}^*$, then $x_1{}^* \cong 0.1$ which is large, but within reason considering that depths to basement of 3 - 4 km are common (Wesson et al., 1973).

Due to the selective siting of the USGS CALNET on the most competent rock in a given region, at frequencies where attenuation dominates the site effect our measurements probably represent a regional upper bound.

B) Peaked Response

Another interesting aspect of the high frequency site effect is the peaked behavior exhibited by some granite sites (Figure 3.4). At 1.5 Hz, there is very little difference in site response among the granite sites which vary by only a factor of 1.5. But at high frequencies, larger variations in site amplification is observed. The maximum difference at 12 Hz corresponds to over a factor of 5 in amplitude. The extremely peaked nature of some of the site curves (2 of 9)

indicates that very small scale resonances may be affecting these high frequency measurements, or that the effective Q is frequency dependent with respect to the other granite sites which may be controlled by different scale lengths of crustal variations beneath the site comparable to the wavelength of 12 Hz waves, coupled with especially high intrinsic Q. Examination of 1:250,000 scale geology maps, however, reveals no difference between these sites. Since the wavelength of 12 Hz shear waves in granite is about 240 m, we must look at much smaller scale maps, or do field work in order to identify the structures responsible for the peaks. The station exhibiting the sharpest peak at 12 Hz is located in Pine Canyon (BPC) to the west of Salinas. Another strong peak is observed at the Salinas Radio site (BSR) which is located on a mountain top. These are some of the few observations of abrupt changes of the site response at high frequencies that are strong enough to affect the measurement of corner frequencies of microearthquakes. Tucker et al. (1984) also noticed a highly variable site effect at high frequencies at hard rock sites in Garm. Some of these variations were attributed to destructive interferences at tunnel sites, but factor of 8 variations between 5 and 10 Hz at ridge sites were not easily explained by simple topographic effects (Bard and Tucker, in press).

3.4 Conclusions

We have demonstrated one aspect of the usefulness of

coda waves through the calculation of the site amplification
effect for a large array of stations in central California.
There are many advantages to our method. Coda waves are
expected to give a stable indication of the average site
effect of shear waves. The coda are easy to measure; results
are independent of the data reduction procedure used. The
use of coda allows a simple separation of the site from the
source and decay terms. A disadvantage of our method is that
the results are expressed relative to an unknown average
reference station; we later plan to use a suite of small
earthquakes to remedy this in the manner of Chouet et al.
(1978). The presence of inefficiently dissipated near
surface trapped modes has been noted at certain sites, where
our results may overestimate the average site effect of shear
waves, but observations of anomalously high Q_c (slow decay)
or long duration should identify these cases. The coda
measurement employs heavy smoothing in the frequency domain,
thus stability is gained but frequency resolution is
diminished. More sophisticated techniques of spectral
estimation such as that due to Thomson (1982) may improve
the quality of the results. Even though the selective siting
of the USGS CALNET stations on the most competent rock in a
given area has resulted in a sampling bias, a large variation
in site amplification is still observed. Our results show
that:

1) There is a tremendous variation of the site effect
throughout central California. At 1.5 Hz, amplitude ratios

as high as 20 are observed. These variations will affect the
measurements of earthquake source parameters such as seismic
moment. To first order the site effect depends on surface
geology, but large variations within a geological unit are
often seen. For example, stations sited on granitic basement
rocks exhibit a highly variable site effect at high
frequencies. Since seismologists place great trust in
granite and other basement sites, these effects should be
studied more thoroughly.

2) Variations in impedance are responsible for most site
response differences at low frequencies. Amplification
generally decreases with age for sedimentary units, and is
the lowest at basement sites on granite or the Franciscan
formation. In extreme cases such as the sites in the
Hollister area it is neccessary that energy trapped by the
3-D structure of the valley sediments be called upon to
explain the high amplification. Durations measured by Bakun
(1984) and velocity changes inferred by Poupinet et al.
(1984) support this hypothesis. The identification of
trapped modes requires a modification of the idea that coda
are simply backscattered body waves at these sites.
Topographic effects are minimal at low frequencies. Since
seismometers are selectively sited on the hardest rock in a
given area, at frequencies where impedance dominates the site
response our measurements probably represent a lower bound.

3) Changes in near site attenuation are responsible for
most variations of site amplification at high frequencies.

The highest amplification, thus the lowest near site attenuation, is observed in the Gabilan granites. The near site attenuation is intermediate at Franciscan and many sediment sites located away from the San Andreas fault zone. High near site attenuation is observed at sites near the San Andreas fault, whether on sediment or granite. High frequencies are complicated by peaked behavior at some stations. This could be the result of small, and as yet undiscovered, resonant structures or a frequency dependent Q. Due to selective siting on hard rock, at frequencies at which attenuation dominates the site effect our measurements represent an upper bound.

This study represents only a small step in the understanding of the seismic coda and its usefulness. The vast amount of digitized and potentially digitizable data collected by the U.S.G.S. in the western U.S. justifies further work along these lines. This study can be expanded to include many more stations in California, including a number in the Sierra foothills which may offer ideal reference characteristics. This will enable us to calculate coda source spectra throughout California based on a common reference, preferably a number of stations sited on the hardest and largest bodies of basement rock.

Table 3.1 Station Descriptions

Station	Location	Geologic Symbol
BAVV	Antelope Valley	KJ_f (Franciscan)
BBGV	Big Mountain	Ku
BBNV	San Benito	Pmlc
BCGV	Cienega Rd.	gr
BEHV	Elkhorn Ranch	QP
BEMV	Emmet	KJ_f
BHSV	Hastings	m
BJCV	Johnson Canyon	gr
BJOV	Mt. Johnson	gr
BLRV	Lewis Ranch	gr
BMCV	McPhail's Peak	gr
BMHV	Mt. Harlan	gr
BMSV	Mercy Hot Sprngs	Ku
BPCV	Pine Canyon	gr
BPFV	Pfeiffer Pt.	KJ_f
BPIV	Pinnacles	Mv^r
BPPV	Pinion Peak	gr
BMRV	Rolling Bench Mk	Ku
BRVV	Little Rabbit Val	Mmc
BSBV	Swanson's Bluff	QP
BSCV	Stone Canyon	gr
BSGV	Shirttail Gulch	gr
BSLV	Silva Ranch	Pc
BSRV	Salinas Radio	gr
BVLV	Bear Valley	Mm

BVYV	Vineyard	gr
CACV	Antioch	Mu
CADV	Anderson Res.	ub
CAIV	Angel Island	KJ_{fv}
CALV	Calaveras Res.	KJ_f
CAOV	Arnold Ranch	KJ_f
CBRV	Bollinger Canyon	Mu
CBSV	Byron Hot Springs	Ku
CBWV	Brookwood Res.	Mu
CCOV	Coe Ranch	J_k
CCYV	Coyote Hills	KJ_{fv}
CDAV		Mu
CDOV	Doolan Rd.	Pmlc
CDSV	Don Santos Rd.	Pmlc
CDUV	Duarte Ranch	
CDVV		KJ_f,Ku,ub
CLCV	Lake Chabot	Ku
CMCV	Mills College	Pv^r
CMHV	Mt. Hamilton Rd.	Mm, Mu
CMJV	Mission San Jose	Mu
CMLV	Mt. Lewis	KJ_f
CMMV	Mt. Mocho	KJ_f
CMOV	Morgan Terr. Rd.	K
CMPV	Mike's Peak	Ku
CMRV	Mines Rd.	KJ_f
COSV	Mt. Oso	KJ_f
CPLV	Palomares Rd.	K

CPNV		K
CRAV	San Ramon	Pmlc
CRPV	Russellman Park	ub
CSAV		Mu? QP? Ku?
CSCV	Silver Creek	KJ_f
CSHV	Cal Sta Hayward	ub, J_k
CTLV	Tesla Rd.	Pmlc
CVLV		QP?
HAZV	Anzar Rd.	gr
HBTV	Batista	ϕ
HCAV	Canada Rd.	K
HCBV	Chamberlain	ϕ
HCOV	Corn Cob Canyon	Qc
HCPV	Crevison Park	
HCRV	Chase Ranch	KJ_{fv}
HCZV	Cardoza Dairy	Qal
HDLV	Dillon Ranch	gr
HFEV	San Felipe	Ku
HFHV	Flint Hills	QP
HFPV	Fremont Park	ls
HGSV	Gilroy Hot Sprngs	KJ_f
HGWV	Gilroy West	KJ_f
HJGV	San Juan Grade	gr
HJSV	John Smith Rd.	Ku
HKRV	Kincaid Ranch	QP
HLTV	Lone Tree Rd.	Ku
HMOV	Monterey	gr

HORV	O'Connell Ranch	Pc
HPHV	Park Hill	QP
HPLV	Pacheco Lake	KJ$_f$
HPRV	Peckham Rd.	Pml
HQRV	Quien Sabe Ranch	Mv
HSFV	St. Francis Retr.	Mv
HSLV	San Luis Dam	Ku
HSPV	Sheep	K
JALV	Almaden Res.	KJ$_f$
JBCV	Bear Creek Rd.	E
JBGV	Bear Gulch Rd.	Pml
JBLV	Camp Ben Lomond	gr
JBMV	Black Mtn.	KJ$_f$
JBZV	Buzzard Lagoon	Pml
JCBV	Cheesbro Res.	ub
JECV	Eureka Canyon Rd.	Mm, Pml
JEGV	El Granada	gr
JHLV	Holmstrom Ranch	Ku
JHDV	Huddart Park	E
JLTV	Los Trancos Woods	QP
JLXV	Lexington Res.	KJ$_f$
JMGV	Milagra Ridge	KJ$_{fv}$
JPLV	Pleasant Valley	Qc
JPPV	Portola St. Park	Pml
JPRV	Presidio	Qs
JPSV	Pescadero	Pml
JRGV	Rodeo Gulch Rd.	Pml

JRRV	Redwood Retreat	KJ_f
JRWV	Ravenswood	KJ_f
JRXV		Mm
JSAV	San Andreas	KJ_{fv}
JSCV	Steven's Creek	Ml, KJ_f
JSFV	Stanford Telesc.	Mm
JSGV	Saratoga Golf	QP
JSJV	St. Joseph Sem.	QP
JSMV	Sawmill Rd.	ϕ
JSSV	Soda Springs Rd.	KJ_f
JSTV	Sta. Theresa Hill	ub, KJ_f
JTGV	Trout Gulch Rd.	Pml
JUCV	U.C. Sta. Cruz	ms
JWSV	Woodside	E
NGVV	Green Valley Rd.	
NMHV	Hamilton Ranch	
NLHV	Lake Herman	
NPRV	Point Reyes	
NTPV	Mt. Tamalpais	
PADV	Adelaida	Mm
PAGV	Antelope Grade	ub
PANV	San Antonio Res.	Mm
PAPV	Alder Peak	KJ_f
PARV	Alder Peak	KJ_f
PARV	Anticline Ridge	Pml
PBWV	Bitterwater Creek	Pml
PBYV	Bryson	Ku

PCGV	Cerro Alto Cmpgr.	Kl
PCRV	Curry Mtn.	Ku
PGHV	Gold Hill	bi
PHAV	Harlan Ranch	Pml
PHCV	Hearst Castle	KJ_f
PHGV	Hog Canyon	QP
PHRV	Hernandez Valley	KJ_f
PJLV	Jolon Rd.	Mm
PLOV	Lonoak Rd.	Pml
PMGV	Sta. Margarita	gr
PMPV	Monarch Peak	KJ_f
PMRV	Maxie Ranch	Ku
PPFV	Parkfield	Qt, QP
PPRV	Paso Robles	QP
PPTV	Peach Tree Valley	Pml
PRCV	Roach Canyon	Ku
PSAV	San Ardo	Pml
PSEV	See Canyon	Mm
PSHV	Shandon	Mm
PSRV	Scobie Ranch	Ml
PTRV	Twissleman Ranch	QP
PTYV	Taylor Ranch	Pml
PWKV	Work Ranch	QP

Table 3.2   Site Effect Results and Standard Errors

$$X = 2 \ln (A/\overline{A})$$
$$S = \text{Standard Error} \quad \text{(Napiers)}$$

Station	1.5 Hz		3 Hz		6 Hz		12 Hz		24 Hz	
	X	S	X	S	X	S	X	S	X	S
BAVV	-1.5	.1	-2.1	.0	-2.1	.0	-2.3	.1	-2.9	.5
BBGV	0.4	.1	0.4	.1	0.6	.0	-0.1	.1		
BBNV	0.2	.3	0.4	.2	-0.2	.3	-0.1	.2		
BCGV	0.5	.1	0.4	.0	1.0	.0	1.3	.0	1.7	.1
BEHV	1.6	.1	1.2	.1	1.0	.0	0.1	.1		
BEMV	-1.3	.1	0.6	.1	-0.7	.0	-1.5	.1	-2.2	.1
BHSV	-0.5	.1	0.6	.1	1.6	.1	1.9	.1		.
BJCV	-2.7	.1	-2.6	.1	-1.8	.0	-0.1	.0	0.8	.1
BJOV	-2.5	.1	-1.6	.1	1.4	.0	2.0	.0	2.3	.1
BLRV	1.1	.1	0.5	.1	-0.2	.0	-0.6	.1	-1.9	.1
BMCV	-2.8	.1	-2.3	.1	-0.7	.0	0.6	.0	0.1	.1
BMHV	-2.3	.1	-1.5	.0	-1.2	.0	0.5	.0	0.8	.1
BMSV	0.1	.1	0.6	.1	0.3	.1	-0.5	.1		
BPCV	-2.2	.1	-1.7	.1	0.8	.0	3.0	.0	1.1	.1
BPFV	-0.8	.2	0.1	.1	0.5	.1	1.3	.1	0.	
BPIV	-2.0	.1	-1.7	.1	-0.9	.0	-0.4	.0	0.7	.1
BPPV	-1.8	.1	-0.4	.1	0.5	.1	0.9	.1		
BRMV	0.6	.1	1.5	.1	1.8	.1	1.2	.1		
BRVV	0.0	.1	-0.4	.1	-1.1	.1	-0.5	.1	-1.6	.2
BSBV	2.7	.1	2.0	.1	1.9	.1	1.9	.1		
BSCV	-0.3	.1	-0.9	.0	-1.2	.0	-1.0	.0	-0.7	.1
BSGV	-2.2	.1	-1.8	.1	-0.1	.0	2.0	.0	2.4	.1
BSLV	2.9	.1	2.7	.1	2.2	.1	0.9	.1		
BSRV	-2.0	.1	-1.1	.1	0.9	.1	1.9	.1	-0.0	.2
BVLV	0.7	.1	0.4	.1	-0.4	.0	0.0	.1	-1.0	.1

BVYV	-0.7	.1	-1.0	.1	-0.6	.0	0.6	.0	0.0	.1
CACV	1.9	.2	1.7	.1	1.2	.1	1.3	.2		
CADV	0.1	.1	0.4	.1	0.0	.1	-0.8	.2		
CAIV	-0.7	.2	-0.3	.2	0.9	.1	0.3	.1		
CALV	-2.0	.1	-1.8	.1	-1.8	.0	-2.3	.1		
CAOV	-1.3	.2	-1.1	.1	-1.7	.1				
CBRV	0.4	.1	0.2	.1	0.2	.1	-0.4	.1		
CBSV	1.2	.1	1.5	.1	2.2	.1	1.8	.2		
CBWV	0.5	.2	0.0	.1	0.1	.1	-0.1	.2		
CCOV	0.3	.1	-0.1	.1	-0.9	.1	-1.2	.1		
CCYV	-1.3	.1	-1.5	.1	-1.1	.1	-0.2	.1	1.2	.1
CDAV	0.7	.2	1.1	.2	0.1	.1				
CDOV	1.3	.1	1.7	.1	0.6	.1	-1.3	.2		
CDSV	0.5	.1	0.6	.1	1.2	.1	0.3	.2		
CDUV	3.1	.2	2.4	.1	1.9	.1				
CDVV	-1.1	.2	-1.1	.1	-0.1	.1	-1.0	.2		
CLCV	1.2	.2	1.4	.1	1.5	.1				
CMCV	2.4	.2	1.3	.1	0.6	.2	1.5	.2		
CMHV	-0.3	.1	-0.3	.1	-0.5	.1	-0.7	.1		
CMJV	-1.3	.1	-1.0	.1	-0.8	.1	-1.7	.1		
CMLV	-0.3	.2	-1.3	.1	-1.6	.1				
CMMV	-1.2	.2	-1.5	.1	-1.5	.1	-1.9	.2		
CMOV	-0.2	.2	0.8	.2	0.7	.1	0.2	.2		
CMPV	0.7	.1	0.4	.1	-0.1	.1	-1.3	.2		
CMRV	-1.5	.2	-1.6	.2	-2.3	.1	-2.3	.1		
COSV	-0.7	.2	-0.4	.1	-0.4	.1	-1.3	.1		
CPLV	-0.6	.1	-1.1	.1	-1.0	.1	-0.6	.1	-0.4	.3
CPNV	2.8	.3	2.0	.2	1.4	.2	1.3	.2		
CRAV	0.6	.2	-1.0	.2						
CRPV	0.3	.2	1.1	.2	0.2	.1	-0.3	.2		

CSAV	3.4	.2	2.6	.1	1.7	.1	0.4	.2		
CSCV	-0.1	.2	0.3	.1	-0.2	.1	-1.0	.2		
CSHV	-0.7	.1	-1.0	.1	-1.0	.1	0.8	.1	0.4	.3
CTLV	1.2	.1	0.3	.1	0.5	.1	-1.2	.1		
CVLV	0.3	.2	-0.1	.1	0.0	.1				
HAZV	-0.8	.1	-1.4	.1	-2.3	.0	-1.7	.0	-1.2	.2
HBTV	0.2	.1	-0.2	.1	-0.9	.1	-0.8	.1	-1.3	.3
HCAV	-0.1	.1	-0.6	.0	-0.9	.0	-0.8	.0	-2.5	.1
HCBV	0.4	.1	0.5	.0	0.6	.0	-0.6	.1		
HCOV	2.2	.1	1.7	.1	1.0	.1	1.0	.1		
HCPV	-0.9	.2	0.2	.1	0.4	.1	-0.9	.1		
HCRV	-1.3	.1	-1.8	.1	-1.1	.0	0.4	.0	-0.6	.1
HCZV	2.0	.1	1.2	.1	1.8	.1	0.7	.1	1.5	.2
HDLV	-1.0	.1	-0.8	.1	0.2	.0	0.5	.0	-0.3	.1
HFEV	-0.3	.1	-0.6	.0	-1.1	.0	-1.3	.0	-1.8	.1
HFHV	3.0	.1	2.2	.0	1.7	.0	-0.5	.1	3.1	.1
HFPV	-1.9	.1	-2.0	.1	-1.8	.0	-0.8	.0	-0.0	.1
HGSV	-1.3	.1	-1.7	.0	-1.6	.0	-1.4	.0	-2.1	.1
HGWV	-1.5	.1	-1.9	.1	-2.0	.0	-1.9	.0	-1.0	.1
HJGV	-1.5	.1	-1.7	.1	-1.4	.0	-0.8	.0	-0.3	.1
HJSV	-0.1	.1	-0.7	.1	-1.6	.0	-1.4	.1	-1.5	.1
HKRV	3.2	.1	2.6	.1	2.3	.0	1.2	.1	-0.1	.4
HLTV	-0.9	.1	-1.0	.1	-1.4	.0	-2.5	.1		
HMOV	-2.5	.2	-1.8	.1	-0.7	.1	0.0	.1	0.9	.1
HORV	2.8	.1	1.3	.1	0.4	.0	-0.9	.1	-2.0	.4
HPHV	2.9	.1	2.6	.1	2.4	.1	1.1	.3		
HPLV	-1.6	.1	-1.7	.1	-1.6	.0	-2.6	.1		
HPRV	2.1	.1	1.2	.1	1.2	.1	1.2	.1	1.1	.3
HQRV	-1.1	.1	-0.6	.0	-1.0	.0	-1.6	.1		
HSFV	1.1	.1	1.4	.0	0.6	.0	-1.1	.1		

HSLV	0.7	.1	1.4	.1	1.4	.1	1.1	.2		
HSPV	-0.8	.2	-0.7	.1	0.2	.1	-0.2	.1		
JALV	-1.4	.1	-0.6	.1	0.2	.0	0.2	.1	1.1	.1
JBCV	-0.3	.3	-0.7	.2	-0.6	.1	-1.3	.2		
JBGV	1.2	.1	1.2	.1	1.1	.1	1.3	.1	0.2	.3
JBLV	-1.5	.1	-1.5	.1	-1.0	.1	-0.3	.1	2.6	.1
JBMV	-1.0	.1	-1.3	.1	-1.8	.1	-1.2	.1	-0.6	.1
JBZV	1.7	.1	1.8	.1	2.4	.1	2.6	.1	2.0	.1
JCBV	-0.7	.1	0.4	.1	0.1	.0	-0.2	.0	-0.1	.1
JECV	0.7	.1	1.2	.1	0.7	.1	-0.6	.2		
JEGV	0.1	.2	0.3	.1	1.0	.1	1.1	.1		
JHLV	-1.9	.2	-1.8	.1	-0.8	.1	0.3	.1		
JHPV	-0.0	.1	0.0	.1	-0.7	.1	-0.2	.1	-0.9	.2
JLTV	0.4	.1	1.6	.1	1.7	.1	0.8	.1	-0.1	.2
JLXV	-0.9	.1	-0.7	.1	-0.3	.1	-0.1	.1	0.2	.1
JMGV	-0.8	.2	-0.5	.1	-0.3	.1	0.9	.1	-0.3	.4
JPLV	1.4	.1	1.1	.1	0.9	.1	0.9	.1		
JPPV	0.2	.1	-0.1	.1	-0.4	.1	0.4	.1	0.7	.1
JPRV	0.4	.2	0.7	.1	1.0	.1	0.8	.1		
JPSV	1.1	.1	0.9	.1	0.6	.1	-0.2	.1		
JRGV	1.9	.2	2.6	.1	2.8	.1	2.5	.1	2.2	.1
JRRV	-1.8	.1	-1.9	.1	-0.7	.0	-0.1	.0	0.1	.1
JRWV	-2.1	.2	-2.8	.1	-2.0	.1	-1.8	.1	-3.3	.2
JRXV	-2.3	.3	-3.9	.3	-4.7	.3				
JSAV	-0.9	.2	-0.6	.1	-0.7	.1	0.2	.1	0.6	.3
JSCV	-0.8	.1	-0.6	.1	-0.6	.1	-0.5	.1	-1.2	.1
JSFV	1.7	.1	1.1	.1	0.4	.1	-0.5	.1	0.1	.1
JSGV	1.1	.1	0.8	.1	0.9	.1	0.5	.1	0.1	.1
JSJV	0.9	.1	0.7	.1	0.9	.1	1.2	.1	1.0	.1
JSMV	0.8	.1	0.2	.1	0.5	.1	0.1	.1	0.8	.2

JSSV	-0.6	.1	-0.4	.1	-1.0	.1	-1.0	.1	-0.3	.2
JSTV	-0.1	.1	-0.3	.1	-0.3	.1	0.5	.1	0.7	.1
JTGV	0.9	.1	1.0	.1	1.1	.1	1.5	.1	0.2	.2
JUCV	-1.6	.2	-1.1	.1	-0.6	.1	-0.4	.1	-0.9	.2
JWSV	1.7	.2	1.5	.2	1.1	.1	1.2	.1		
NGVV	0.4	.3	0.7	.2	0.5	.1	-0.1	.2		
NHMV	2.7	.3	1.8	.2	0.3	.2				
NLHV	1.0	.2	1.0	.1	0.6	.1	-0.2	.2		
NPRV	0.1	.3	0.3	.2	0.9	.2				
NTPV	-0.8	.3	-0.0	.2	0.1	.1	0.9	.1		
PADV	0.4	.2	0.6	.1	1.0	.1				
PAGV	-0.3	.2	0.0	.1	0.3	.1	-0.3	.2		
PANV	0.0	.3	1.7	.2	1.9	.1				
PAPV	-1.9	.2	-0.9	.1	-0.5	.1	0.5	.1		
PARV	1.0	.2	0.5	.2	0.5	.2				
PBWV	1.2	.1	0.3	.1	0.5	.1	2.2	.1	1.8	.2
PBYV	-0.0	.2	0.1	.2	1.7	.1	1.3	.1		
PCGV	-1.8	.3	-1.6	.2	-1.4	.1	-0.8	.2		
PCRV	-1.3	.1	-1.1	.1	-1.0	.1	-1.4	.2		
PGHV	-2.0	.1	-2.6	.1	-2.5	.1	-2.3	.1		
PHAV	1.4	.1	1.6	.1	0.9	.1	0.4	.1		
PHCV	-0.8	.2	-0.5	.1	-0.9	.1	-2.3	.2		
PHGV	1.1	.1	1.1	.1	0.6	.1	0.2	.1		
PHRV	2.3	.1	1.3	.1	0.2	.1	-0.5	.1		
PIVV	1.9	.1	1.6	.1	2.1	.1	1.4	.1		
PLOV	1.7	.1	2.3	.1	1.8	.1	1.9	.1	2.0	.2
PMGV	-2.2	.3	-1.8	.2	-1.2	.1	-0.1	.1		
PMPV	-0.1	.1	-0.5	.1	-1.0	.1	0.1	.1	-0.9	.2
PMRV	-2.1	.5	-1.8	.2	-1.6	.2	-0.1	.2		
PPFV	1.1	.1	1.1	.1	0.2	.1	-0.1	.1		

PPRV	0.0	.3	0.4	.2	0.7	.1	1.9	.2		
PRCV	-0.8	.1	-0.5	.1	0.3	.1	0.4	.1	-0.2	.4
PSAV	2.7	.1	2.0	.1	1.1	.1	1.8	.2		
PSEV	0.2	.3	1.0	.1	2.5	.1	0.3	.2		
PSHV	1.3	.2	0.7	.1	1.3	.1	1.0	.2		
PSMV	-0.0	.1	0.1	.1	-1.0	.1	-1.4	.1		
PTRV	1.9	.2	2.2	.2						
PTYV	-0.7	.1	-0.2	.1	-0.1	.1	-0.5	.1		
PWKV	1.0	.1	0.4	.1	0.0	.1	0.5	.1		

TABLE 3.3

Topography and Site Effect at 1.5 Hz for Granite Stations

station	site	elevation (m)	topography	$\dfrac{\text{height}}{\text{half-width}}$
JBL	-0.7	792	peak (Ben Lomond Mountain)	.25
HFP	-0.9	705	valley	
BSR	-1.0	395	peak	.3
BPI	-1.0	329	valley	
BPC	-1.1	183	valley	
BSG	-1.1	192	mouth of canyon	
BMH	-1.2	811	mountain pass	.2
BJO	-1.2	1052	peak (Mt. Johnson)	.15
BJC	-1.3	207	mouth of canyon	
BMC	-1.4	1022	peak (McPhail's Peak)	.15

Figure Captions

Figure 3.1:

Simplified version of the geology of the Coast Ranges in central California. Basement rocks in the area are the Franciscan to the northeast of the San Andreas and to the southwest of the Nacimiento faults, with the granite-metamorphic complex associated with the Salinian block in between. CALNET high gain vertical instrument sites are represented by triangles.

Figure 3.2:

Place names referred to in the text.

Figure 3.3a-d

a,b) Geographical distribution of the natural log of site amplification (Napiers) with respect to the average station for the frequency bands centered at 1.5 and 3 Hz. Triangles represent stations that have yeilded standard errors less than 0.2, squares are used if standard errors are greater than 0.2. A factor of 20 difference in amplitude is observed between the Hollister sediments (center) and the Gabilan range granites. Other high areas include Cenozoic sediments east of the Bay Area, near Watsonville, and the upper reaches of the Salinas river drainage south of the Gabilan range. Additional low areas include the expanse of Franciscan to the east of the San Andreas, lying along the

Sargent fault, and southwest of the Nacimiento fault, and isolated granite outcropping north of Santa Cruz and near San Luis Obispo to the south. c,d) Distribution of the natural log of site amplification with respect to the average station for the frequency band centered at 6 and 12 Hz. The most definable pattern is high amplification to the southwest of the San Andreas including the Salinian basement sites, and low amplification to the northeast of the San Andreas, and southwest of the Nacimiento faults, including many Franciscan sites.

Figure 3.4:

The site effect (Napiers) as a function of frequency for selected stations grouped by surface geology. "Granite" stations are from Gabilan and Santa Lucia range sites (stars mark sites exhibiting peaked behavior at 12 Hz), most "Franciscan" stations lie along the east side of the Sargent or San Andreas faults, or in the Diablo range (stars mark sites depleted in high frequencies, both lie in the Diablo anticline), "Fault Zone" sites lie in the Hollister sediment trough or directly southeast along the San Andreas on granite, while "sediments" sites are located away from the San Andreas, the majority near Watsonville. These plots were made only using stations at which a full complement of frequencies were measured, 1.5 -24 Hz. The average station represented by the zero line has been adjusted accordingly. Note the different roll-offs with frequency between the four

groups of stations, the result of near site Q variations, and
the different low frequency levels which reflect the
variation in near site impedance, complicated by the
possibility of low frequency resonances. Station locations
can be found in Figure 3.5.

Figure 3.5:

Locations of stations used in Figure 3.4. The code is
as follows: g = Granite (stars are sites exhibiting high
frequency peaks), f = Franciscan (stars are sites depleted in
high frequencies), 1 = fault zone sites, and 2 = non-fault
zone sediment sites.

Figure 3.6:

Histograms of site measurements (Napiers) divided by
standard error. The vertical axis is the total number of
measurements, while the horizontal is the natural log of
relative amplitude. White represents standard errors less
than 0.1, gray, less than 0.2, and black, all measurements.
The standard errors reflect the distribution of data. The
asymmetry between good and fair measurements at 1.5 Hz is due
to the large number of sediment sites lying near the outer
edge of the array. Hollister sites stand out at 1.5 Hz and
are marked by a star. A bar indicates the range of
amplification explainable by the impedance effect for a
contrast of 8.25, representing unconsolidated sediments
versus granite.

Figure 3.7:

Two recordings of an aftershock of the Coyote Lake earthquake, August 6, 1979, magnitude 1.5, depth 7km. Instrument amplifications are identical. The origin time is at 0 seconds. The O'Connell Ranch (HOR) station is located on Permian sediments near Hollister, while the San Felipe (HFE) station is located on nearby upper Cretaceous sediments. Note the long ringing of low frequency energy at HOR as compared to the "normal" decay observed at HFE.

GEOLOGY of the
CENTRAL CALIFORNIA
COAST RANGES

▲ CALNET station

Cenozoic nonmarine

Cenozoic marine

Cenozoic volcanic

Late Mesozoic shelf & slope

Franciscan & ultramafic

Salinian granite & metamorphic
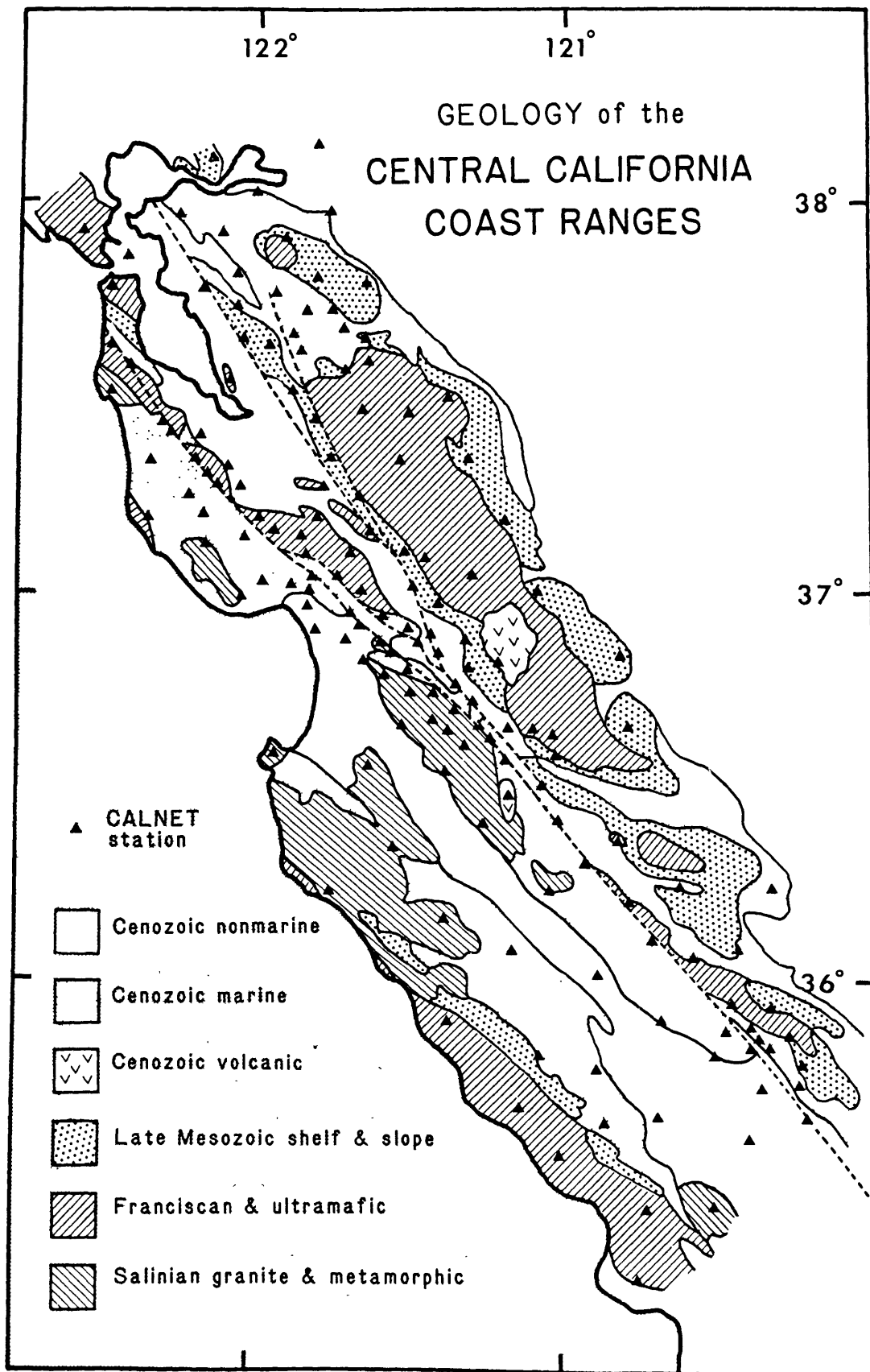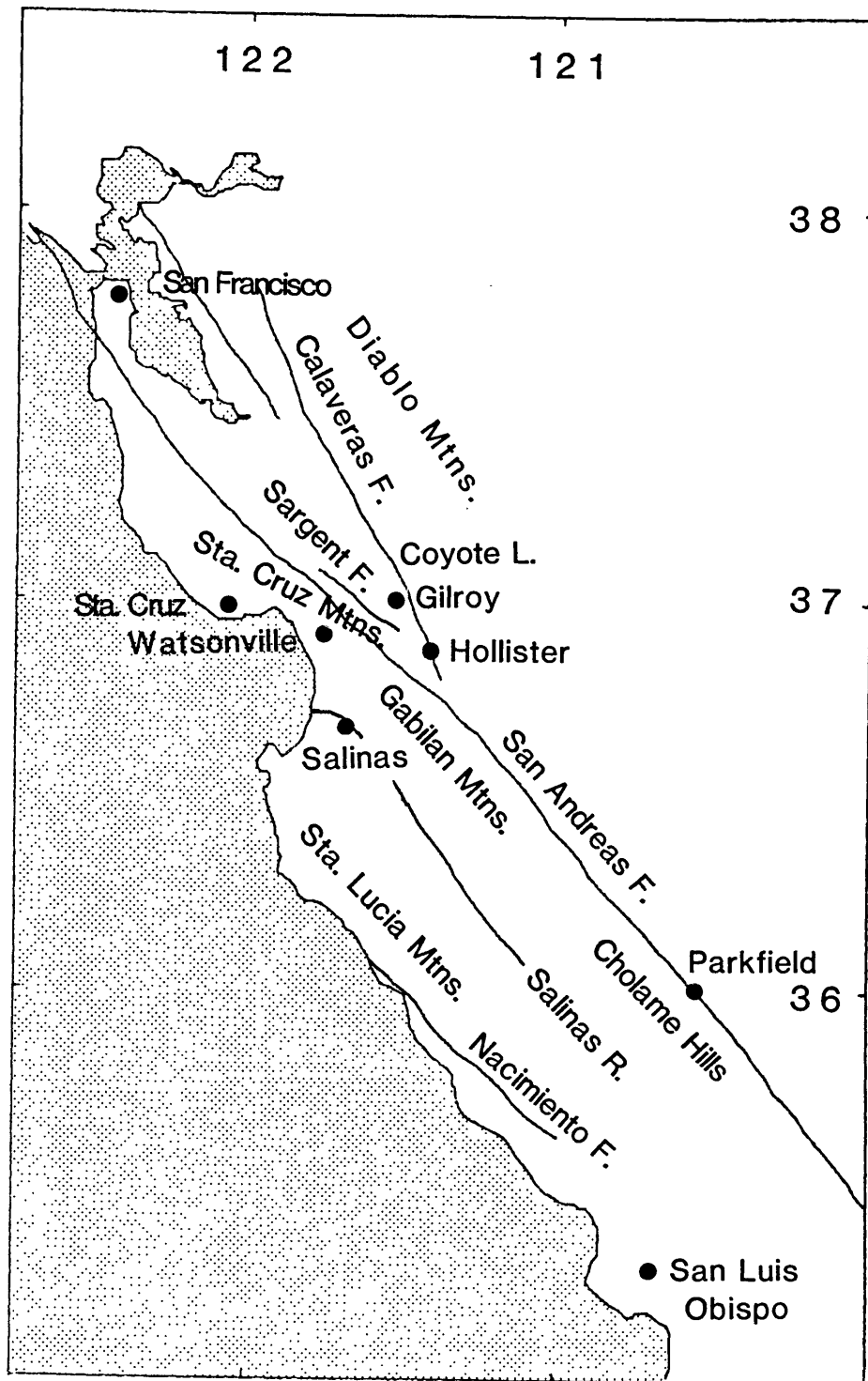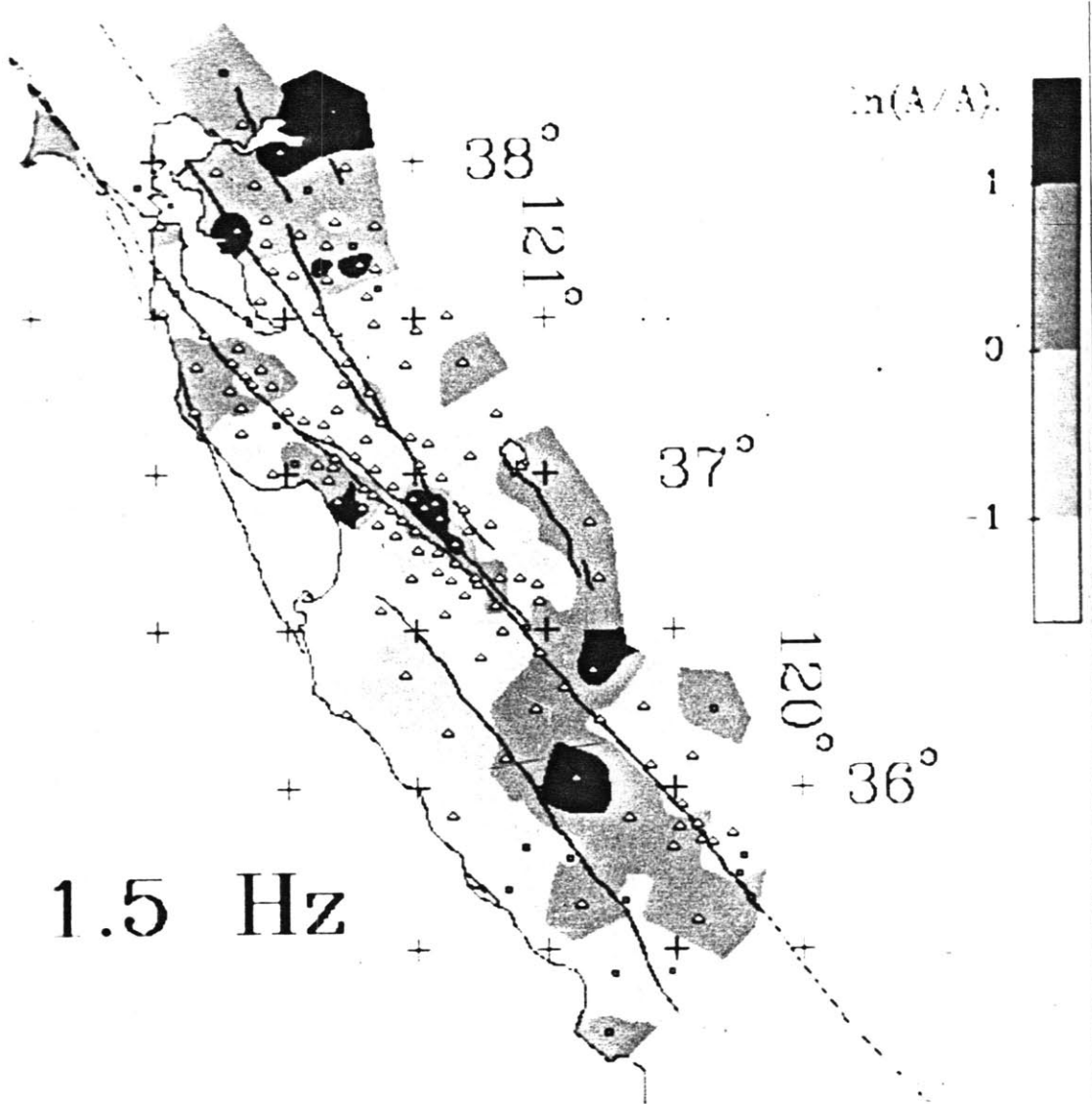
Figure 3.1

Figure 3.2

Figure 3.3a
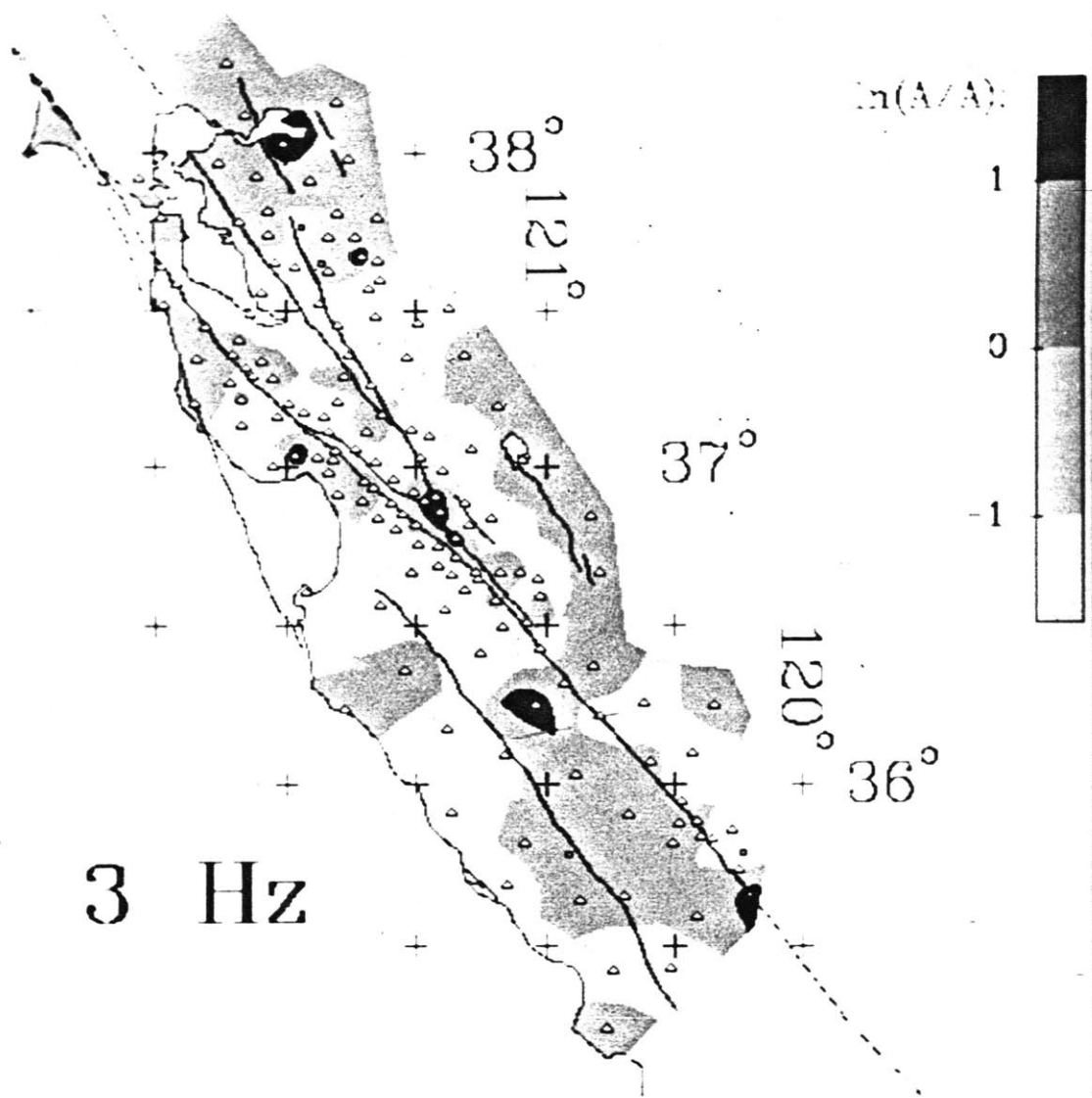
Figure 3.3b
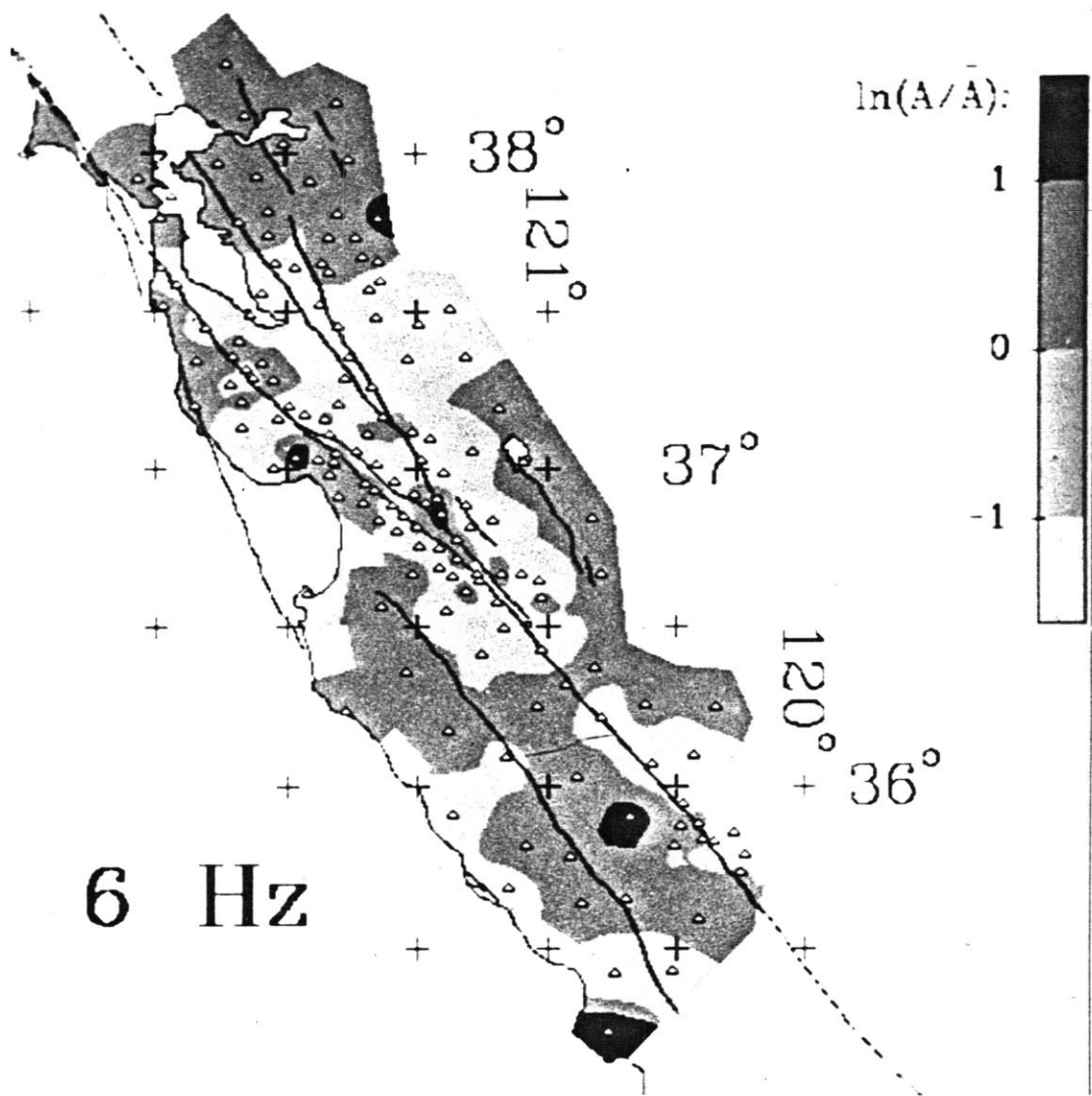
Figure 3.3c
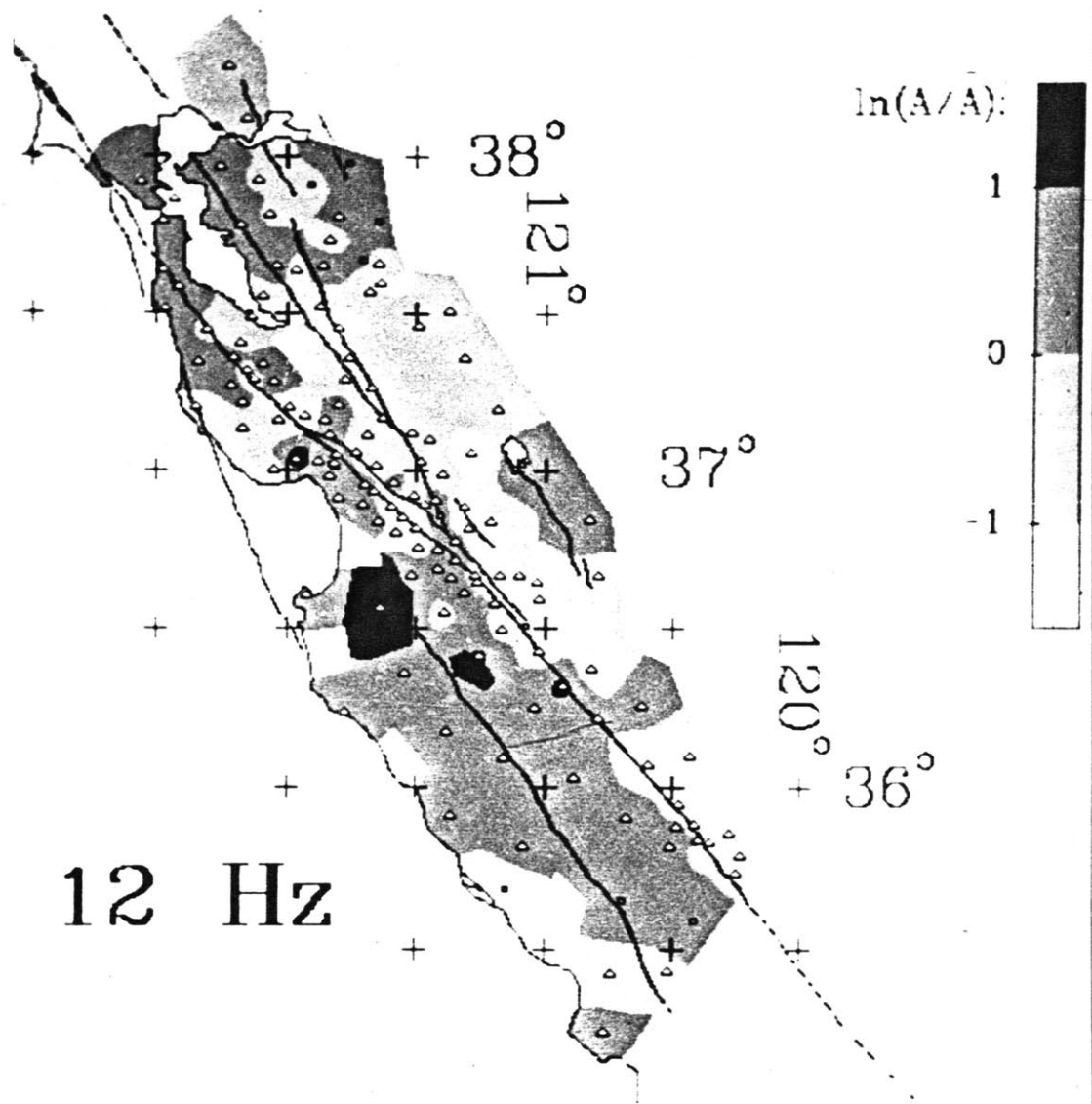
Figure 3.3d
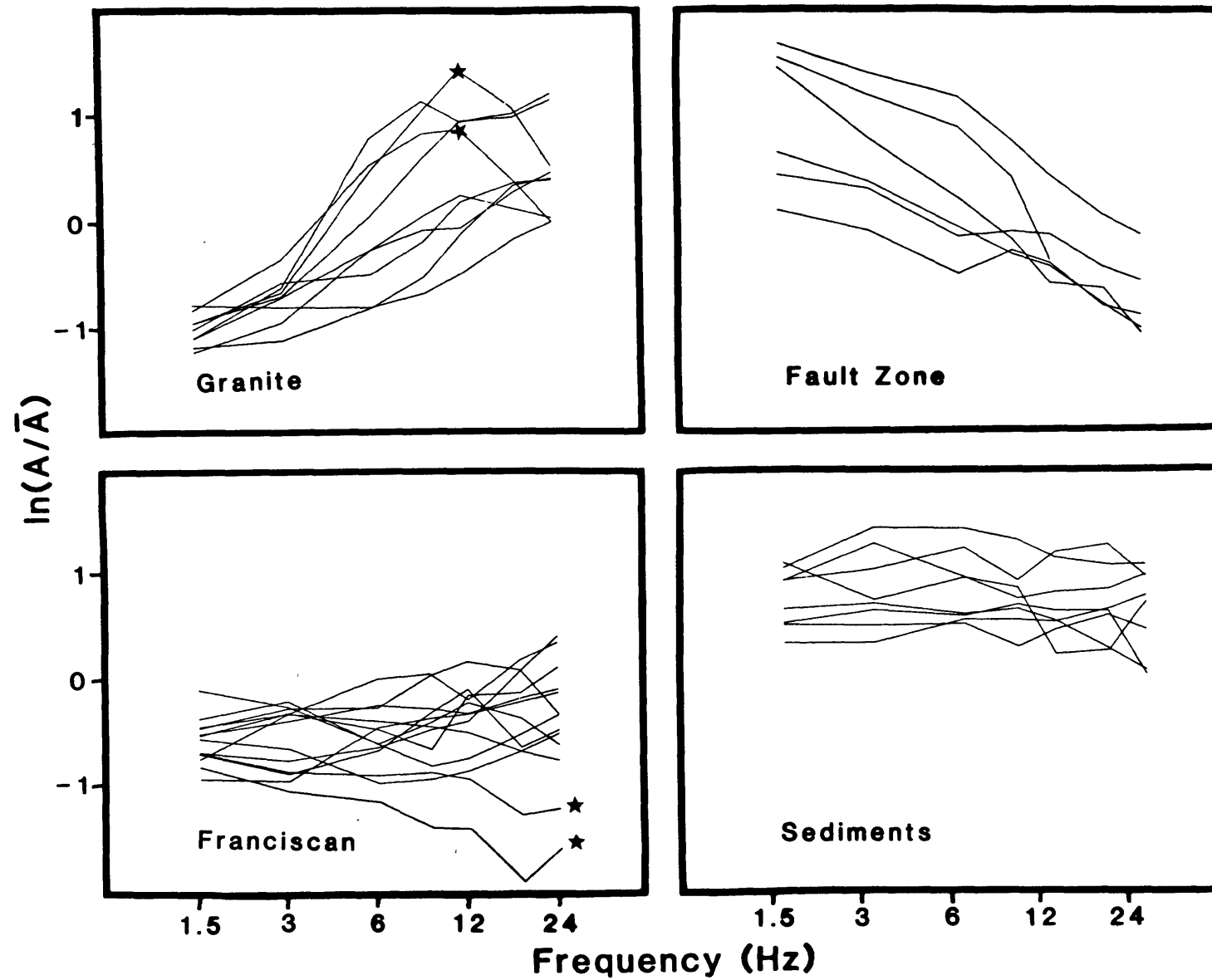
Figure 3.4
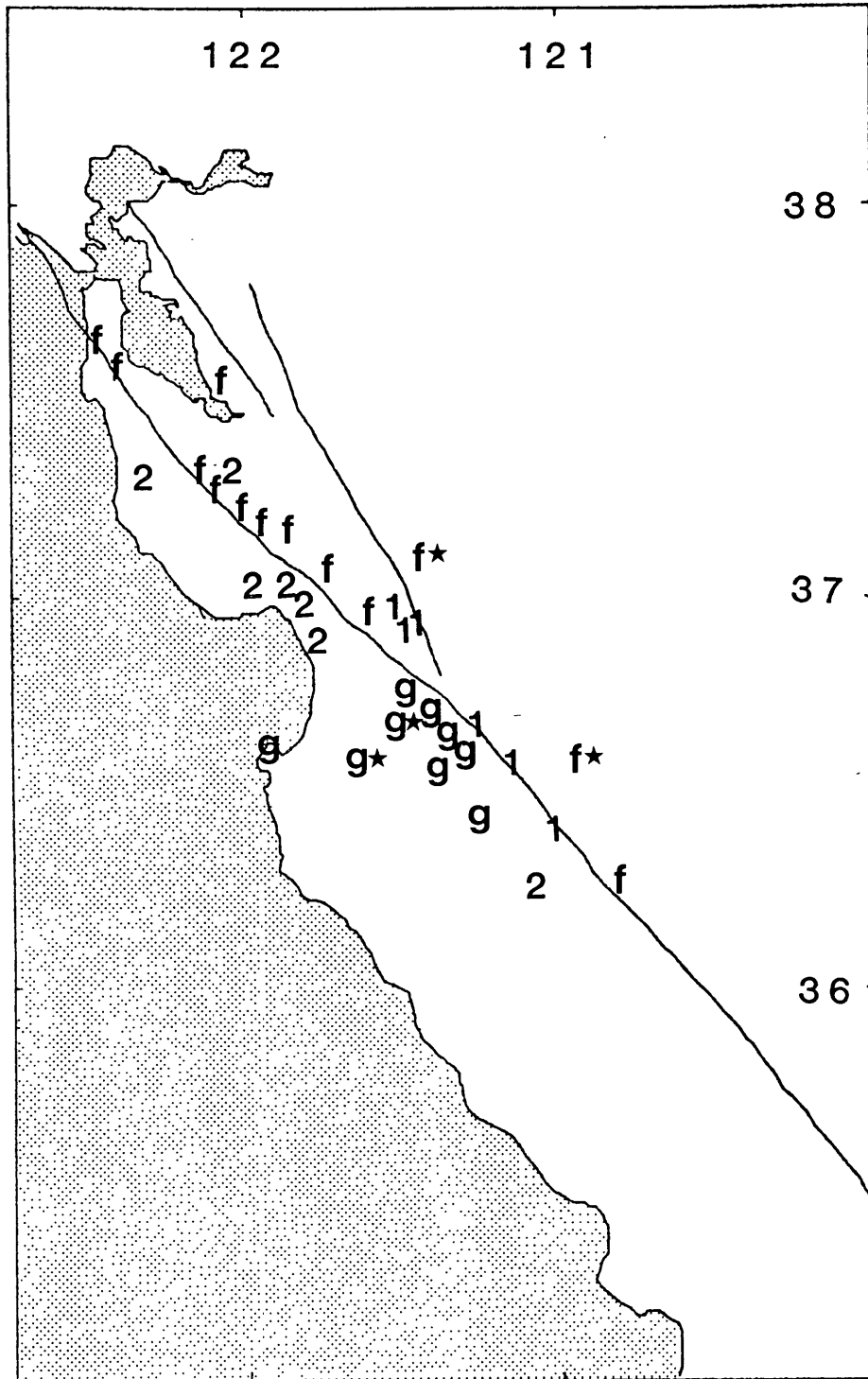
Figure 3.5
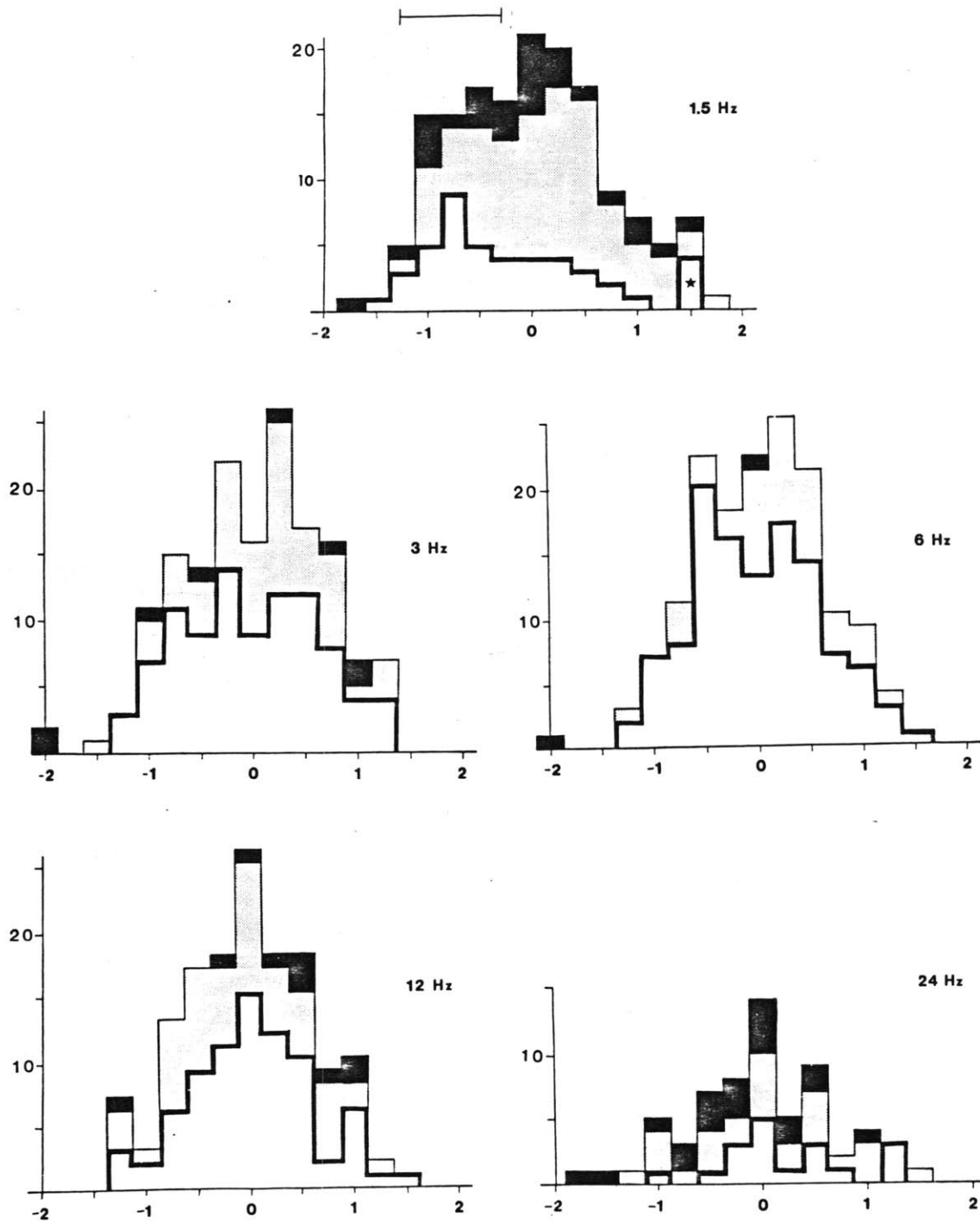
Figure 3.6
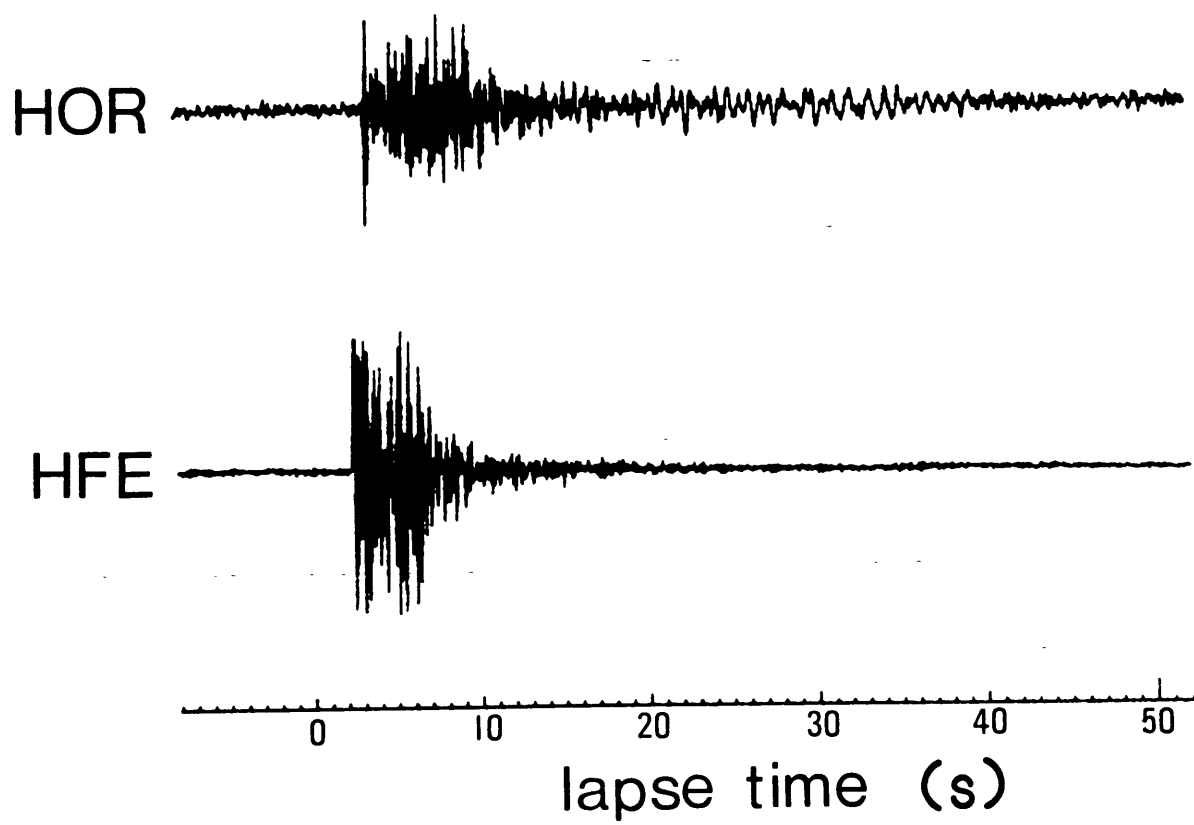
Figure 3.7

Chapter 4: <u>The Source Effect</u>

The high frequency energy radiated by a seismic source carries information about source processes, geometry and anelastic properties of the near source medium. Important observables that describe the shape of the source displacement spectra are the high and low frequency asymptotes, the corner frequency f_0, defined as the frequency at which the two asymptotes intersect, and f_{max}, which band limits acceleration spectra from above (Figure 4.1). Source dimensions are routinely inferred from the corner frequency, while a description of the non-elastic response of the faulted medium to the high stress of the crack tip can be inferred from f_{max} (Papageorgiou and Aki, 1983a, b), if f_{max} is not controlled by path or site effects, as suggested by Hanks (1982). Predictions of strong ground motion are based on estimates of the bandwidth of acceleration spectra which are bounded by f_0 and f_{max}. It is important, therefore, to understand the origin of f_{max}, whether it be due to the effect of source, path or site.

Unfortunately, high frequencies are profoundly affected by their passage through the extremely heterogeneous upper crust of the earth. Phenomena such as scattering and multipathing (interfering waves arriving along separate paths) make the implementation of propagation corrections difficult. Estimates of the path effect Q_β using direct

waves vary considerably. Measurements made at short distances ($\sim$ 10 km) can be explained by a low $Q_\beta \sim$ 75-100, independent of frequency. This was done by Bakun and Bufe (1975) who used spectral ratios of one large and many small events with the same epicenter. Assuming that the low frequency displacement spectrum of the small events is flat, the ratio removes the path effect from the large event for frequencies less than the corner frequencies of the small events. Correcting the observed high frequency roll-off of the large event to the roll-off of the ratio gives Q_β. Measurements of direct waves at larger distances, many using the S-to-coda method outlined in Chapter 2, yield a highly frequency dependent Q_β. Q_β can be as low as 100 at 1.5 Hz and as high as 1000 at 24 Hz. These observations are becoming quite common and will be reviewed in Chapter 5. Measurements have been made in California by Singh et al. (1982), Papageorgiou and Aki (1983a, b) and this study (Figure 5.14, Chapter 5). Singh et al. place a constant, low Q_β above 3.75 km, with a frequency dependent Q_β below. Since high frequencies (> 6 Hz) propagate much more efficiently at depth, the near site Q_β will be more important than the total path Q_β, especially at distances > 10 km. This idea is supported by the observation that pulse widths depend more strongly on the site than on the path in California (Reiter and Monfort, 1977). In light of the extreme variability of crustal Q_β, it is wrong to apply a constant Q correction in all situations.

Obviously, correcting for site and path effects is a difficult task in analyzing direct waves for source characteristics. I propose to use coda wave recordings to isolate the source from the propagation and site effects in much the same way as the site response calculations that were described in the previous chapter.

The use of coda to isolate source spectra is not new; Chouet et al. (1978) applied single scattering theory to isloate the source factors for events in California, Hawaii and Japan. The method used here (see Chapter 2) relies on less restrictive assumptions and incorporates a number of stations into the measurement. The beauty of the coda wave method is that the source-path-site separation is simple; restrictive source-receiver geometries do not have to be adhered to as in the direct wave case. Since the coda can be thought of as backscattered energy summed randomly, the multipathing problem ceases to exist, and scattering losses are contained in the path effect of coda waves which is constant for a given region. In addition, awkward azimuthal source radiation corrections can be ignored. Chouet et al. showed that coda wave estimates of source parameters such as corner frequency are very stable, and agree well with estimates using direct shear waves made in the same region.

In this chapter, aspects of the study of seismic sources that are pertinent to our study will be reviewed, followed by a presentation of results using CALNET data.

4.1 Far-Field Spectra of Seismic Sources

In order to study the seismic source, models must be created which will lead to the synthetic generation of the observable waveforms and spectra. This is achieved, as outlined by Aki and Richards (1980), using the elastodynamic representation theorem which allows the time varying elastic field to be uniquely determined from a description of the displacement discontinuity on a surface (in the absence of body forces and stress discontinuities). Inserting the Green's function for a homogeneous, isotropic medium of infinite extent, keeping only far-field terms, specializing to unidirectional rupture and employing an approximation equivalent to the Fraunhofer diffraction criteria leads to a simple formula for far-field spectra (Aki and Richards, Equation 14.14). A number of approaches are possible at this point. A wide range of models have been proposed; the earliest were based on primitive ideas of what the slip function should look like (Haskell, 1966), while later models have incorporated more dynamically realistic features. These models can be differentiated according to their predicted corner frequencies and high frequency asymptotes. Models are often categorized as ω-squared, ω-cubed, or intermediate depending on the slope of the high frequency fall-off. Aki (1967) showed that the ω-squared model best fits observations of spectral ratios of recordings sharing the same path, and also explains the M_s-m_b relationship. To match theory and data it was assumed

that earthquakes of all sizes are similar. This means that non-dimensional products of physical parameters involved in the fault process are independent of earthquake size which implies:

-final slip = D ~ linear fault dimension = L

-rupture velocity = constant since velocities of the medium are constant.

-seismic moment = M_0 ~ L^2D ~ L^3

-static stress drop = $\Delta\sigma$ = constant since total strain is constant (being non-dimensional)

-locus of moment vs. corner frequency has slope -3 on a log-log plot.

The similarity assumption is very restrictive, allowing only one free parameter to be fit to data. While the assumption works well for large events, it seems to break down when smaller events are considered. This may be expected as the source dimensions start to approach the inhomogeneity size of the earth medium surrounding the fault.

Aki (1980c) lists a number of observations of the violation of similarity, some for large events. Specifically, violations occur in instances where the measured stress drop is observed to increase with source size. Chouet et al. (1978) noted many deviations of the moment-corner frequency locus from its predicted form in a world-wide study. Their results from central California show that magnitude 4 and 5 events share similar corner

frequencies, while the larger events exhibit more rapidly decaying high frequency behavior. This is interpreted by Aki (1980c) in terms of a fault with barriers. Das and Aki (1977) used a finite difference simulation to show that a rupture could skip a region of high strength, producing a smaller amount of integrated slip, and slower high frequency spectral decay, than the case in which the rupture passes cleanly along the fault length. Thus, earthquakes of different magnitudes can have similar dimension, or corner frequency, while the larger of the two exhibits a higher rate of spectral decay at high frequencies as observed by Chouet et al. (1978).

The discovery of the importance of fault heterogeneity on observed waveforms and spectra has resulted in a suite of source models consisting of sums of smaller events. Papageorgiou and Aki (1983a, b) have constructed such a model that also incorporates non-elastic effects at the crack tip. This results in a less "δ-like" stopping phase, and rapid high-frequency spectral decay to which f_{max} is attributed. f_{max} is most readily observable in acceleration spectra, of which it is the upper band limit, but it also can be found in the displacement spectra of small earthquakes as the "limiting corner frequency." Alternatively, Hanks (1982) attributes f_{max} to the site effect, demonstrating a strong variation in f_{max} between sediment and hard rock sites near Oroville. Even from the high quality Oroville data, f_{max} seems difficult to choose

(see Hanks' Figures 4 and 5), however, the fairly large
number of observations lend credibility to Hanks'
conclusion. But the observation of a limiting corner
frequency for magnitude 1-2 events by Chouet et al. (1978)
should not be influenced by the site effect. We seek to
shed more light on this controversy in the next section.

4.2 Results and Discussion

We wish to see if the coda method can help to resolve
some of the controversies concerning source radiation at
high frequencies. The earthquakes used in this study have
duration magnitudes centered around 1.8 and 2.8. The
smaller events are measured at up to 10 stations each, while
the larger events are measured at up to 50 stations each,
which should provide sufficient redundancy. The large
events yield fewer high-frequency measurements, while small
events yield fewer low-frequency measurements. The
assumptions necessary to perform the source calculation are
fairly non-restrictive. It is required that the coda shape
be the same for all sources at a given station. Variations
between stations are allowed. It has been noted
(Chapters 3, 5) that coda decay does vary from station to
station; the most significant differences are found at
sediment sites, such as those near Hollister. These
stations can be included in the calculation unless their
coda shapes also depend on source distance or depth which
would be the case if the coda was dominated by energy from

trapped modes excited by direct body or surface waves. Unfortunately, this problem was not resolvable with the current data set.

As described in Chapter 2, the results will be expressed relative to the "average" source. This may be confusing since the plots will not look like traditional source scaling-law plots. To overcome this difficulty the results will be simulated using various forms of the scaling law. Eventually, results such as these should be rectified by making direct determinations of the source spectra for a number of small events near the best stations in the network in the manner of Chouet et al. (1978).

Results of the source regression are shown in Figure 4.2. Only those events for which a full complement of frequencies were measured are included. Standard errors of the results for the large events are less than 0.05 for 1 - 12 Hz, and near 0.1 for 24 Hz; for small events, near 0.1 at 1.5 Hz, and less than 0.1 for 3 - 24 Hz.

The results can be examined for evidence of variable near source Q, or more precisely, near source δx^* (see Section 3.3.2). Below the corner frequency the source spectrum is expected to be flat, deviations can be explained by near source medium variability. The corner frequencies of the small set of events (B) should not be much less than 12 Hz (see Chouet et al. 1978); the results from these events indicate that δx^* does exist, yet the source results do not show nearly the variation seen in the site results

from the previous chapter (Figure 3.4). This is due to the additional effects of impedance and resonance on the site measurement, as well as a wide range of near site δx^*. The set of small events is appropriate for checking the near source δx^* since most events were chosen randomly over a long segment of the San Andreas fault. It is concluded that medium properties as expressed by δx^* show stronger variation with position on the earth's surface than with position along the fault plane.

Simulated results are shown in Figure 4.3a, b for the ω-squared and ω-cubed models, assuming similarity. The simulation was obtained from the far-field displacement spectra given by Aki and Richards (1980):

$$\Omega(\omega) = \frac{\Omega(o)}{[1 + (\omega/\omega_0)^2]}$$

for the ω-squared model, and:

$$\Omega(\omega) = \frac{\Omega(o)}{[1 + (\omega/\omega_0)^2]^{3/2}}$$

for the ω-cubed model, where $\Omega(o)$ is proportional to the seismic moment M_0. The moment-magnitude relation found by Bakun and Bufe (1975) for central California was used:

$$\log_{10}(M_0) = (16.2 \pm 0.1) + (1.52 \pm 0.05)M_L$$

assuming M_L is accurately given by the routinely measured

coda duration magnitude. The assumption of similarity leaves one free parameter which was fixed by taking the corner frequency of a magnitude 3 event equal to 4 Hz, as found by Chouet et al. (1978) for Bear Valley, California.

Taken together, the coda source results more closely match the ω-squared model; this is especially true for the group of smaller events, while the large events exhibit a faster high frequency roll-off. We choose to look at the small events in more detail. When they are split up into two groups, representing events spread along the San Andreas and those concentrated in the Coyote Lake region of the Calaveras fault, a different pattern emerges (Figure 4.4a, b). The San Andreas events (b) more closely match the ω-squared law while the Coyote Lake events (a) seem to exhibit a constant shape. This is not a strong result, since the magnitude range for the Coyote Lake events is quite narrow, and the expected corner frequency is close to our upper band limit. But if there is a constant corner frequency among these events, as indicated by a comparison with simulated results, it can be concluded that the limiting corner frequency, or the inferred f_{max}, is a local fault zone property, and can be found in spite of possible complications due to the site. If the limiting corner frequency is a localized effect, we cannot expect to find it in the set of events spread over 300 km of the San Andreas fault. This is consistent with local trends of increasing (inferred) stress drop with increasing moment, found in the

compilation of Hanks (1977), as noted by Aki (1980c). It is imperative that more data be analyzed from the Coyote Lake region and other areas in order to determine the validity of the constant corner frequency result.

Returning to the larger events, we note that their observed high frequency decay is much more rapid than expected from the ω-squared model. Standard errors of the results are typically 0.1 at high frequencies for these events so this observation is significant. Chouet et al. (1978) make a similar observation at Bear Valley, but for magnitude 5 events rather than magnitude 3 as is seen here. Aki (1980c) interpreted the Bear Valley magnitude 5 result in terms of a fault with barriers as described in the preceding section. It is generally thought that steep high frequency asymptotes indicate a smaller contribution from the stopping phase of earthquake motion, which in turn may be related to the distribution of strength (resistance to slip) along a fault. We have demonstrated that our method gives very stable estimates of the high frequency spectral decay which may be used effectively to study the relationship between fault heterogeneity and source spectra, both in a spatial and temporal sense.

4.3 Conclusions

We have used coda waves and non-restrictive assumptions to calculate source spectra for over 90 micro-earthquakes in central California. Although the data set is not ideal for

a study of this nature, initial results promise great potential for future work. It is found that:

1) Anelastic properties as expressed by δx^* exhibit a stronger variation across the earth's surface than along a fault zone at depth. Yet, near source δx^* does exist; attempts to map this quantity should be carried out.

2) Spectra from micro-earthquakes in the Coyote Lake area of the Calaveras fault have similar shapes. This is taken as an indication of the existence of a limiting corner frequency that is independent of the site effect, as found by Chouet et al. (1978). The result presented here is not strong since only a narrow range of magnitudes was used, and the expected corner frequencies lie near the high end of our band. Further study using a more appropriate set of events should yield very interesting results.

3) Spectra from magnitude 3 events roll-off faster than expected from the ω-squared model. Hanks (1979) has proposed that high frequency spectral decay is related to fault stress inhomogeneity along with other observables such as b-value. The method presented here gives very stable estimates of high frequency source radiation and may be used in conjunction with other studies to investigate the inhomogeneous nature of fault zones.

Figure Captions

Figure 4.1:

Displacement of (u) and acceleration (a) for the ω-square model. Dotted line indicates the locus of corner frequencies under the similarity assumption.

Figure 4.2:

Results of source effect regression. Events are grouped by A) magnitudes 2.7 - 3.0, B) magnitudes 1.4 - 2.1.

Figure 4.3:

Simulation of the source effect results under the similarity assumption for a) the ω-squared model, b) the ω-cubed model.

Figure 4.4:

Actual results and their simulation under the similarity assumption for the ω-squared model for a) events from the Coyote Lake area of the Calaveras fault, b) events from the San Andreas fault. See Figure 2.7 for locations.
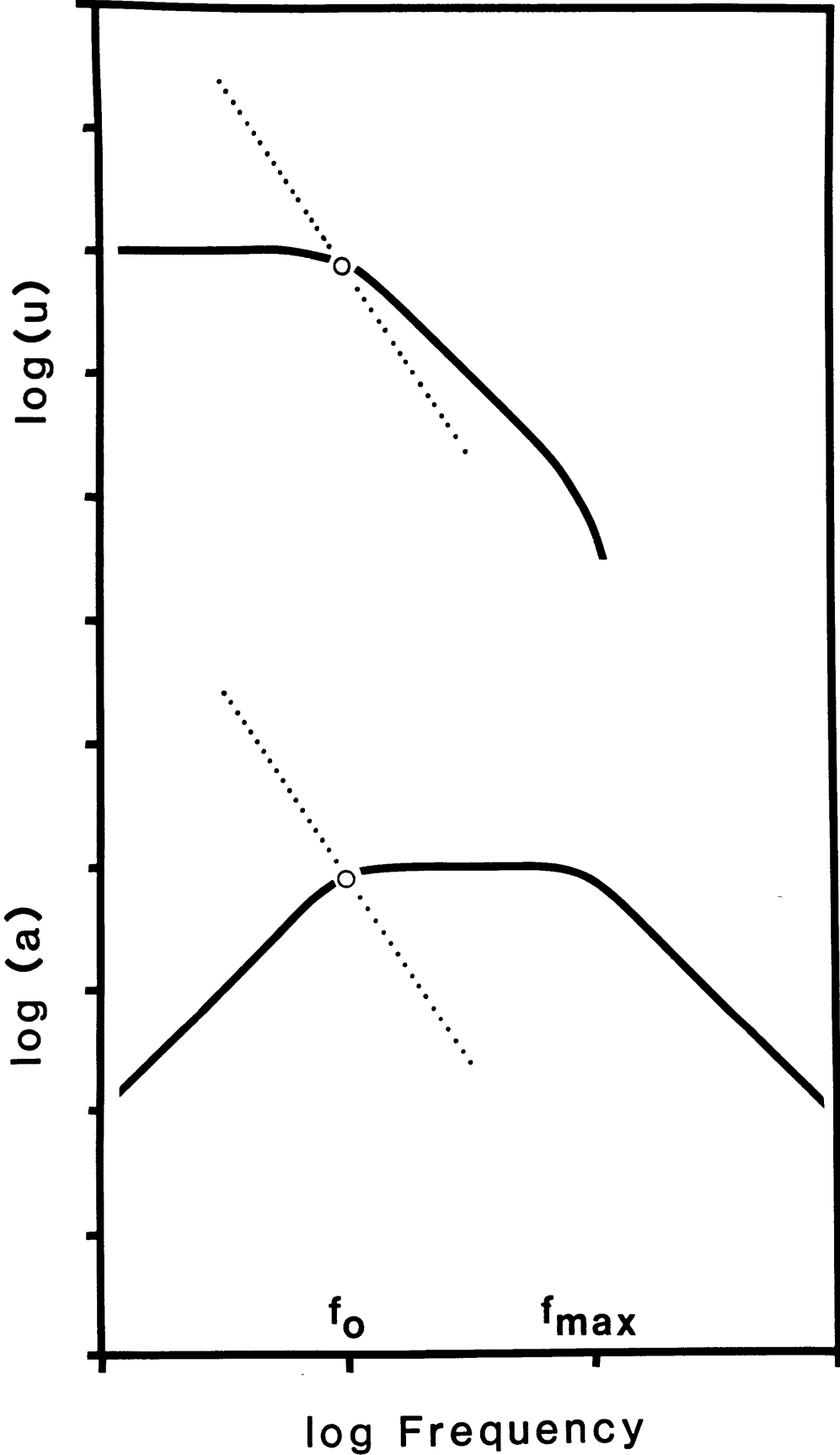
Figure 4.1
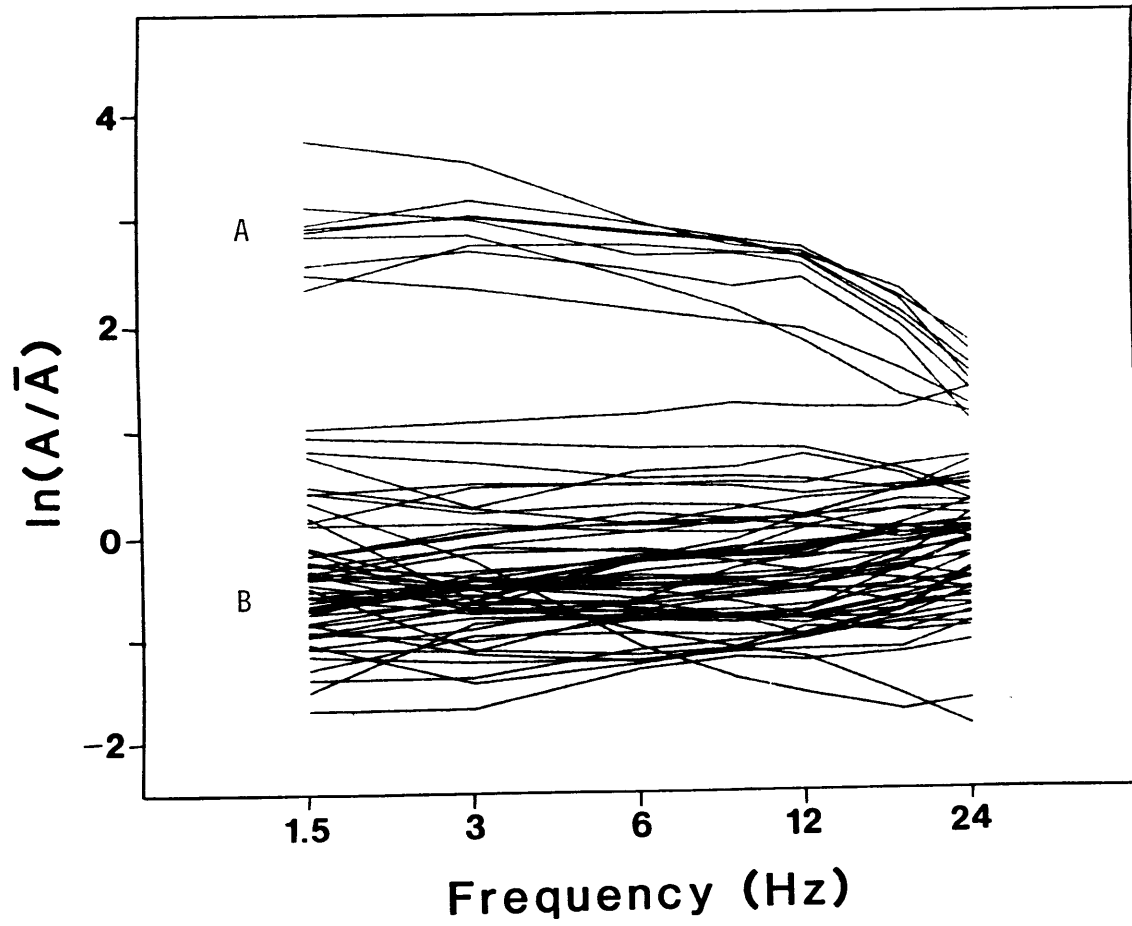
Figure 4.2
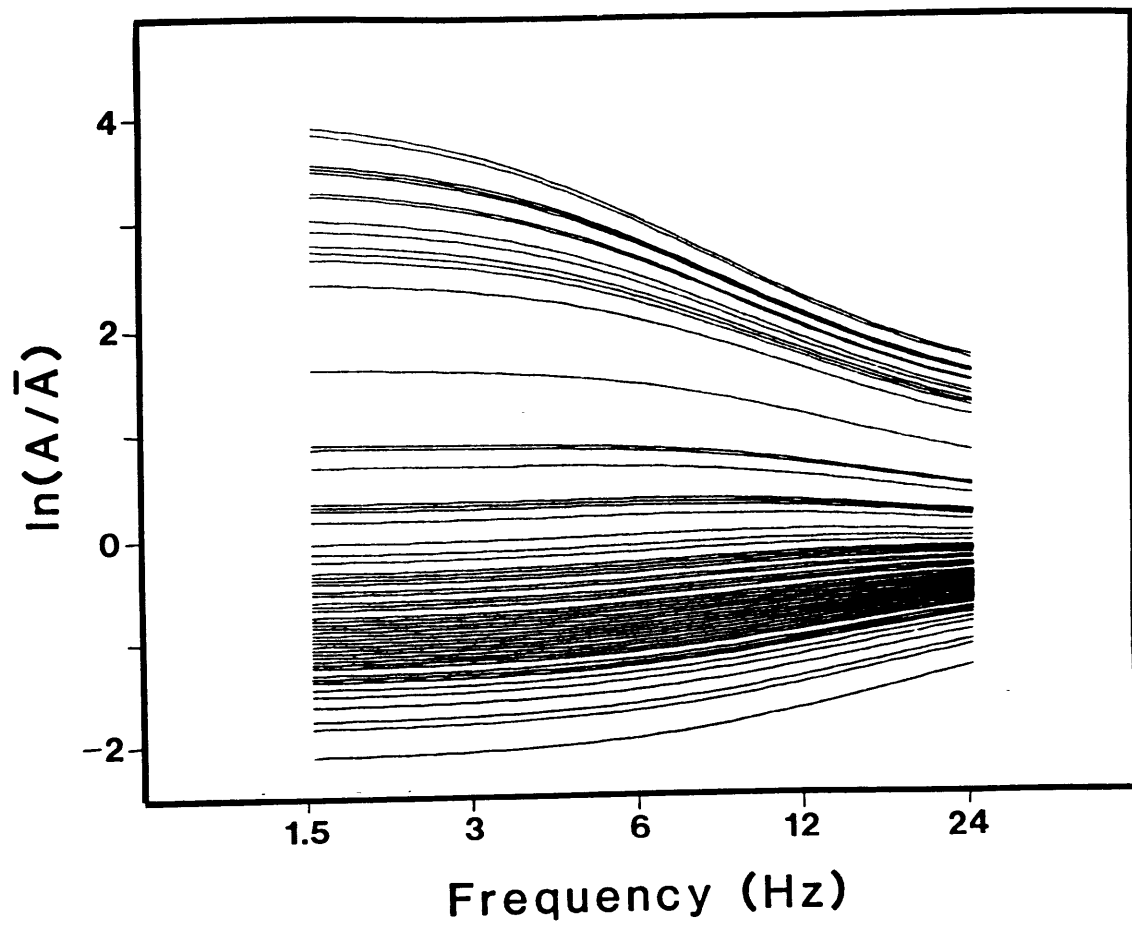
Figure 4.3a
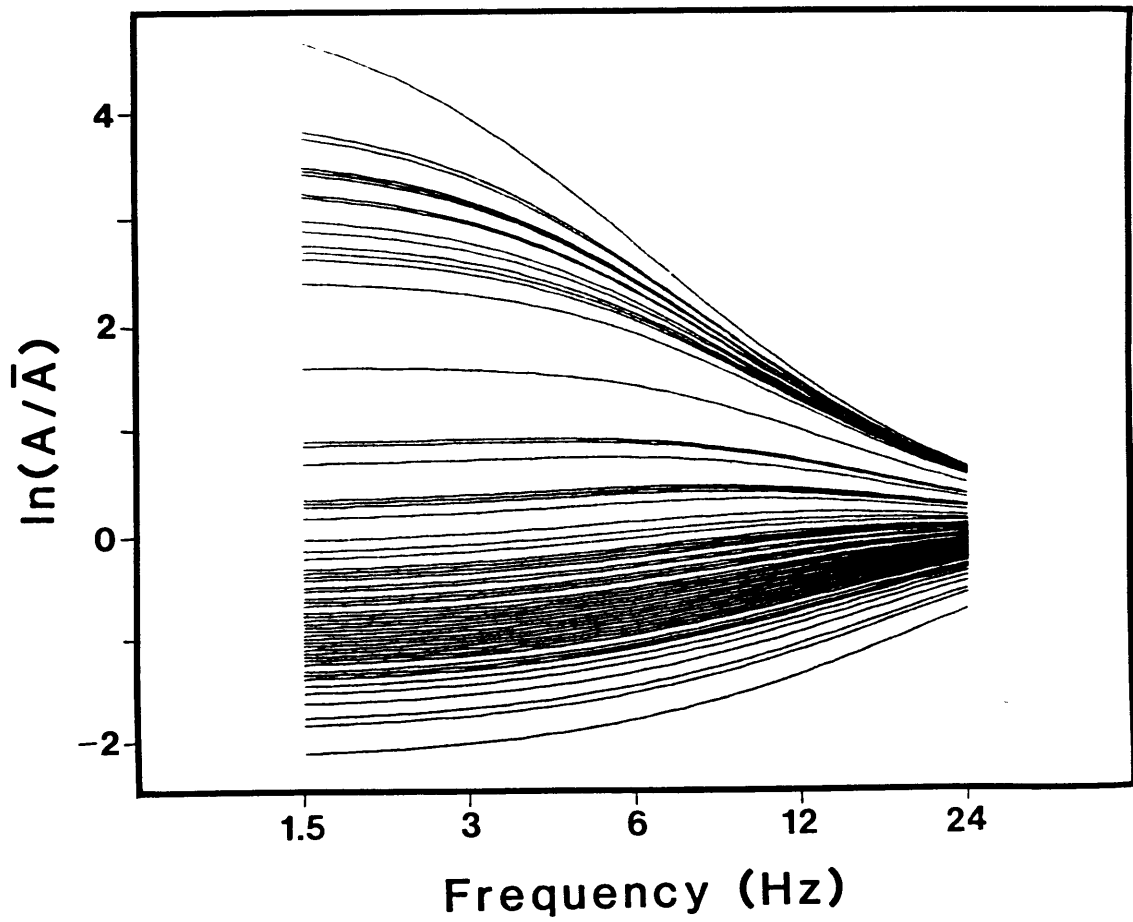
Figure 4.3b

Figure 4.4a

128
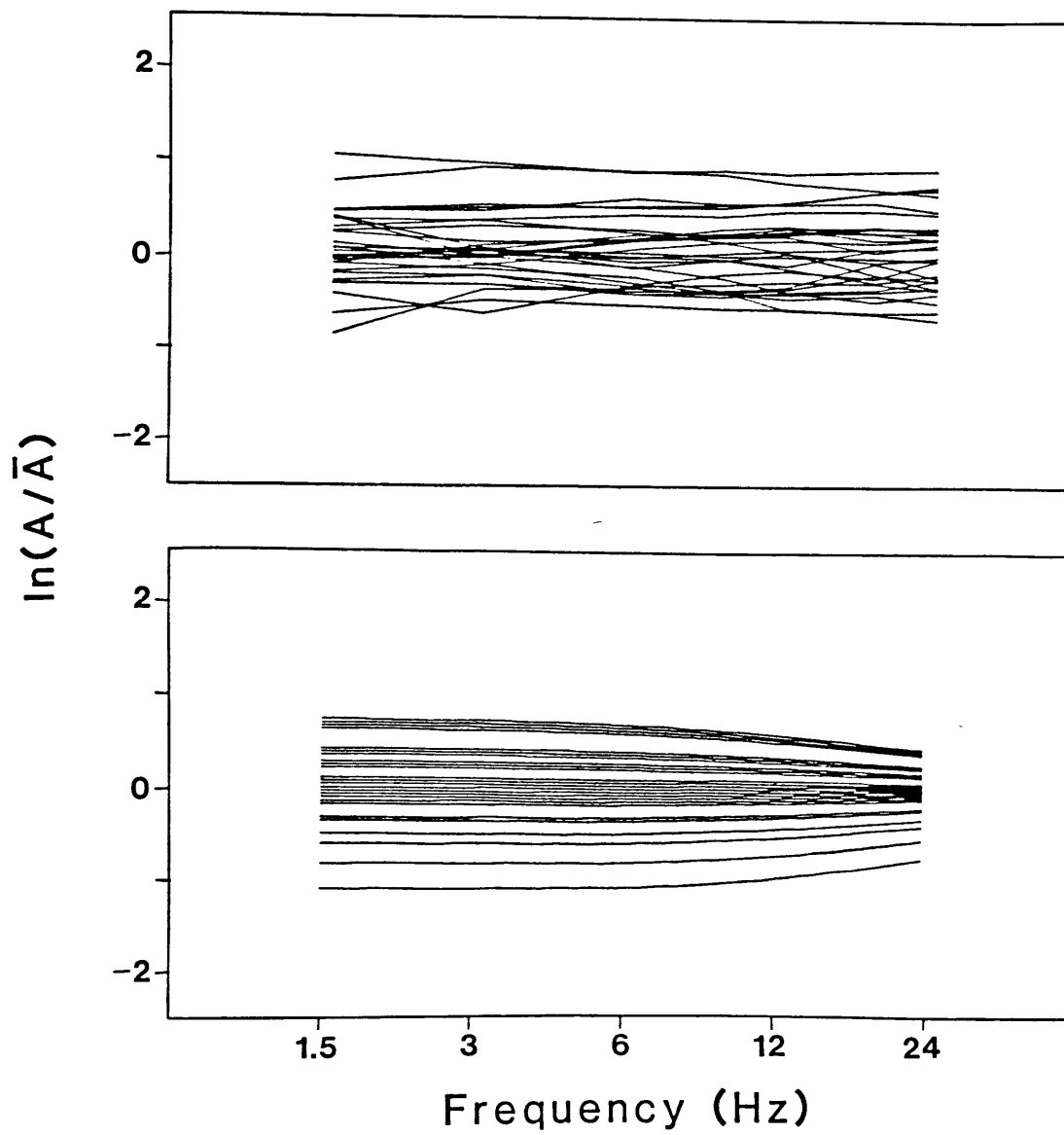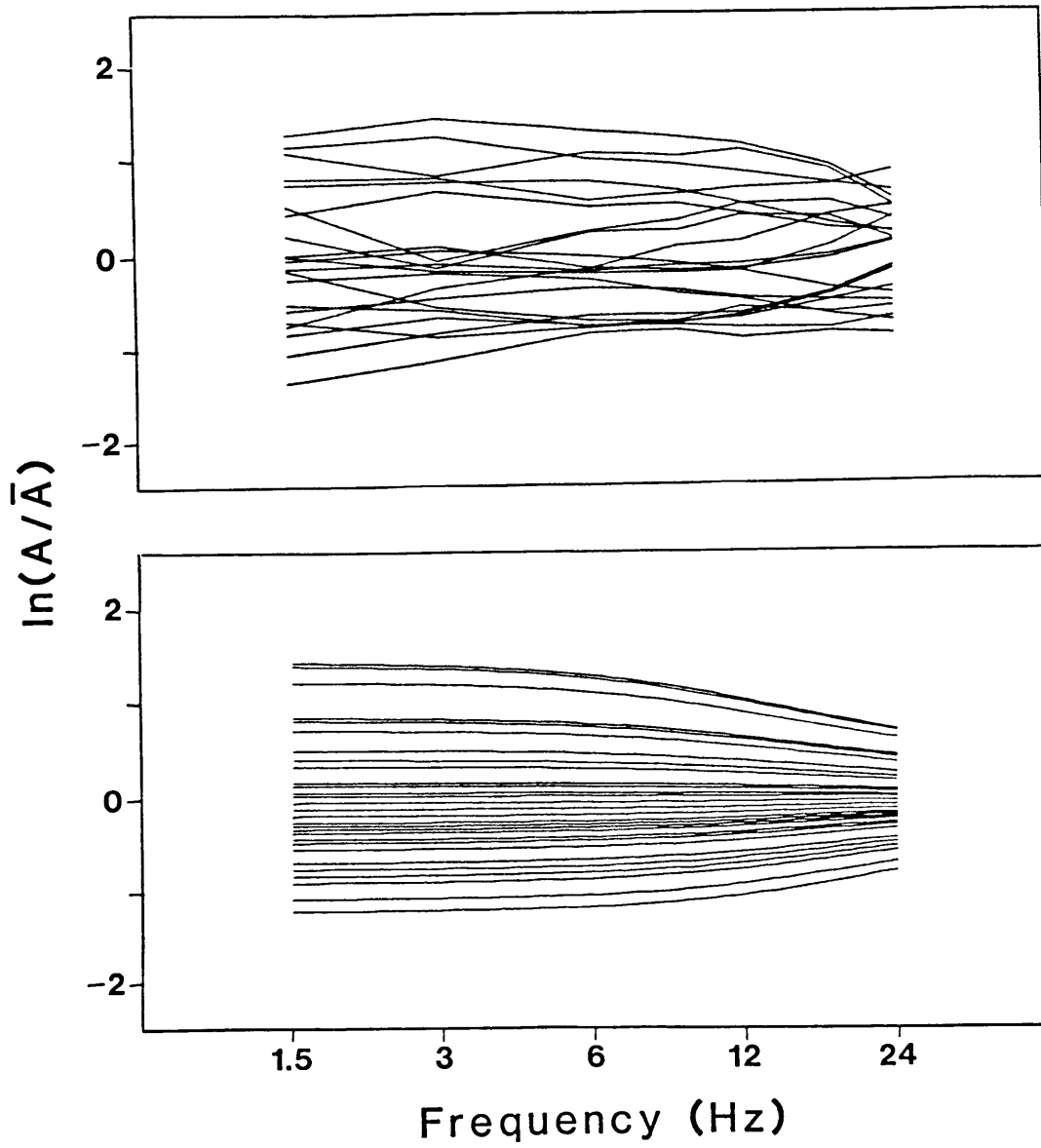
Figure 4.4b

Chapter 5: <u>THE PATH EFFECT</u>

The coda carries information about the medium through which the coda energy has travelled, in addition to information about source and site characteristics. In order to estimate the medium effect or Q_c, a specific model of the propagation of coda waves is needed. In this chapter we will briefly review previous work on coda decay, mentioning simple models, observations of Q_c and the equivalence noted between Q_c and Q_β. Measurements using the CALNET array will then be discussed, including an exhaustive search for the factors upon which Q_c depends.

5.1 <u>Review of Observations of Coda Q</u>

The steadily increasing availability of spectral analyzer and digital data has allowed the measurement of Q_c in many parts of the world. In the following, specific coda models and the agreement found between Q_c and Q_β will be briefly discussed, along with the observed dependence of Q_c on frequency, tectonic environment, lapse time (due to enlarging volume sampled) and origin time (due to temporal fluctuations in the earth medium). A useful compilation of measurements can be found in Wu (1984).

5.1.1 <u>Specific Coda Models</u>

In order to study the propagation effects on the seismic energy comprising the coda we need to create a model

of its generation. The simplest models assume randomly located inhomogeneities and isotropic source and scatterers. Aki and Chouet (1975) considered single backscattered (weak scattering) surface and body waves, as well as the diffusion (strong scattering) of body waves for coincident source and receiver. Their results have a simple form (Equation 2.3, Chapter 2) containing Q_c, a spreading constant (α) and source and medium scattering strengths as variables. Comparison with data revealed that α could not be constrained well. Values of α representing 2 and 3-D spreading were then fixed, which only slightly influenced the determination of Q_c. The variation of Q_c between different regions was found to be much stronger than variations induced by changing α.

The body wave single scattering model was extended by Sato (1977a) who retained all the above assumptions except that the source and receiver were allowed to move apart. He obtained:

$$P(\omega,t) = |S(\omega)|^2 \, K(\alpha) \exp -\omega t / Q_c$$

$$K(\alpha) = \frac{1}{\alpha} \ln \left(\frac{\alpha+1}{\alpha-1} \right)$$

$$\alpha = t/t_s$$

where t_s is the travel time of S waves and $S(\omega)$ contains source and scattering terms and assorted constants. This result coincides with the model of Aki and Chouet for $t > 2t_s$. The Sato model is used in this study, since occasional data

are collected at lapse times less than $2t_s$, but tests using both models have yielded equivalent results. Further extensions of the body wave backscattering model by Sato have included the effects of wave conversions (1977b) and non-isotropic source and scatterer (1982b, 1984), the latter containing numerical results for three components. Gao et al. (1983) have attempted to extend the scalar wave calculation to include multiple scattering. Fine-tuning the coda model should not drastically affect measured Q_c values, so in practice we use the simplest models.

5.1.2 Factors Influencing Q_c

The earliest measurements of Q_c using spectral analyzer data revealed a striking dependence on frequency. This has been reenforced by many observations worldwide. Q_c is observed to increase with frequency between 1.5 and 24 Hz, roughly following an f^N law. The frequency dependence expressed by the factor N varies from region to region in such a way that Q_c converges at high frequencies. The factor N seems to be dependent on the tectonic environment, varying between 0.8 in California and Japan (Aki and Chouet, 1975) and the Hindu Kush (Roecker et al., 1982) to less than 0.5 in the Eastern U.S. (Pulli and Aki, 1981).

Q_c has also been noticed to increase with lapse time, or effective volume sampled by the coda (Tsujiura, 1978; Roecker et al., 1982; Pulli, 1984; this study, Figure 5.1). This has been attributed to an increase in Q_β with depth

which could be due to closure of cracks and the inability of the mantle to support sharply defined inhomogeneities if Q_β is dominated by scattering in the range 1-24 Hz. The presence of multiply scattered waves late in the coda will also cause Q_c to increase with lapse time (Gao et al., 1983). The variation of $Q_c(f)$ with lapse time is almost as large as its variation between regions. This means that care must be taken in comparison of results from different studies; the lapse time effect must be taken into account.

In addition to the strong and widely observed influences of frequency, tectonic environment and lapse time, coda Q_c has also been noticed to depend on origin time. These observations are not common, yet they receive much attention since they indicate changes in the earth medium. Monitoring these changes in Q_c could be helpful as an earthquake prediction tool. Chouet (1979) first noticed temporal changes in Q_c in a data set that spanned one year from Stone Canyon, California. Q_c decreased gradually throughout the year; striking changes in the coda decay could be seen in the raw data, especially at high frequency (24 Hz). Dependence on magnitude and location was ruled out, as were the effects of rainfall and instrument problems. Aki (1980b) noticed that the frequency dependence of this variation of Q_c with time was very similar to that of the variation from region to region; both were attributed to variations in the heterogeneity of the earth under the assumption that scattering is primarily responsible for

attenuation.

The search for more evidence of temporal fluctuation of Q_c is ongoing. Fehler (1979) noticed changes in coda envelopes associated with pressurization of a Hot Dry Rock reservoir. Wyss (1983) measured velocity changes and noted corresponding changes in the coda decay associated with a magnitude 7.2 Hawaiian earthquake. This work is interesting because geodetic measurements are available for this area. Changes in seismicity in South Carolina were correlated with coda envelope fluctuations by Rhea (1984), however this study was based on a small amount of data. Other tantalizing work remains unpublished (e.g., Jin, pers. comm.).

5.1.3 Relation Between Q_c and Q_β

One of the most interesting developments in the study of coda waves has been the discovery that the quality factors of coda and of S waves are very similar. Perhaps inspired by a study by Fedotov and Boldyrev (1968) who found a frequency dependent Q_β in the Kuril Islands, and the knowledge of a frequency dependent Q_c, Aki (1980a) used the S to coda method (see Chapter 2) to calculate Q_β in the Kanto region, Japan. He found that Q_c and Q_β correspond within error bounds for frequency $>$ 3 Hz. The difference at 1.5 Hz has been attributed to the different volumes sampled by the direct and coda waves (Aki, 1981). Evidence from the work of Rautain and Khalturin (1978) and Herrmann (1980)

support this observation. More recently Roecker et al.
(1982) noted similarities between Q_β and the Q_c representing
shallow portions of the earth's lithosphere in the Hindu
Kush. These observations are important since they support
the assumption that the coda is composed of back scattered
shear waves. The frequency dependence of Q_β, and thus Q_c,
coupled with much lower frequency Q measurements using
surface waves suggests that Q_β has a minimum at some
frequency less than 1 Hz. This minimum is especially
pronounced in regions of high tectonic "activity." Aki
(1980b) believes that this is due to loss by scattering, and
gives additional evidence in support of this interpretation.
Sato (1982a) showed that a wide range of scalar random media
models could account for the implied variation of Q_β with
frequency. Such a model is described by its autocorrelation
which is parameterized by its rms velocity fluctuation, and
correlation distance, with an exponential, gaussian or
intermediate (Von Kharman) shape. Wu (1982a,b) has
completed similar calculations, including energy scattered
into the forward half-space as transmitted energy, compared
with 29° forward cone implicit in Sato's calculation.
Unfortunately, the backscattering coefficient calculated for
these random media models does not match that estimated from
the amplitude of coda waves. Better agreement was obtained
by extending these calculations to vector waves (Sato,
1984). Ongoing work includes low frequency (< 1 Hz)
measurements of Q_β using L_g (Patton, 1983) and Q_c (this

study, section 5.2.1.B). Attempts to separate intrinsic and scattering attenuation have led to the preliminary conclusion that scattering may not be as important as originally thought (Gao, 1984; Wu, 1984).

5.2 Measurements of Coda Q Using CALNET Data

The high station density and expanse of the CALNET offers an opportunity to measure coda decay on a previously unrealized scale. Objectives are to search for the factors that influence Q_c, including spatial and temporal effects, and to confirm the basic assumption that coda decay is independent of path as expected from the back scattering model. In addition, the comparison between Q_c and Q_β calculated using a fairly small number of direct S waves will be discussed.

5.2.1 Variations of Q_c in California

A) Lapse Time Effects

As seen by many previous workers, Q_c is observed to be heavily dependent on lapse time, or the volume of the earth's lithosphere that the coda samples. Figure 5.1 shows measurements taken at three lapse times: 1) magnitude 1-2 events measured between 5 and 30 s, 2) magnitude 2-3 events measured between 20 and 100 s, and 3) the magnitude 5.9 Coyote Lake earthquake measured on low gain vertical and horizontal components between 100 and 300 s. Also included in the figure is a rough envelope representing the

compilation of Q_c measurements from Wu (1984).

Much has been made of the variation in Q_c between areas of different tectonic "activity," however, the varation with lapse time is just as large, if not larger. Our Q_c measurements from central California easily span one-half of the envelope of measurements. Perhaps even higher Q could be measured beyond 300 s lapse time as found by Rautian and Khalturin (1978) who made measurements up to 1000 s in tectonically active Tadjikistan. Close scrutiny of Wu's compilation reveals that the lowest Q_c measurements were made using small, nearby sources (Roecker et al., 1982; Rovelli, 1982), while the highest Q_c measurements were made using larger, far away events (Pulli, 1984). Pulli also measured a few nearby events at short lapse times (less than 100 s), finding a dramatic decrease in Q_c for New England. The point of this discussion is that although Q_c is dependent on region or tectonic environment, this dependence is tempered by the lapse time effect. The regional effect seems stronger than it actually is since crustal Q_c has been measured more often in tectonically active environments where small nearby events are common, while Q_c measurements in inactive regions must rely heavily on more distant events.

B) Low Frequency

The Coyote Lake earthquake has been examined in order to look at low frequency coda decay. Measurements of Q_c at

frequencies less than 0.75 Hz are not common, which is
unfortunate since Q^{-1} of shear waves has been postulated to
peak somewhere near 0.5 Hz (Aki, 1980b). Identification of
this peak will help to constrain the parameters of models
such as scattering that attempt to explain Q_β. Of course Q_c
and Q_β have not been shown to coincide at these low
frequencies, and the modal composition of the coda is an
open question. But whether the coda contains backscattered
S or surface wave energy, Q_β should be reflected by Q_c in
some manner. Figure 5.2 shows the results of the Coyote
Lake earthquake work, plotted along with other low frequency
observations. Q_c^{-1} appears to level off at low frequencies,
and even begin to turn over, forming a peak about
0.3-0.4 Hz. The peak is not significant owing to the large
standard error associated with the 0.2 Hz measurement. The
error increases at lower frequencies as the 1 Hz instruments
are pushed to their limit. The Q_c shown is for single
scattered body waves; assuming the coda is composed of
surface waves flattens the peak. In either case the
leveling off of Q_c^{-1} at frequencies less than 0.75 Hz for
lapse times 100-300 s can be considered well established in
California.

C) Regional Variations in Short Lapse Time Data

After assigning separate values of Q_c to different
groups of data based on lapse time, we wish to see whether
or not there is any further unexplained variation in coda

decay. To do this, residual variances are compared for data fit by constant Q_c, and a Q_c that is free to change for each record. Data from large events (mag. 2-3) and small events (mag. 1-2) are treated separately. Results of this comparison (Table 5.1) show that the residual variance only changes slightly for large events, while the difference for small events is more substantial. This is interpreted to mean that the codas from the large events do not show much systematic variation, as a constant Q_c describes them well. This is expected from the backscattering model since later arriving coda energy will have sampled a good portion of the total study area. The coda from the smaller events will have sampled a much smaller volume (approximately a half-sphere of radius 30 km) so there is room for variation across the array. Data were grouped by geographical area, geology, source, station, distance, depth, and azimuth with respect to the structural trend in order to discover any systematic variation in Q_c.

The largest variations in short lapse time Q_c were found to correlate with geographical area or geology. The data were divided up according to where the center point of each source-receiver pair fell as shown in Figure 5.3. The most stable measurements come from areas 2 and 3, representing crust associated with the Franciscan, and areas 4 and 5, representing the crust under the Gabilan granites; these results are shown in Figure 5.4 along with Q_c from the large events. These measurements represent a crustal

average. Shear waves travelling for 20 seconds will have time to penetrate approximately 30 km before returning to the surface. Crustal thickness in this area is about 24 km in the Gabilans and 30 km in the Diablo range (Walter and Mooney, 1982). The Q_c is insensitive to shallow crustal differences. Wesson et al. (1973) and Mooney and Luetgart (1982) show that the Franciscan in the Santa Cruz Mountains (our area 2) contains a shallow high velocity body, thought to be greenstone. The effect of this structure is seen in our site effect measurements at high frequency, but no difference in Q_c is observed between area 2 and area 3 in the Diablo range.

The difference between granite and Franciscan crustal Q_c is striking. At low frequencies the two measurements are very similar, while quite different from the longer lapse time results. At high frequencies the measurements diverge; a factor of 2 difference is observed at 24 Hz. The granite curve merges with that for longer lapse times at 12 and 24 Hz. This is curious since it indicates that high frequency shear waves propagate just as efficiently in the crust of the Salinian block as they do at greater depths. Walter and Mooney (1982) believe that the Salinian block crust is made up of granite and the gneiss into which the granite intruded. Only slight velocity changes are observed indicating that the crust is fairly homogeneous on a large scale. The Diablo range crust is thought to be composed of Franciscan meta-graywacke with gabbroic material at greater

depths. While these adjacent portions of crust are geologically very different, their average crustal velocities are almost identical. With this in mind, the Q_c measurement takes on new significance; it is far more sensitive to regional changes in geology than are gross measurements of seismic velocity.

It remains to be seen whether or not the Q_c measurements can help to constrain the composition of the crust. The difference between the Franciscan and granite Q_c is similar to differences mneasured between "hot" and "normal" areas of the crust. P. Roberts (pers. comm.) measured Q_c for lapse times up to 25 s at Long Valley, California. The Q_c for this hot region is lower and much less frequency dependent ($Q_c \sim f^{0.5}$) than is normally observed at short lapse times. Since the Franciscan measurement behaves similarly, although not to the same degree, perhaps it is reflecting a thermally dependent intrinsic Q. This is only speculation; however, heat flow in the Diablo range is quite high (greater than that measured for the Basin and Range province, Roy et al., 1972). In addition, low velocity zones have been found in the crust associated with the Franciscan (Blümling and Prodehl, 1983). The low Q_c observed at high frequencies may be a combination of both thermally activated intrinsic Q and scattering loss in the highly deformed Franciscan. A low velocity zone has also been postulated to lie in the Salinian block crust (Stewart, 1968). The high Q_c we have

measured in the Gabilans does not seem to reflect this.

Of course the Q_c measurement might be affected by crustal thickness, which increases away from the continental margin, and is 5-9 km greater under the Diablo compared to the Gabilan range (Kind, 1972; Oppenheimer, 1985). But a few measurements made in Franciscan terrane along the coast to the south-west of the Nacimiento fault seem qualitatively similar to their Diablo range counterparts. In addition, all frequencies should be affected equally if crustal thickening were entirely responsible for the short lapse time Q_c variation. This is not observed.

Our result is important because it points out the utility of mapping crustal Q_c, especially at high frequency. An inverse problem for $Q_c(x)$ can be formulated in the usual way:

$$Q_c(t_0) = \int_{V(t_0)} Q_c(\overline{x}) \ K(\overline{x}, t_0) \ d\overline{x}$$

where K is a probability density kernel determined by the assumed model of coda wave propagation, V is the volume over which K is non-zero, t_0 is lapse time and x is the space variable. Singh and Herrmann (1983) employed a similar approach in mapping Q_c across the continental United States. Unfortunately, our current data set is too sparse to map Q_c effectively.

D) Dependence of Q_c on Site Conditions

In Chapter 3, observations of site amplifications using coda waves spanned a much broader range than expected, leading to the idea that near surface trapped modes can be an important part of the coda, especially at sediment sites at low frequency. If such trapped energy is inefficiently dissipated, an increase in Q_c should be coupled with a large site effect measurement. This is observed in extreme cases as pointed out in Chapter 3. To see how prevalent this effect might be, Q_c was calculated for data grouped by recording station (Figures 5.5a,b). There is considerable variation in these values of Q_c, however at least 63% of the observations fall within one standard error from their mean, indicating that the variation is expected statistically. Some of the high frequency, short lapse time measurements reflect the correlation of Q_c with geology discussed above. Systematic variations could still be significant, but absolutely no correlation was found between these values of Q_c and the site effect measurements (Figure 5.6a). When the site Q_c is compared to the results of Poupinet et al. (1984, see chapter 3), a modest correlation is observed (Figure 5.6b), however the correlation dissapears when Hollister stations HOR, HPH and HKR are removed. We must conclude here that there is no conclusive evidence for inefficiently dissipated trapped modes at sites where Q_c could be measured, except for the few exceptional cases near Hollister discussed in Chapter 3.

E)   Verification of Coda Stability Assumption

We continue checking basic assumptions of coda shape stability by dividing data by epicentral distance, depth and source-receiver azimuth measured from the structural trend. Results are included in Figures 5.7-5.9. Some variation can be seen in these results, however none are systematic outside of the regional effect seen at short lapse times and high frequencies. Special attention was paid to the depth problem. Hill and Levander (1984) show that energy can be scattered into, and then be trapped within, a low velocity zone with surface roughness and will later contribute to the coda. Low velocity surface layers could act in this way, so that a shallow event could generate a relatively large coda. Also, if near site trapped modes are excited by incident surface waves, this should be apparent as variations of coda amplitude and Q_c with depth. No significant variations are observed; however our data do not sample depth well, especially the set of 15 large events. Instead of relying on Q_c, we can study magnitudes measured from coda duration and Wood-Anderson amplitude M_L. The U.S.G.S. calculates duration magnitudes while the seismographic stations at University of California at Berkeley measure M_L. A plot of $M_L - M_{coda}$ versus depth is shown in Figure 5.10. It was hoped that any surface layer influence on amplitude, thus duration, would be evident in such a plot. Unfortunately, shallow events are not common, so this result is inconclusive. Perhaps quarry blasts should be looked at to

evaluate the magnitude of the scattering effect due to
surface topography.

F) Temporal Effects

Temporal fluctuations are among the more intriguing
observations of coda decay. This subject is pursued by
looking at two data sets: 1) a collection of
micro-earthquakes centered in time around the Coyote Lake
earthquake (August 1979, M_L=5.9) and 2) a collection of
magnitudes measured using both coda duration and
Wood-Anderson amplitudes from the Bear Valley area.

Thirty usable micro-earthquakes were drawn from the
CALNET data set falling between December 1977 and August
1979. These events were chosen to lie in the magnitude
range 1-2 so that the measureable portion of the coda (5
-30s) would represent a crustal average. Only 15
earthquakes of appropriate quality, size and location could
be found prior to the Coyote Lake earthquake over the period
for which data are available. Fifteen more events were
chosen from the large set of aftershocks. Plotting the
results on a time line did not reveal any systematic changes
in Q_c prior to the Coyote Lake earthquake. To improve the
estimates, the data were placed in two groups, representing
"foreshocks" and aftershocks. These Q_c results are not very
different (Figure 5.11). Poupinet et al. (1984) have looked
at the codas from doublet earthquakes in this area and
observed no changes in velocity before and after the Coyote

Lake earthquake for paths in the faulted region. Since
their results are quite precise, it is not surprising that
the measurements of Q_c reported here show no systematic
variation with time.

Coda duration and Wood-Anderson magnitudes were
compared for the period 1969 - 1981 in the Bear Valley area
south of Hollister. This is the same area in which Chouet
(1979) observed temporal fluctuations of Q_c between July
1973 and June 1974. The duration magnitudes have been
collected routinely by the USGS as described in a study by
Lee et al. (1972). The Wood-Anderson magnitudes (M_L) are
measured by the Seismographic Stations of the University of
California. A large amount of scatter is observed in the
M_L - M_{coda} data plotted in Figure 5.12. When the data are
smoothed by year, a more systematic trend appears. These
results predict that durations are increased with respect to
magnitude during the period in which Chouet's study took
place. But Chouet noticed a decrease in Q_c with time which
should correlate with a decrease in duration. The results
of these two studies do not coincide. Interestingly, the
coda duration seems to increase after the Bear Valley
earthquake (February 1972, M_L = 5.0, Ellsworth, 1975) which
is similar to an observation by H. Sato (pers. comm.) for
the Eastern Yamanashi earthquake (August 1983, $M \cong 6$).
Variations in M_L - M_{coda} can be explained in another manner.
Bakun (1984) showed that site corrections as large as 0.5
should be included when calculating duration magnitudes.

The CALNET has evolved significantly through the 1970's which could be responsible for the M_L - M_{coda} observation. Using Bakun's results, this effect could be removed, however site corrections are only given for a subset of the CALNET.

5.2.2 Measurement of Q_β in Central California

The quality factor of shear waves (Q_β) has been measured using the S-to-coda ratio method described in Chapter 2. The S wave data come from a small set of three-component low gain stations operated as part of the CALNET. These stations are shown in Figure 5.13. Amplitudes were estimated using a smoothed FFT with window width of 5.12 s. Coda amplitudes can be measured using the corresponding high-gain vertical components. Slightly less than 100 direct S wave measurements were found that were on scale, yet were well above the signal-to-(P coda) noise. These direct waves had travelled up to 90 km, which confines their paths to the crust (see Levander and Kovach, 1981). Results of this calculation are plotted in Figure 5.14 along with the Q_c discussed in the previous sections. Error bars are large due to the relatively small amount of data that were used. In addition, the direct waves all follow turning ray paths and their amplitudes are sensitive to velocity variations at the turning point. This effect has been avoided in many studies by using data from deep events, but may be averaged out if enough data are used.

As found by Roecker et al. (1982), the Q_β measurement matches crustal measurements of Q_c. In this case, Q_β is similar to Salinian block and Franciscan crustal Q_c at low frequencies. At high frequencies Q_β follows the Salinian block Q_c, however the errors here are fairly large. The high frequency behavior of Q_β may be the result of over sampling the Salinian block since low signal to noise data are not included. Shear arrivals have been noted to be most clearly defined at the Salinian granite sites (Rick Lester, pers. comm.).

5.3 Conclusions

Measurements have been made of the coda wave decay parameter Q_c using the extensive CALNET database. In an attempt to separate out the major factors that influence Q_c we found that:

1) basic assumptions of the stability of coda shape are satisfied. The observed Q_c showed no systematic variations with epicentral distance, depth and azimuth from epicenter to station. The anticipated correlation between site Q_c and site effect turned out to be fairly weak, leaving us to conclude that inefficiently dissipated trapped modes dominate the coda only in exceptional cases.

2) significant differences exist between crustal Q_c for the Salinian and Franciscan regions. This is especially apparent at high frequencies where a factor of 2 difference is observed. The low Q_c in the Franciscan crust may be a

combination of scattering and intrinsic Q. Q_c seemes to be more sensitive to the geological differences between the two regions than the average crustal velocity. This demonstrates the prospects of mapping Q_c, even considering the accompanying low resolution.

3) Q_c is heavily dependent on the lapse time over which it is measured. This is interpreted as a reflection of attenuation decreasing with depth through the crust and upper mantle, however multiple scattering and changing modal composition of the coda may also be important. Q_c seems to be controlled by lapse time as much as, if not more than it is controlled by regional geology.

4) temporal variations of Q_c were not observed in data from 30 micro-earthquakes which ocurred before and after the Coyote Lake earthquake of 1979. Variations in $M_L - M_{coda}$ were also investigated. Systematic changes were found, but could be due to changes in the configuration of the CALNET which was evolving rapidly during this period. However, durations are noted to have increased after a nearby $M_L = 5.0$ event which coincides with other observations of the coda Q precursor. Further investigation of temporal changes should be interesting, but the effect of the network changes must be eliminated. Unfortunately, M_L is only measured routinely for magnitudes greater than 2.5; we expect any crustal changes to be more easily observable in short lapse time Q_c which will be reflected in the durations of much smaller events.

5) Q of shear waves travelling crustal paths agrees with crustal Q_c. This represents an additional test of the observation that $Q_\beta = Q_c$ which supports the supposition that the coda is composed of backscattered shear waves. Our result was obtained using only a small part of the data available from the CALNET. Further study is of interest; perhaps an attempt can be made to detect anisotropy in Q_β.

Table 5.1 <u>Residual Variance (Napiers)2 and Degrees</u>
<u>Freedom for</u>:

1) Q_c = constant

2) Q_c = free

3) Q_c = constant for given sub-region

frequency (Hz)	size	1 $\sigma_r{}^2$	ν	2 $\sigma_r{}^2$	ν	3 $\sigma_r{}^2$	ν
1.5	B	.25	5509	.21	4977		
1.5	S	.15	602	.11	458	.15	588
3	B	.32	11856	.28	11295		
3	S	.26	2902	.21	2567	.25	2800
6	B	.34	16275	.30	15783		
6	S	.30	6918	.24	6513	.27	6688
12	B	.22	4928	.21	4667		
12	S	.22	5011	.17	4619	.19	4880
24	B	.11	180	.11	161		
24	S	.15	1211	.11	1065	.13	1182

B: Lapse times 20 - 100 s from large events

S: Lapse times 5 - 30 s from small events

Figure Captions

Figure 5.1:

Q_c^{-1} measured over different lapse times (time elapsed from the earthquake origin time): 1) Short lapse times (5 - 30 s) from magnitude 1.5 - 2 events in the Coyote Lake area, 2) Lapse times 20 - 100 s from magnitude 2.5-3 events scattered throughout the array, and 3) Lapse times 100 - 300 s from low gain recordings of the Coyote Lake earthquake, magnitude 5.9. Error bars represent twice the standard error, none are shown if they are smaller than the symbol size. The envelope of Q_c measurements world wide is also depicted.

Figure 5.2:

Low frequency measurements of Q_c: A) Alaska (Aki, unpublished data), B) Central Asia (the "b" leg of Rautian and Khalturin, 1978), C) California, this study. Error bars are twice the standard error.

Figure 5.3:

Sub-regions into which the short lapse time data were divided. Areas 2 and 3 represent the Franciscan while areas 4 and 5 represent the Gabilan granites. Symbols mark the source-receiver midpoint for every quality = 1 record for the 6 Hz band.

Figure 5.4:

Q_c^{-1} by sub-region (see Figure 5.3). Filled circles represent areas 2 and 3, open circles areas 4 and 5; triangles are the Q_c from the 20 - 100 s lapse time data.

Figure 5.5:

Q_c^{-1} measured at each station for: a) Lapse times 20 - 100 s, b) Lapse times 5 - 30 s. Results are arranged in descending order.

Figure 5.6:

a) Correlation at 1.5 Hz between station Q_c^{-1} and the site amplification measurement for lapse time 5 - 30 s data. From top to bottom plots show stations, site geology (see Table 3.1), and standard errors. b) Same as "a" except Q_c^{-1} is compared to the change in time delay with lapse time in parts per thousand from the doublet measurement of Poupinet et al. (1984). The correlation coefficient is -0.6 if station BJC is ignored.

Figure 5.7:

Q_c^{-1} measurements grouped by epicentral distance: a) Lapse times 20 - 100 s, b) Lapse times 5 - 30 s. Error bars are one standard error.

Figure 5.8:

Q_c^{-1} measurements grouped by azimuth: a) Lapse times 20 - 100 s, b) Lapse times 5 - 30 s. Error bars are one standard error.

Figure 5.9:

Q_c^{-1} measurements grouped by depth: a) Lapse times 20 - 100 s, b) Lapse times 5 - 30 s. Error bars are one standard error.

Figure 5.10:

$M_L - M_{coda}$ as a function of depth. Symbols represent magnitudes in the upper plot. Data are smoothed by depth interval in the lower plot. Error bars are one standard error.

Figure 5.11:

Q_c^{-1} measured for magnitude 1.5 - 2 events prior to the Coyote Lake earthquake (triangles) and aftershocks (circles). Symbols are placed side-by-side rather than superimposed. Error bars represent twice the standard error, and are only shown if they exceed the symbol size.

Figure 5.12:

$M_L - M_{coda}$ versus time. The Bear Valley earthquake $(M_L = 5.0)$ and the period over which Chouet (1979) conducted his Bear Valley experiment are shown. Symbols represent

earthquake magnitude in the upper plot. Data are smoothed by year in the lower plot. Error bars represent one standard error.

Figure 5.13:

   Three-component low-gain CALNET stations from which the direct S waves were gathered for the Q_β study.

Figure 5.14:

   Comparison of Q_β and Q_c. Q_β^{-1} is represented by open circles; Q_c^{-1} is shown for lapse times 20 - 100 s (triangles), and lapse times 5 - 30 s (K = areas 2 and 3, G = areas 4 and 5, see Figure 5.3). Error bars are twice the standard error.
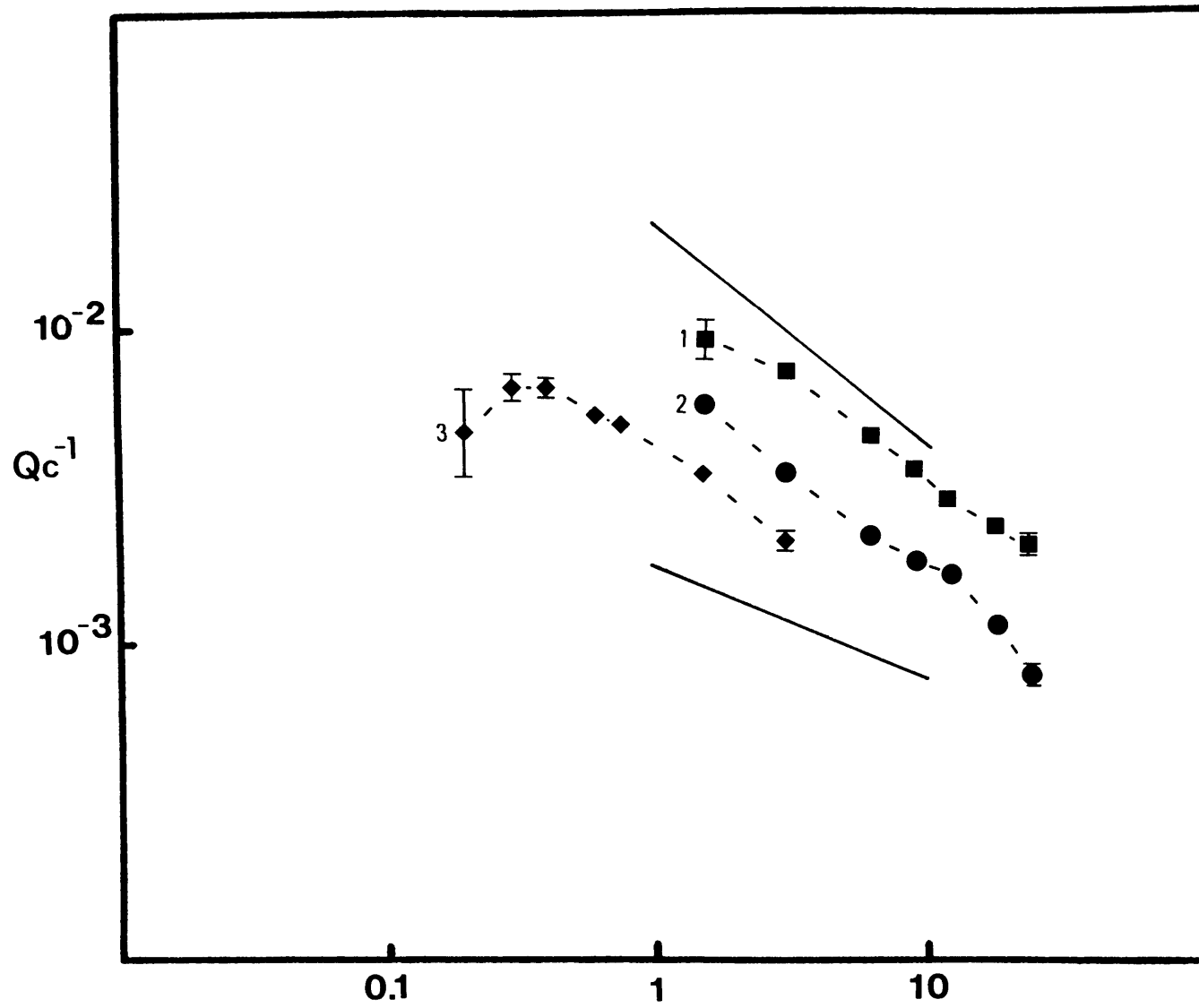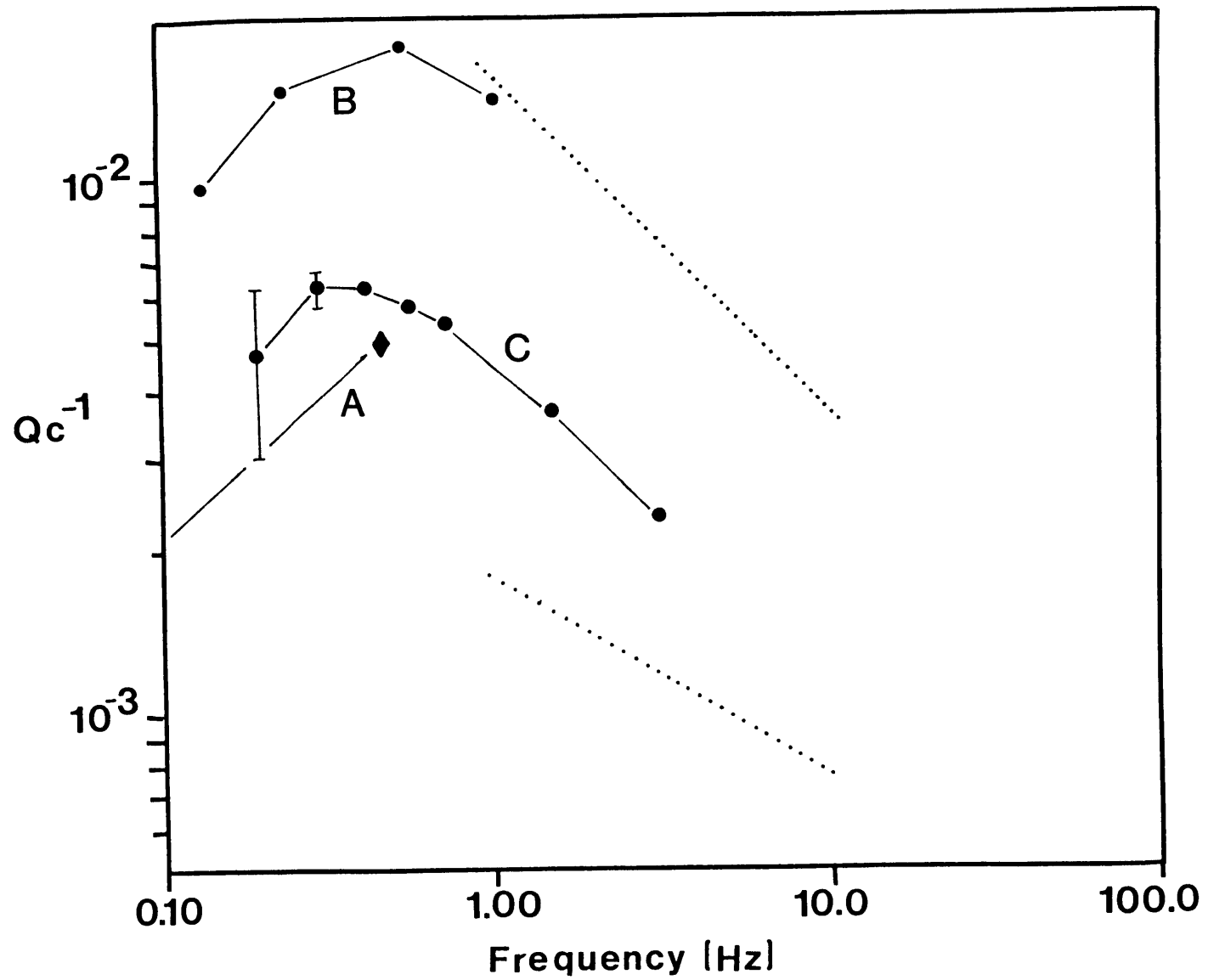
Figure 5.1

Figure 5.2
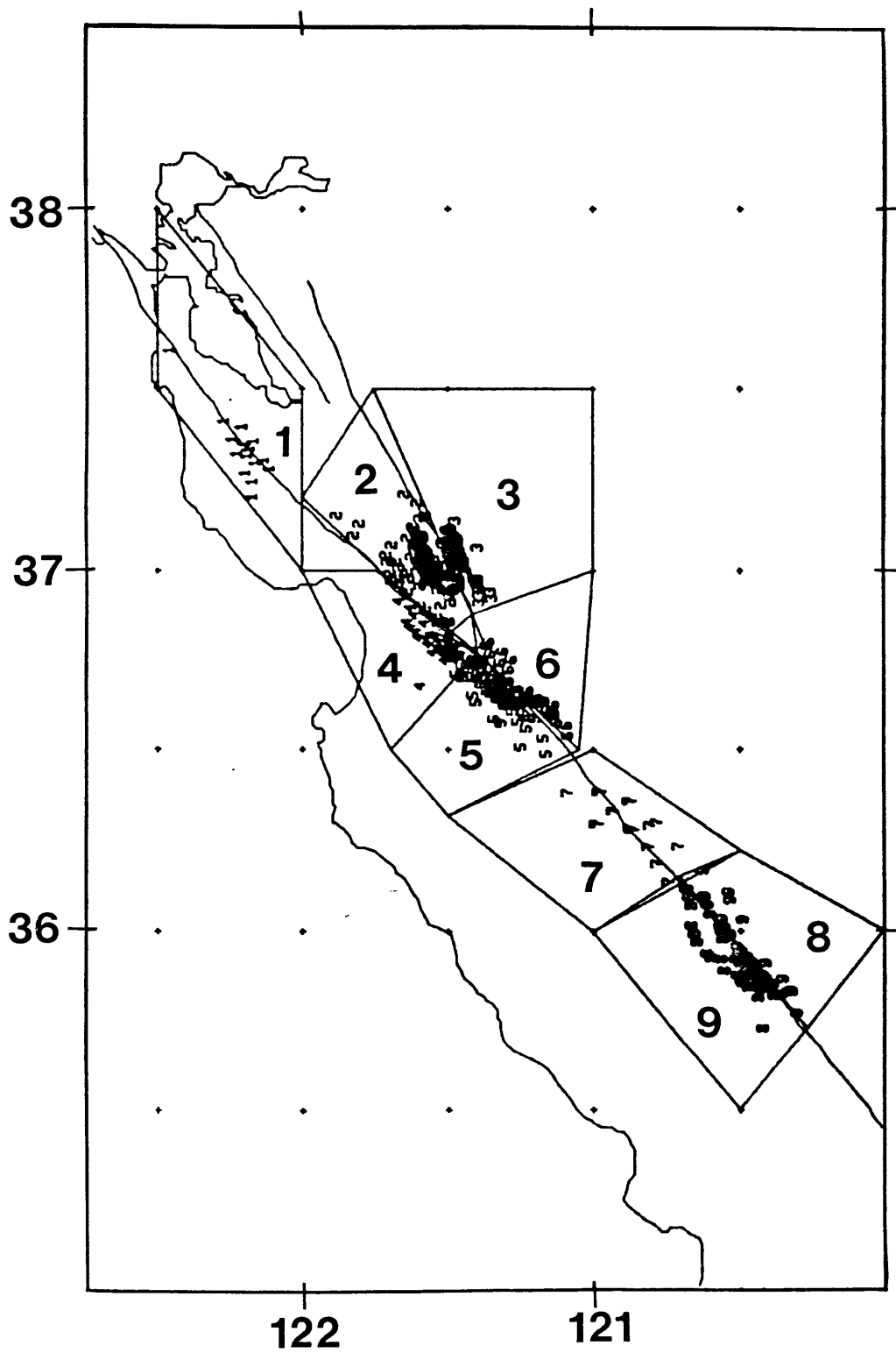
Figure 5.3
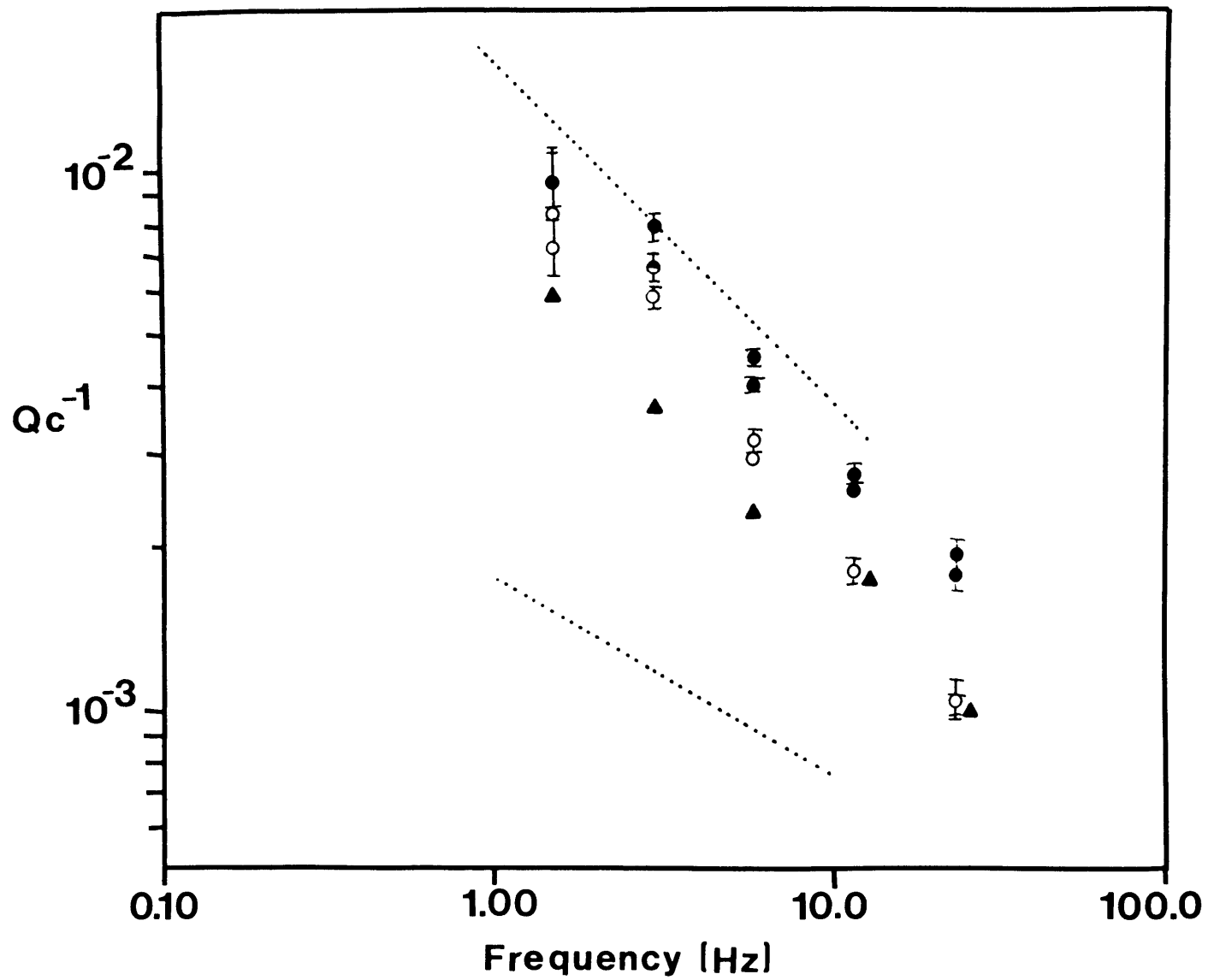
Figure 5.4
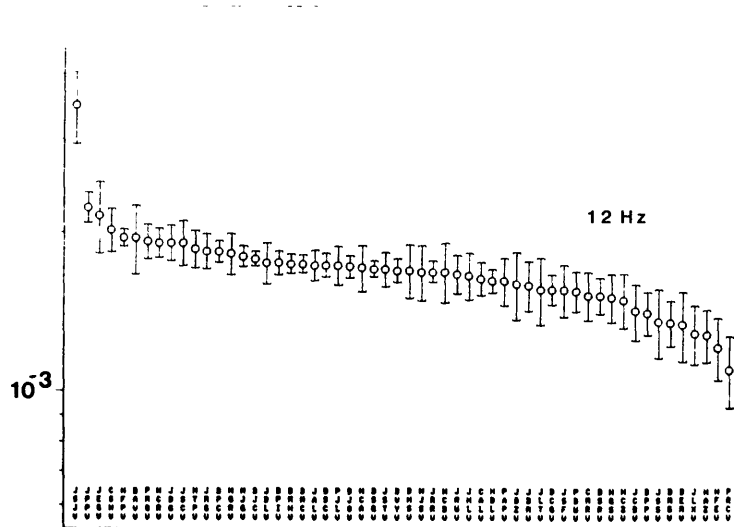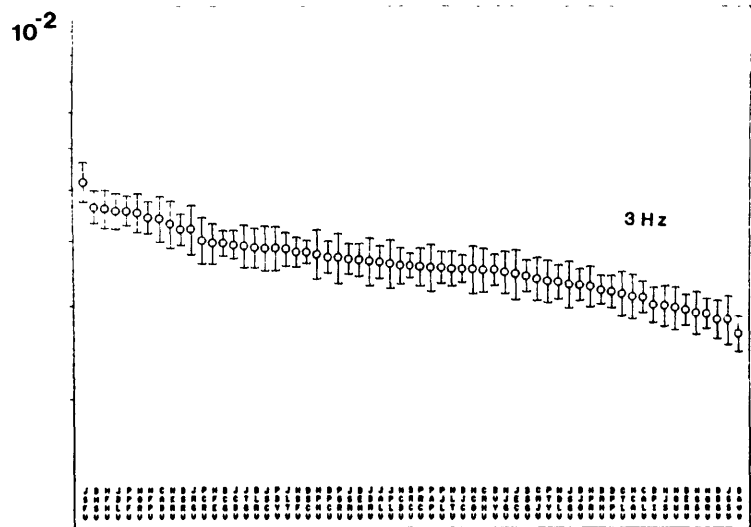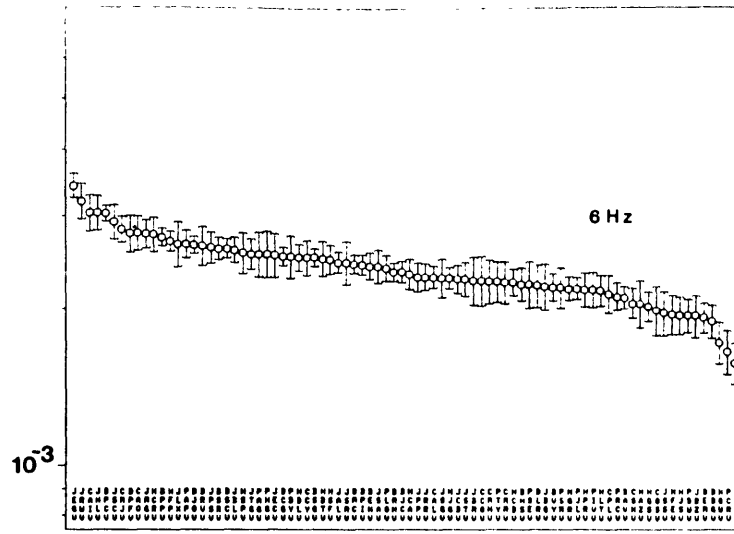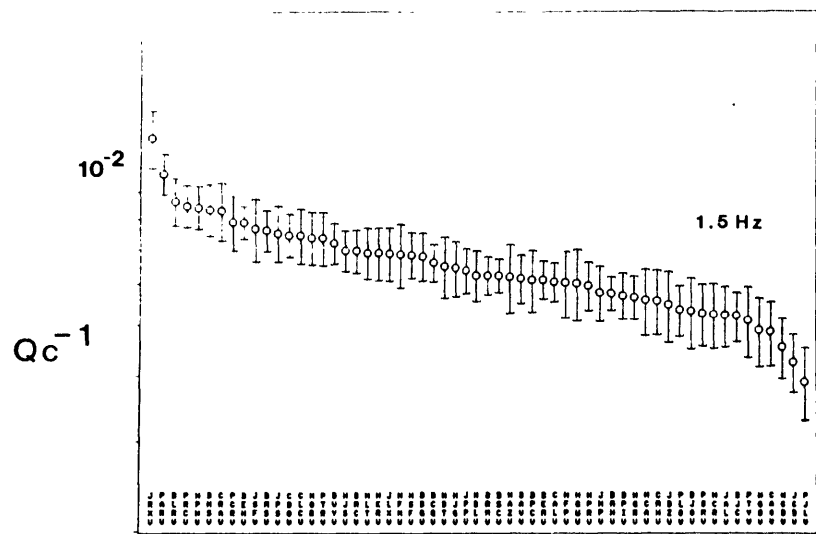
Figure 5.5a

Figure 5.5b

$-\log_{10} Q_c$

$\ln(A/\bar{A})$

Figure 5.6a

Figure 5.6b

The y-axis is labeled $-\log_{10} Q_c$ with values -2.0, -2.2, -2.4.

The x-axis is labeled $d[\delta t]/dt \times 10^3$ with values 0, 1, 2.
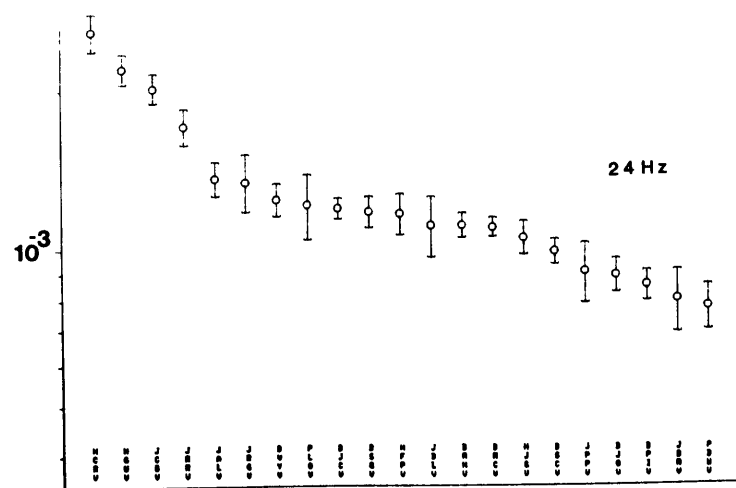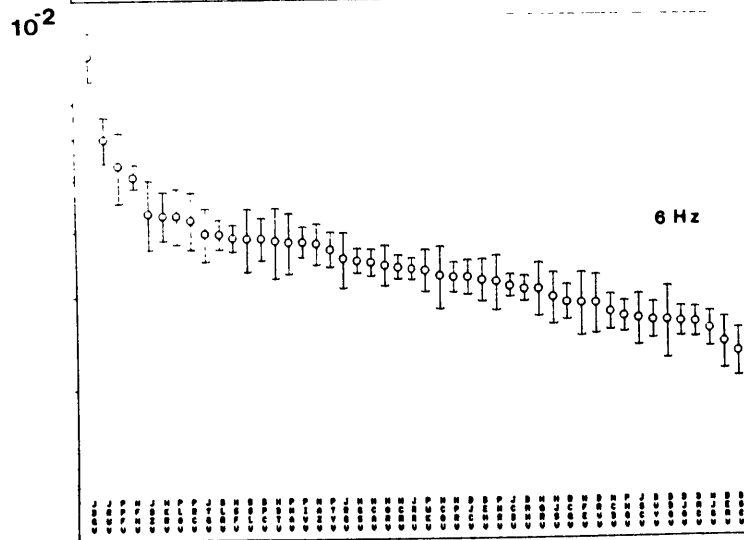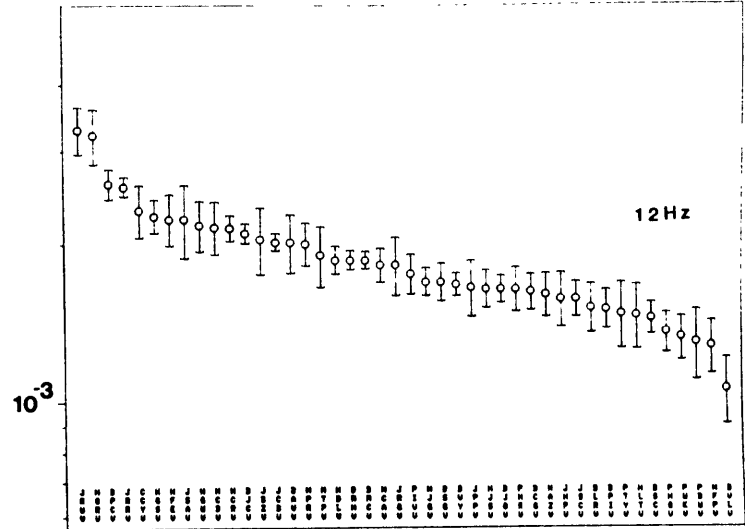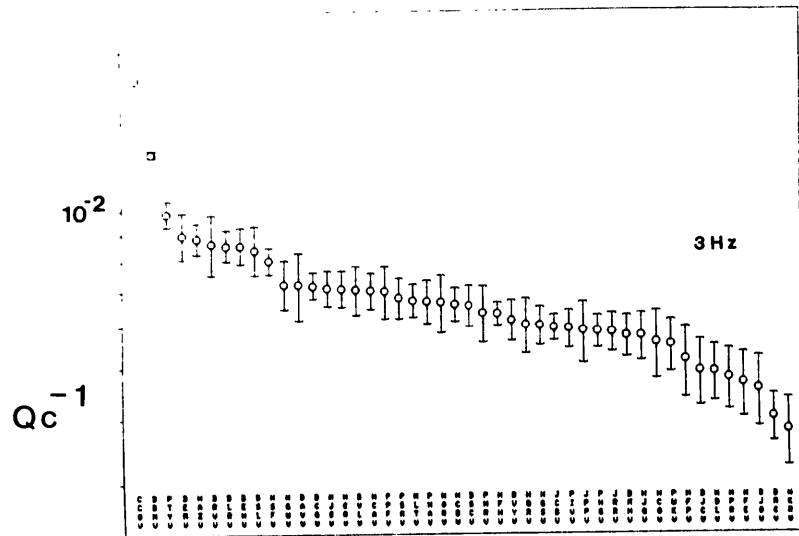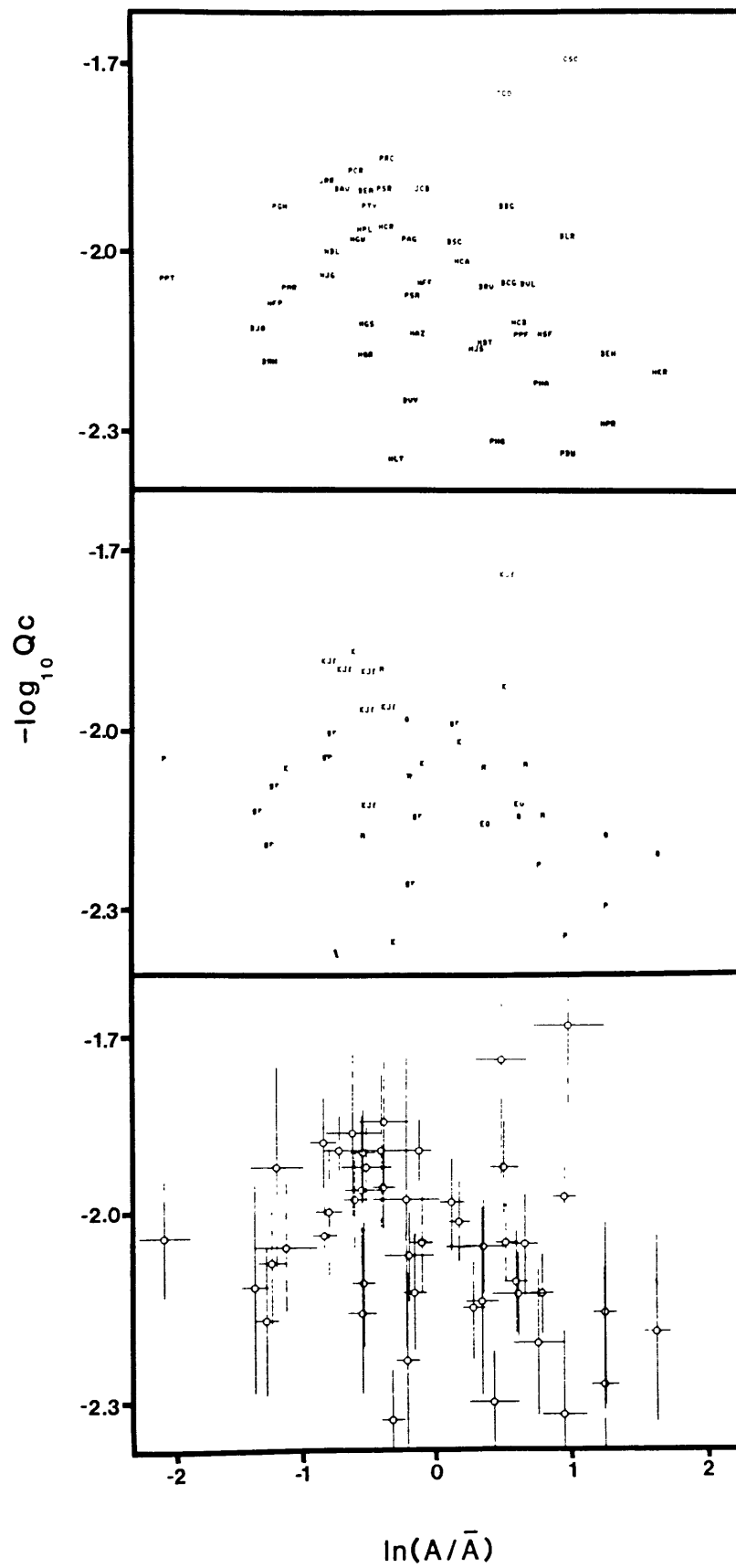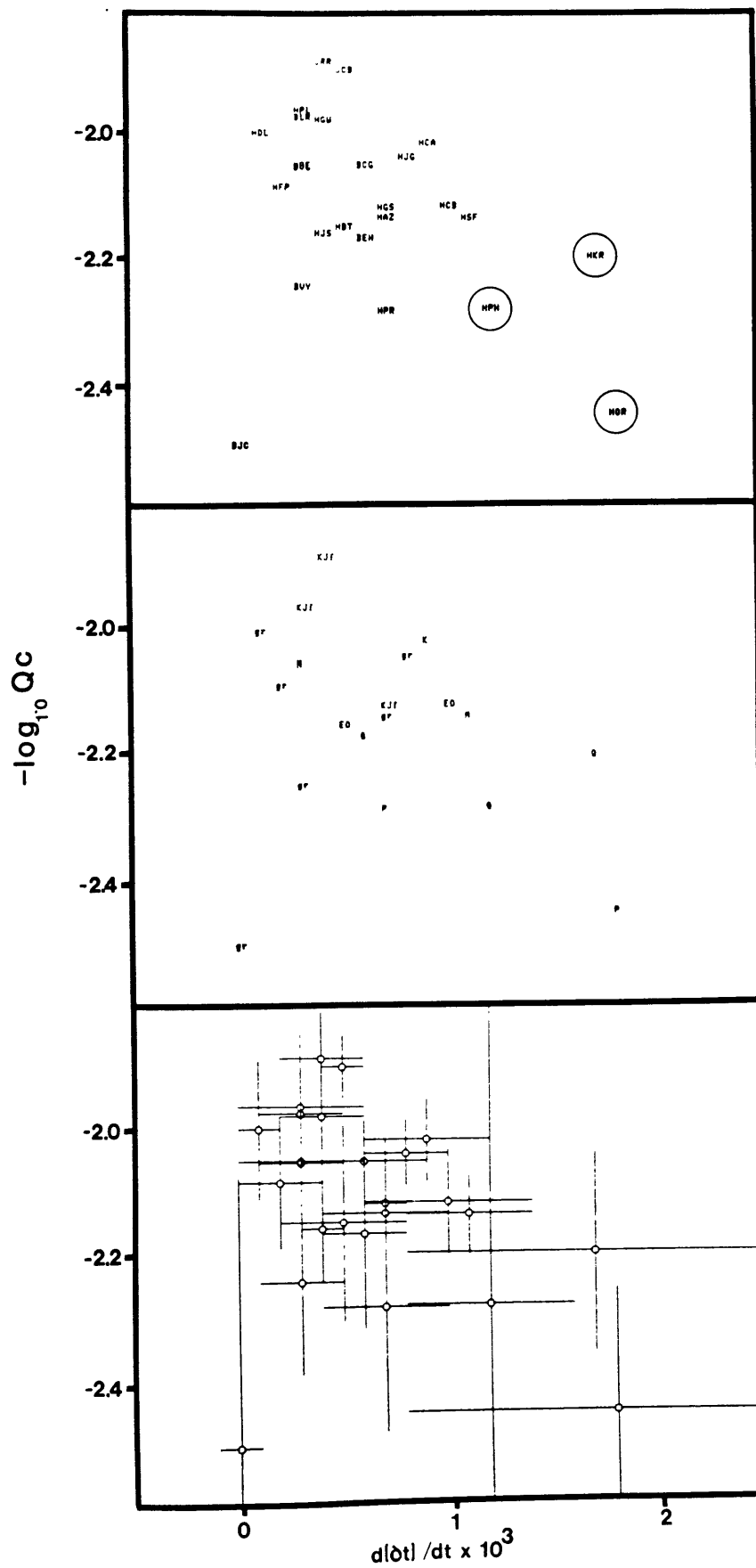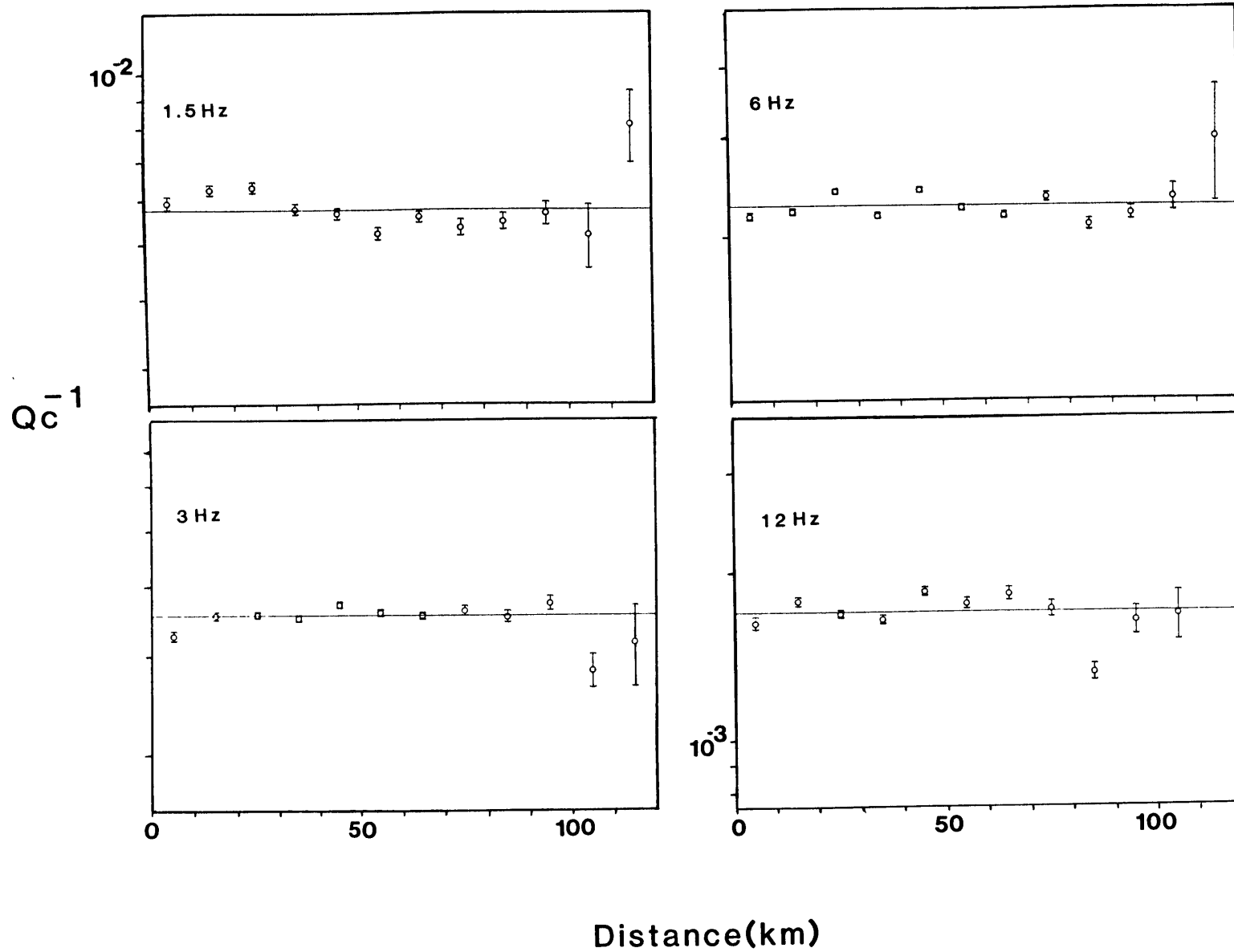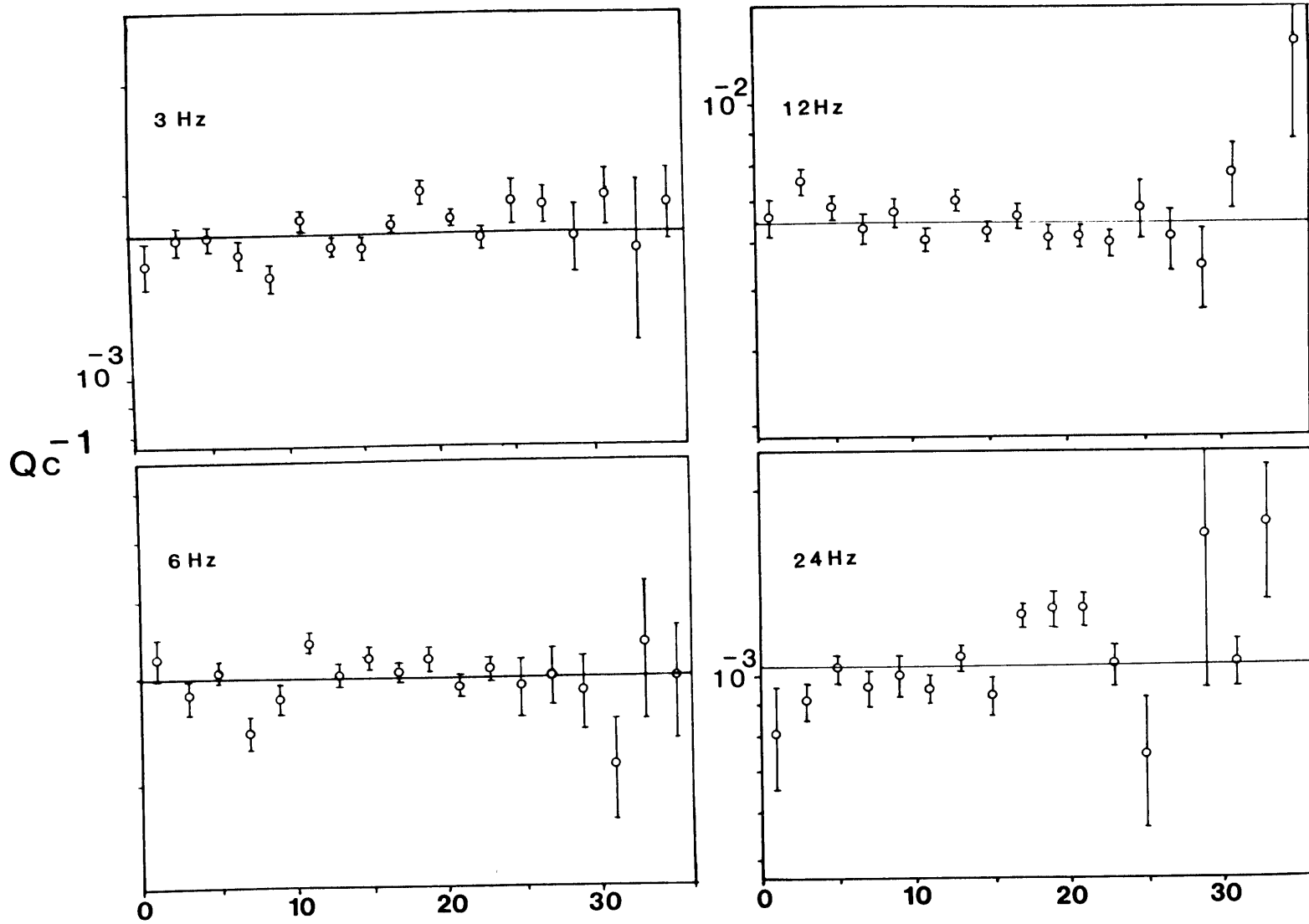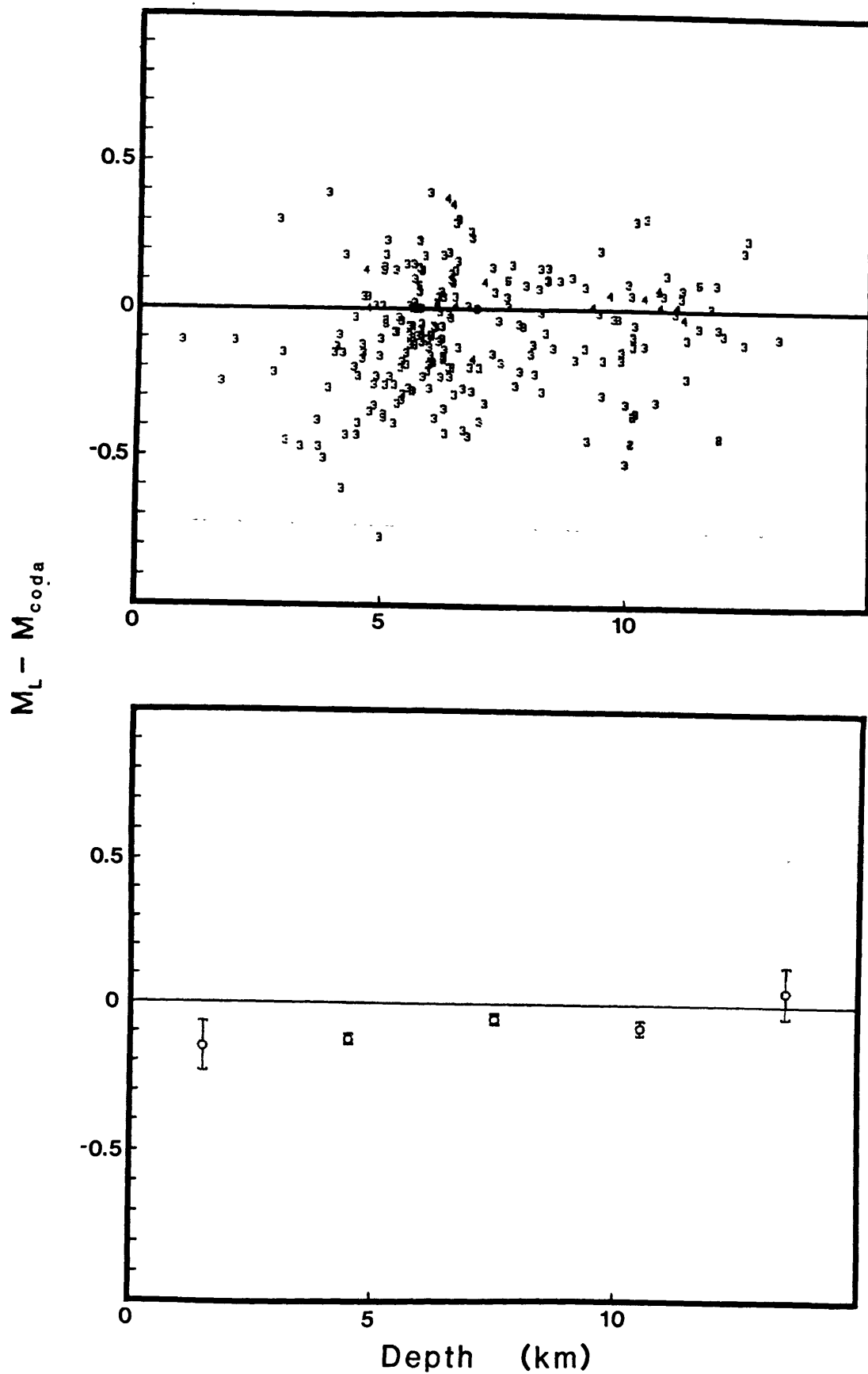
Figure 5.7a
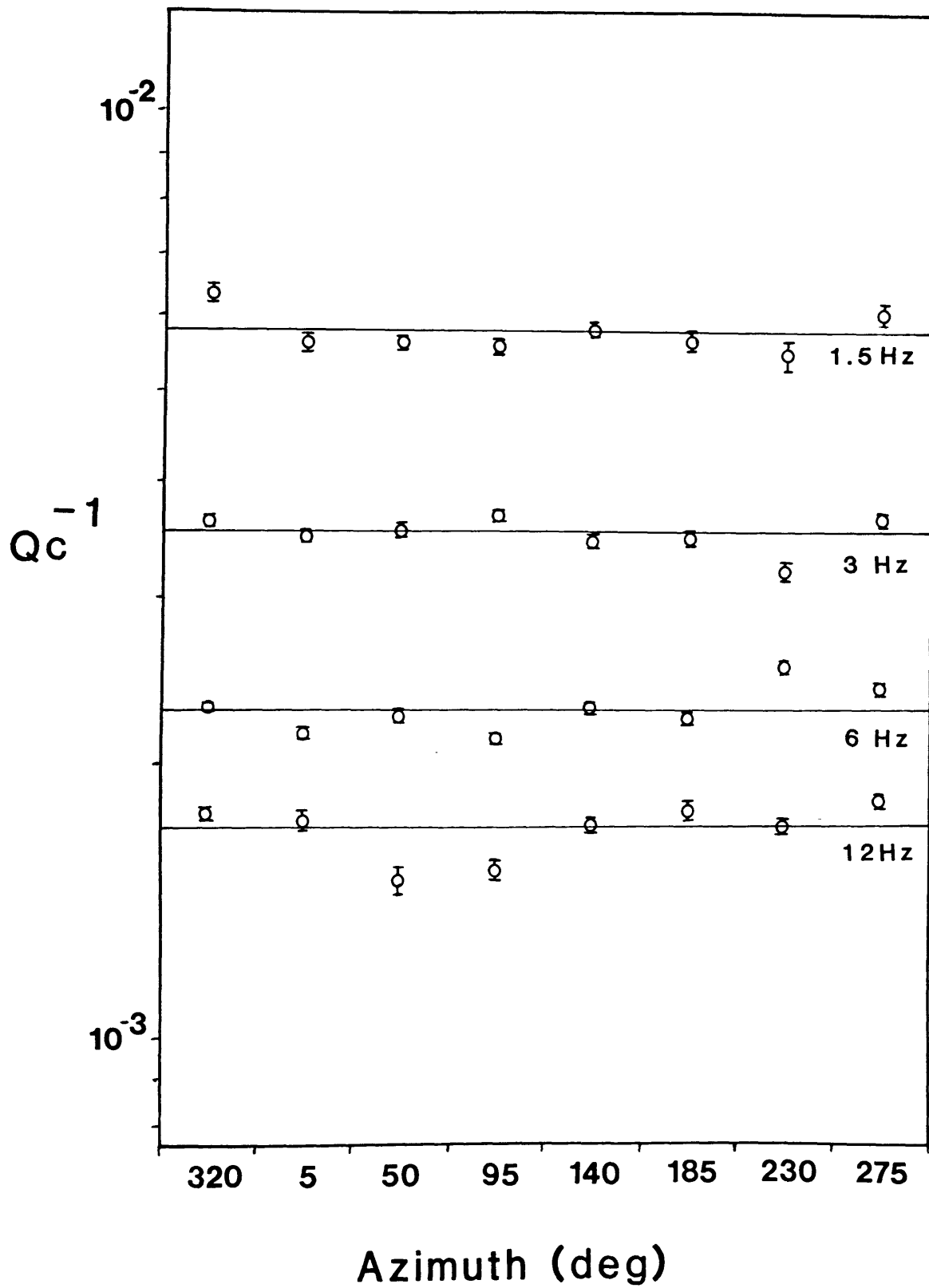
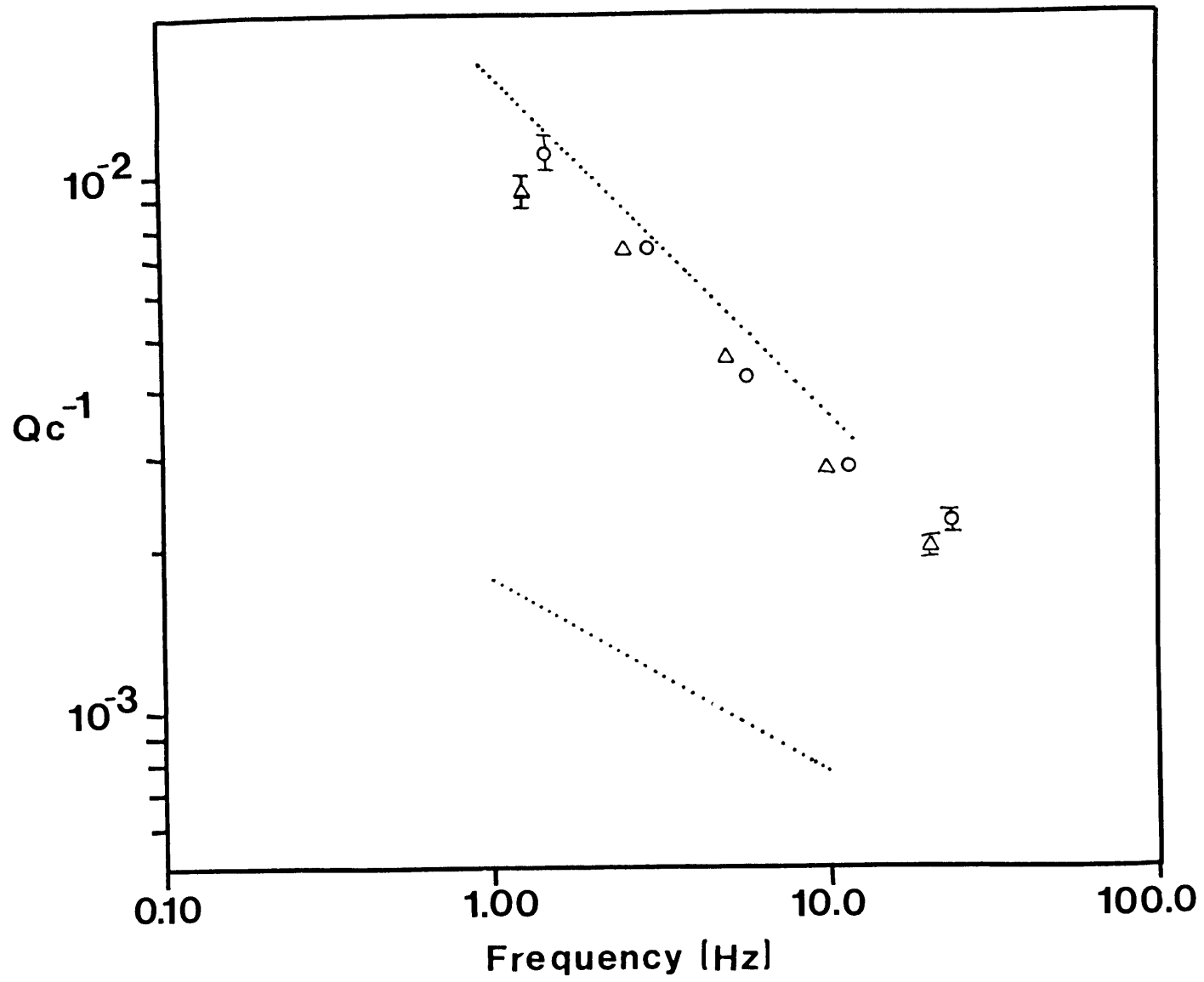Figure 5.7b
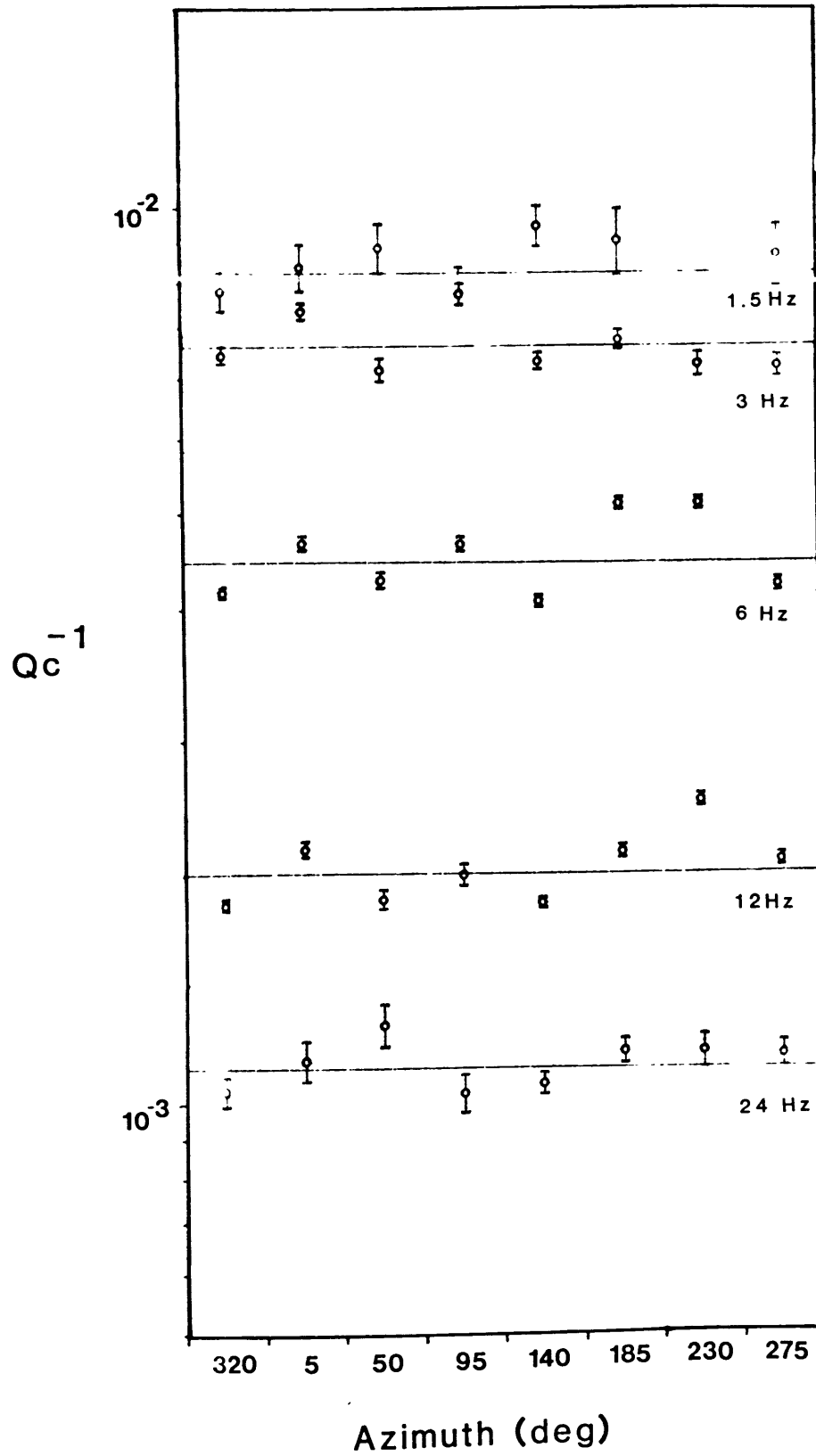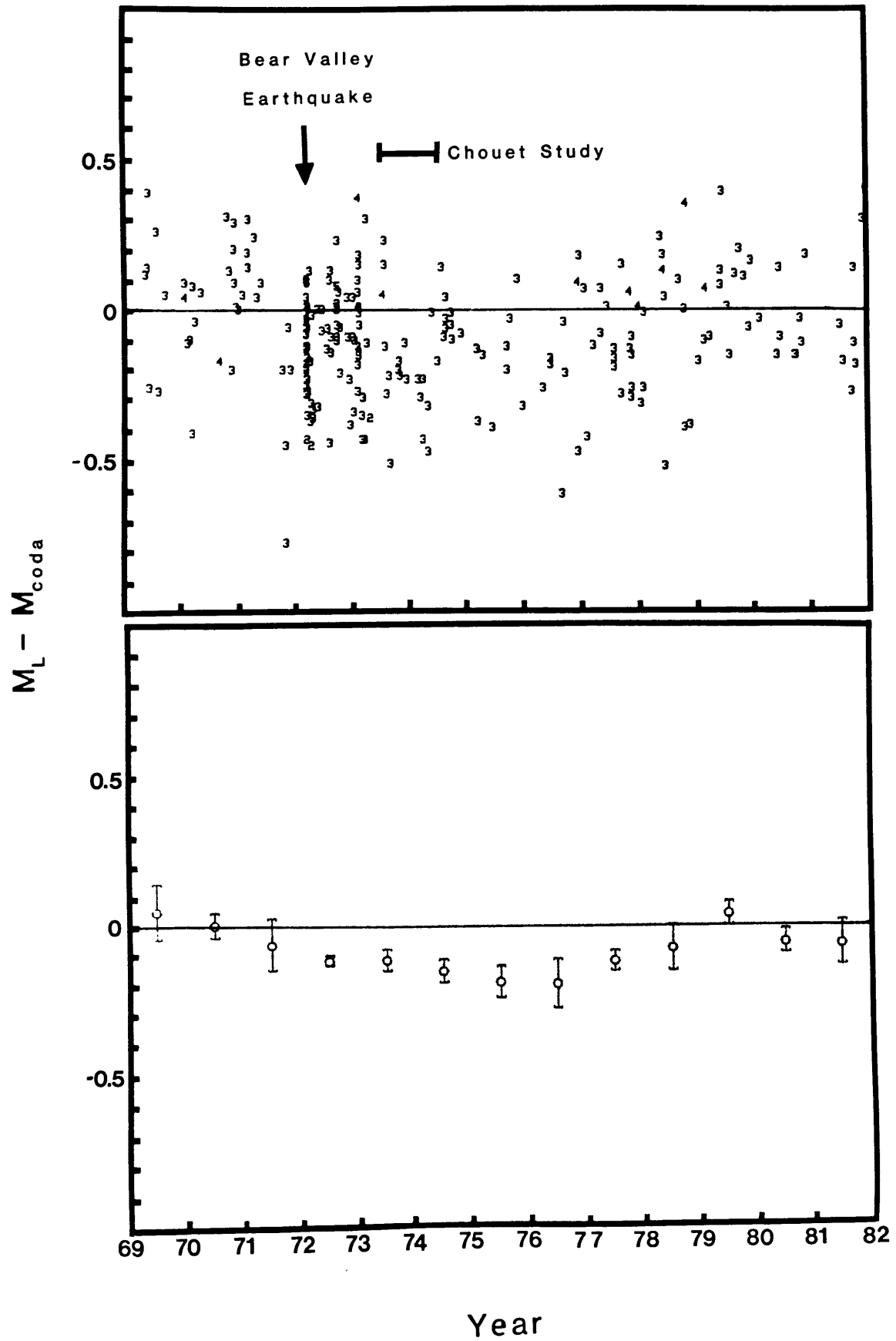
Figure 5.8a

Figure 5.8b
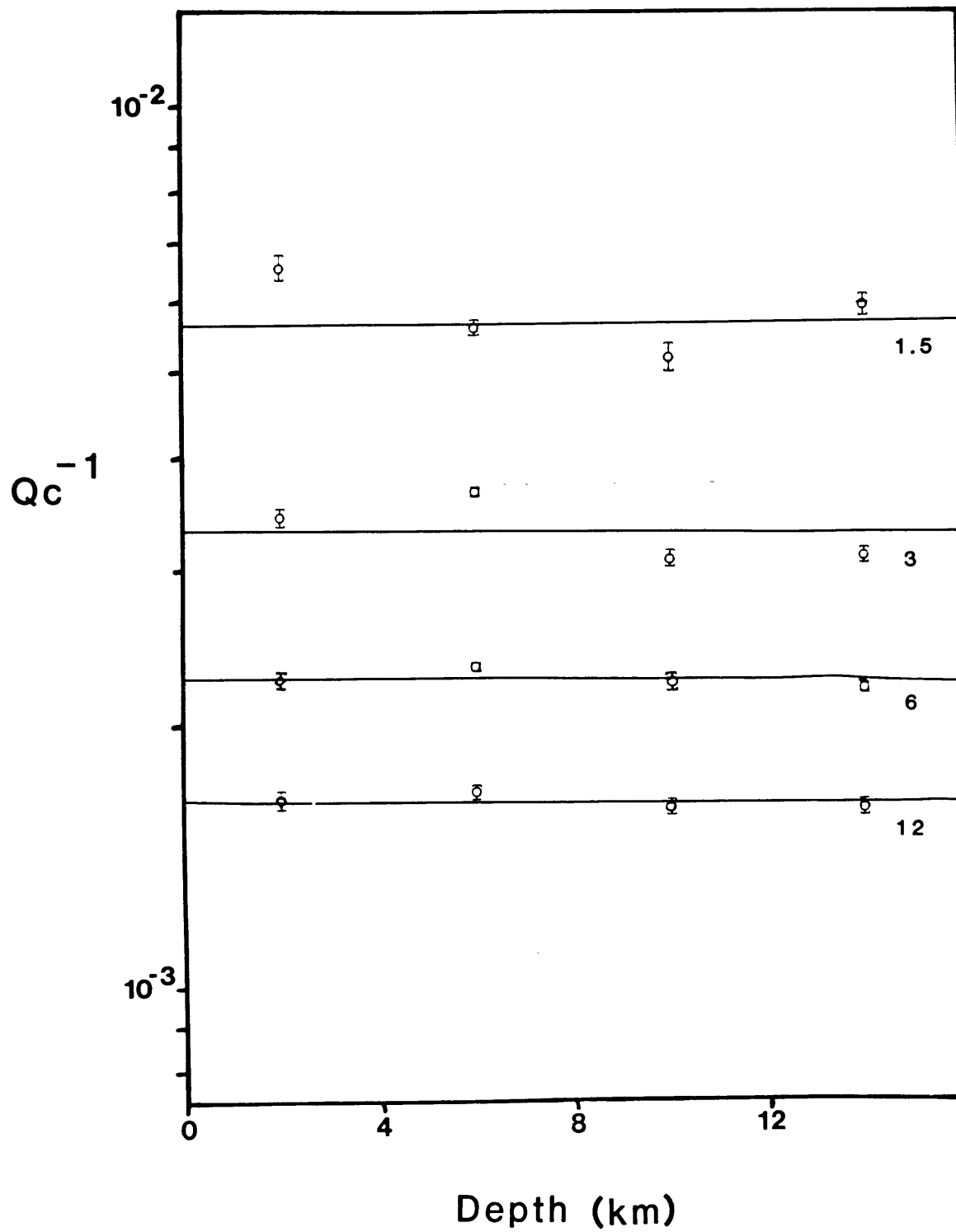
Figure 5.9a
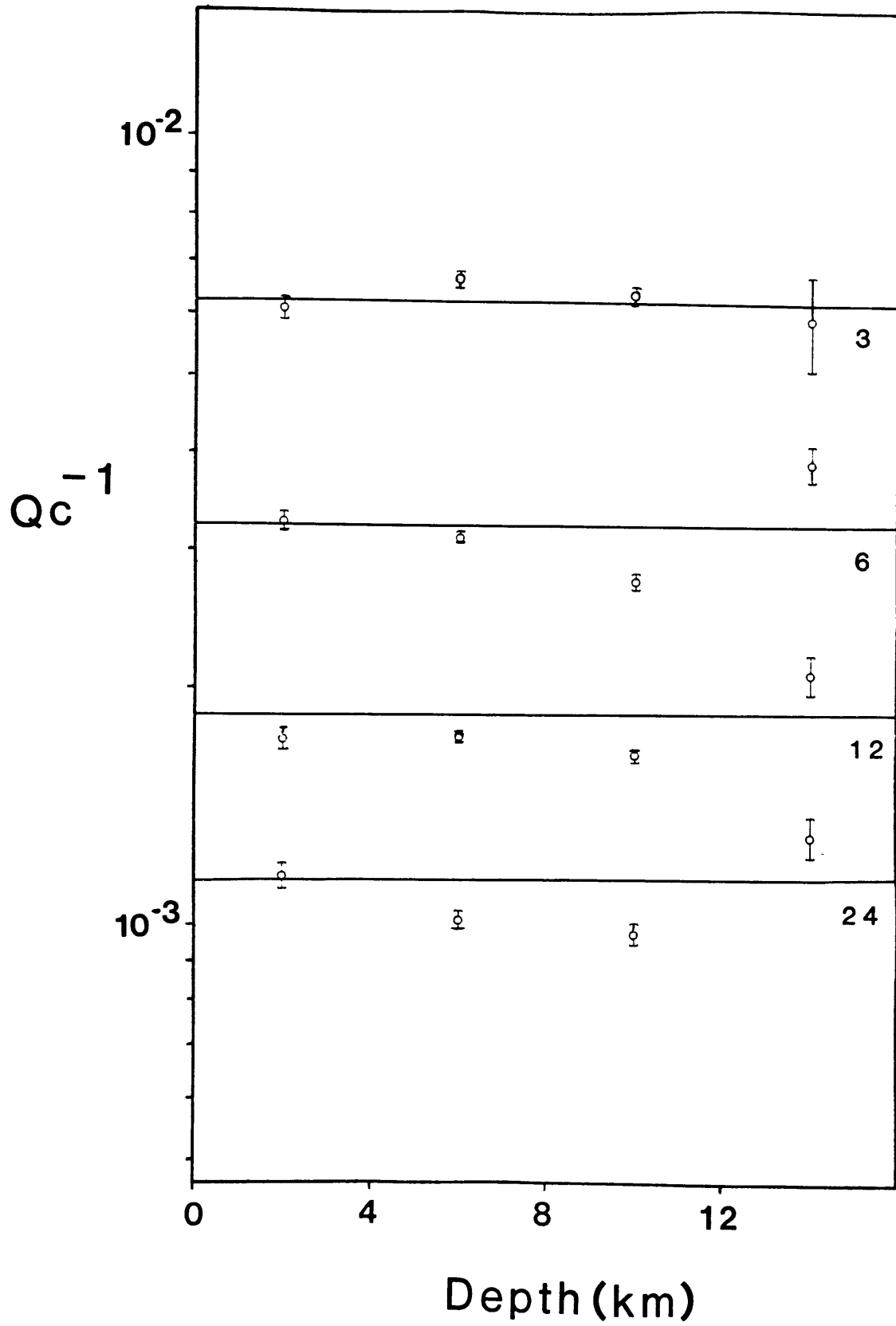
Figure 5.9b

Figure 5.10

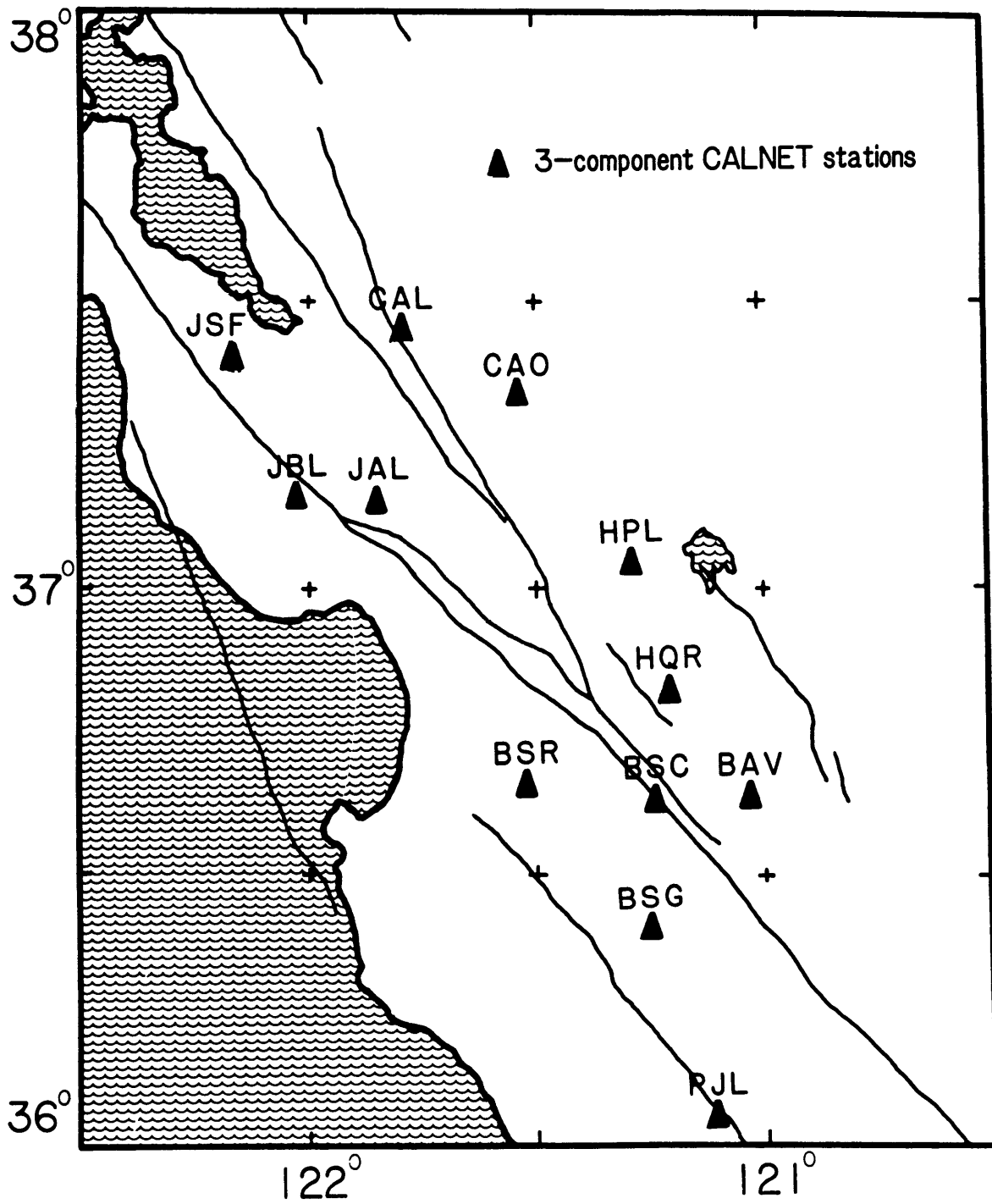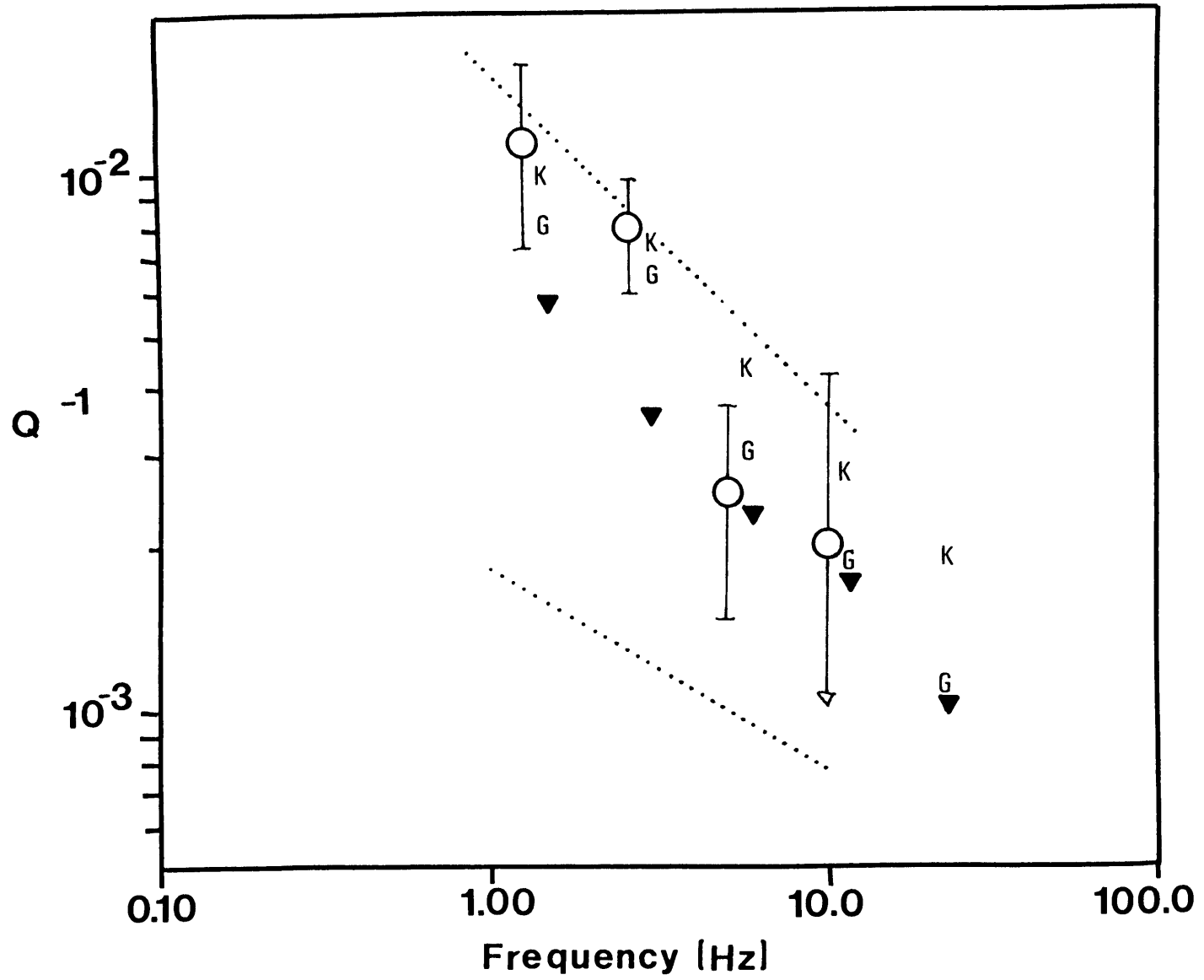Figure 5.11

Figure 5.12

Figure 5.13

Figure 5.14

Chapter 6: <u>SUMMARY</u>

The goals of this research have been to ascertain the degree to which the study of coda waves from local earthquakes can increase our knowledge of the earth, and also to learn about the processes that generate the coda itself. To do this, I have utilized the most extensive coda wave data set ever studied. The methods used are simple extensions of widely used single-station methods, with advantages of less restrictive assumptions and the inclusion of many stations in the calculations. The application of these methods to California data has been effective, yielding intriguing results and helping to define exciting research directions for the future.

The site effect on coda waves is calculated under the non-restrictive assumption that the coda shape is independent of recording site for a given source, as expected from the backscattering model. Previous work has shown that the average site effect on coda waves is the same as the average site effect on direct S waves (Tsujiura, 1978). A very broad distribution of site terms is found at all frequencies; a factor of 20 difference is seen between granite and sediment sites near Hollister at 1.5 Hz. Little evidence is found to support the proposition that high frequency source spectral parameters such as f_{max} are controlled by the site effect (Hanks, 1982). The responses at "hard" and "soft" rock sites can be represented schematically by approximately straight

lines on a log-log plot, indicating that high frequencies are attenuated less than might be expected from a frequency independent near site Q. Sites exhibiting sharp changes in response at high frequencies are the exception rather than the rule.

The coda site effect calculation may be applied in various investigations. Engineers may use it to obtain a stable estimate of the average site response; however, care must be taken at sediment sites where undamped resonances may be strong, as this constitutes a violation of the initial assumptions. The calculation will be of greater use to microearthquake seismologists through network calibration and the identification of ideal reference sites. Recordings of small nearby events at such ideal sites can be used to rectify the source and site effect results in the manner of Chouet et al. (1978).

Source terms were calculated under the assumption that the coda shape is independent of the source for a given station. Although the data were not ideal for a study of this nature, interesting results were obtained. Anelastic medium properties encompassed by the quantity δx^* (see Section 3.3.2) vary less with source than with site location, however, variations do exist. An attempt should be made to map δx^* within the fault zone using a well constrained concentration of sources. The corner frequencies of a group of 30 microearthquakes in the Coyote Lake area appear to be constant, which is important to the debate about whether or

not a source-controlled limiting corner frequency, or f_{max} can be observed. A wider range of magnitudes must be included in order to substantiate the findings presented here. Regional variations of this effect should also be explored in order to infer variations of fundamental parameters describing the anelastic behavior of fault zone materials (Papageorgiou and Aki, 1983a, b). The rectification of our results by the inclusion of independently determined spectra of a number of earthquakes as mentioned above, and the attainment of higher resolution in the frequency domain, are advisable improvements if these studies are to be carried out.

The Q of coda waves (Q_c) was investigated with the method of Aki and Chouet (1975), under the assumption of a specific (single-scattering) coda model. As observed by many workers Q_c is found to be heavily dependent on frequency and lapse time; the latter effect is interpreted as due to an increase in effective Q with depth in the crust and upper mantle (Roecker et al., 1982), although multiple scattering may be partially responsible. The importance of multiple scattering versus depth-controlled Q and scattering strength should be investigated theoretically, perhaps following the method of Gao et al. (1983). Regional variation of Q_c was detected in the short lapse time data (5 - 30 s). The strongest difference exists at high frequencies (12 - 24 Hz) between the high Q Salinian block and the low Q crust associated with the Franciscan Complex. The difference may

be due to low, thermally activated intrinsic Q under the Franciscan, perhaps related to the low velocity zone found by refraction studies in the area (Blümling and Prodehl, 1983). The variation in Q_c is quite large (a factor of 2 at 24 Hz), while average crustal velocities between these geologically distinct regions are very similar (see Walter and Mooney, 1982). The extreme sensitivity to crustal composition found here points out the potential in mapping crustal Q_c, in spite of the expected low spatial resolution ($\sim$ 30 km).

Results of my investigations generally support the model of coda as energy backscattered from randomly-situated heterogeneities in the lithosphere. Observations of coda stability on the earth's surface are consistent with this model, although the earth medium cannot be restricted to be stationary with respect to depth, for depths much greater than that of the deepest seismicity. The model does not hold at certain sediment sites, such as those near Hollister in the southern Santa Clara Valley. The site response at low frequency (1.5 Hz) is much too large to be explained by the impedance effect, and ringing (thus high Q_c) is observed in the codas at these sites. More subtle violations of the coda stability assumption were investigated through the comparison of Q_c and the site effect. Large scatter and low correlation coeficients were obtained at all frequencies, indicating that the model violation only occurs conclusively at the Hollister sediment sites at low frequencies.

REFERENCES

Aki, K. (1956) Correlogram analyses of seismograms by means of a simple automatic computer, J. Phys. Earth, 4: 71-78.

Aki, K. (1967) Scaling law of seismic spectrum, J. Geophys. Res., 72: 1217-1237.

Aki, K. (1969) Analysis of the seismic coda of local earthquakes as scattered waves, J. Geophys. Res., 74: 615-631.

Aki, K. (1980a) Attenuation of shear waves in the lithosphere for frequencies from 0.05 to 25 Hz, Phys. Earth Planet. Interiors, 21: 50-60.

Aki, K. (1980b) Scattering and attenuation of shear waves in the lithosphere, J. Geophys. Res., 85: 6496-6504.

Aki, K. (1980c) Re-evaluation of stress drop and seismic moment using a new model of earthquake faulting, in Source Mechanism and Earthquake Prediction, C. J. Allegre, ed., Editions du Centre de la Recherche Scientifique, Paris.

Aki, K. (1981) Attenuation and scattering of short-period seismic waves in the lithosphere, in Identification of Seismic Sources- Earthquakes or Underground Explosions, E. S. Husebye and S. Mykkelveit, eds., D. Reidel Publishing Co., Dordrecht, The Netherlands, 515-541.

Aki, K. and B. Chouet (1975) Origin of coda waves: Source, attenuation and scattering effects, J. Geophys. Res., 80: 3322-3342.

Aki, K. and P. G. Richards (1980) Quantitative Seismology, W. H. Freeman and Co., San Francisco.

Bailey, E. H., M. C. Blake Jr., and D. L. Jones (1970) On-land Mesozoic oceanic crust in the California Coast Ranges, U. S. Geol. Survey Prof. Paper 770-C: C70-C81.

Bakun, W. H. (1984) Magnitudes and moments of duration, Bull. Seism. Soc. Am., 74: 2335-2356.

Bakun, W. H. and G. G. Bufe (1975) Shear wave attenuation along the San Andreas fault zone in central California, Bull. Seism. Soc. Am., 65: 439-459.

Bard, P.-Y. (1982) Diffracted waves and displacement field over two-dimensional elevated topographies, Geophys. J. R. Astr. Soc., 71: 731-760.

Bard, P.-Y., and M. Bouchon (1980a) The seismic response of sediment-filled valleys. Part 1. The case of incident SH waves, Bull. Seism. Soc. Am., 70: 1263-1286.

Bard, P.-Y., and M. Bouchon (1980b) The seismic response of sediment-filled valleys. Part 2. The case of incident P and SV waves, Bull. Seism. Soc. Am., 70: 1921-1941.

Bard, P.-Y., and B. E. Tucker (1985) Ridge and tunnel effects: Comparing observations with theory, Bull. Seis. Soc. Am., submitted.

Bisztricsany, E. A. (1958) A new method for the determination of the magnitude of earthquakes, Geofiz. Kozlem., 7: 2.

Blümling, P., and C. Prodehl (1983) Crustal structure beneath the eastern part of the Coast Ranges (Diablo Ranges) of central California from explosion, seismic, and near earthquake data, Phys. Earth Planet. Int., 31: 313-326.

Chouet, B. (1976) Source, scattering, and attenuation effects on high frequency seismic waves, Ph.D. thesis, M.I.T., Cambridge, MA.

Chouet, B. (1979) Temporal variations in the attenuation of earthquake coda near Stone Canyon, California, Geophys. Res. Lett., 6: 143-146.

Chouet, B., K. Aki, and M. Tsujiura (1978) Regional variation of the scaling law of earthquake source spectra, Bull. Seism. Soc. Am., 68: 59-79.

Davis, L. L. and L. R. West (1973) Observed effects of topography on ground motion, Bull. Seism. Soc. Am., 63: 283-298.

Del Pezzo, E., A. Rovelli, and G. Zonno (1984) Seismic Q and site effects on seismograms of local earthquakes in the Ancona Region (Central Italy), Annales Geophysicae, submitted.

Der, Z., M. E. Marshall, A. O'Donnell, and T. W. McElfresh (1984) Spatial coherence structure and attenuation of the L_g phase, site effects, and the interpretation of the L_g coda, Bull. Seism. Soc. Am., 74: 1125-1147.

Eaton, J. P. (1979) Frequency response of the U.S.G.S. short-period telemetered seismic system and its suitability for network studies of local earthquakes, U.S.G.S. Open File Report, 77-844.

Eaton, J. P. (1980) Response arrays and sensitivity coefficients for standard configurations of the U.S.G.S. short period telemetered system, U.S.G.S. Open File Report, 80-316.

Ellis, J. R., and A. Lindh (1976) Linearity of VCO-discriminator playback system with respect to zero crossing times, U.S.G.S. Open File Report, 76-873.

Ellsworth, W. L. (1975) Bear Valley, California, earthquake sequence of February-March 1972, Bull. Seism. Soc. Am., 65: 483-506.

Ernst, W. G. (1980) Summary of the geotectonic development of California, in Geotectonic Development of California, G. Ernst, ed., Prentice-Hall, Engelwood Cliffs, N.J., 602-613.

Fedotov, S. A., and S. A. Boldyrev (1969) Frequency dependence on the body wave absorption in the crust and the upper mantle of the Kurile Island chain, Izv. Phys. Solid Earth, 9: 553-562.

Fehler, M. (1979) Seismological investigation of the mechanical properties of a hot dry rock geothermal system, Ph.D. thesis, M.I.T., Cambridge, MA.

Frankel, A. (1982) The effects of attenuation and site response on the spectra of microearthquakes in the northeastern Caribbean, Bull. Seis. Soc. Am., 72: 1379-1402.

Gao, L. S. (1984) Q factor in coda wave analysis: Discriminating the attenuation due to scattering from the attenuation due to general absorption, Pure Appl. Geophys., submitted.

Gao, L. S., L. C. Lee, N. N. Bismas, and K. Aki (1983) Comparison of the effects between single and multiple scattering on coda waves from local earthquakes, Bull. Seism. Soc. Am., 73: 377-389.

Griffiths, D. W., and G. A. Bollinger (1979) The effect of Appalachian Mountain topography on seismic waves, Bull. Seism. Soc. Am., 69: 1081-1105.

Hanks, T. C. (1977) Earthquake stress drops, ambient tectonic stress, and stresses that drive plate motions, Pure Appl. Geophys., 115: 441-458.

Hanks, T. C. (1979) b-values and $\omega^{-\gamma}$ seismic source models: Implications for tectonic stress variations along active crustal fault zones and the estimation of high frequency strong ground motion, J. Geophys. Res., 84: 2235-2242.

Hanks, T. C. (1982) f_{max}, Bull. Seism. Soc. Am., 72: 1867-1879.

Haskell, N. A. (1960) Crustal reflection of plane SH waves, J. Geophys. Res., 65: 4147-4150.

Haskell, N. A. (1966) Total energy and energy spectral density of elastic wave radiation from propagating faults. II. Bull. Seism. Soc. Am., 56: 125-140.

Herraiz, M. (1982) Microsismicidad en el campo proximo, Analisis de generacion de ondas de coda y parametros fisicos asociados, Ph.D. thesis, Universidad Complutense de Madrid, Madrid.

Herraiz, M., and J. Mezcua (1984) Application of coda wave analysis to microearthquake analog data, Annales Geophys., 2: 545-552.

Herrmann, R. B. (1980) Q estimates using the coda of local earthquakes, Bull. Seism. Soc. Am., 70: 447-465.

Hill, N. R. and A. R. Levander (1984) Resonances of low-velocity layers with lateral variations, Bull. Seism. Soc. Am., 74: 521-537.

Hudson, D. E. (1972) Local distribution of strong earthquake ground motion, Bull. Seism. Soc. Am., 62: 1765-1786.

Jennings, C. W. (1958) Geologic map of California, San Luis Obispo sheet, 1:250000.

Jennings, C. W. and R. G. Strand (1958) Geologic map of California, Santa Cruz sheet, 1:250000.

Jennings, C. W. and J. L. Burnett (1961) Geologic map of California, Santa Cruz sheet, 1:250000.

Joyner, W. B., R. E. Warrick, T. E. Furmal (1981) The effect of Quaternary alluvium on strong ground motion in the Coyote Lake, California earthquake of 1979, Bull. Seism. Soc. Am., 71: 1333-1349.

Kind, R. (1972) Residuals and velocities of P_n waves recorded by the San Andreas seismograph network, Bull. Seism. Soc. Am., 62: 85-100.

King, J. L. and B. E. Tucker (1984) Observed variations of earthquake motion across a sediment-filled valley, Bull. Seism. Soc. Am., 74: 137-151.

Lanczos, C. (1961) Linear Differential Operators, Van Nostrand, London.

Lee, W. H. K. , R. G. Bennett, and K. L. Meagher (1972) A method of estimating magnitude of local earthquakes from signal durations, U.S.G.S. Open File Report.

Levander, A. R. and R. L. Kovach (1981) S-wave observations in the Franciscan terrane, central California, Bull. Seism. Soc. Am., 71: 1863-1874.

Montgomery, D. C. and E. A. Peck (1982) Introduction to Linear Regression Analysis, Wiley, New York.

Mooney, W. D. and J. H. Luetgert (1982) A seismic refraction study of the Santa Clara Valley and southern Santa Cruz Mountains, west-central California, Bull. Seism. Soc. Am., 72: 901-909.

O'Neill, M. E. and J. H. Healy (1973) Determination of source parameters of small earthquakes from P-wave rise time, Bull. Seism. Soc. Am., 63: 599-614.

Oppenheimer, D. H. (1985) Moho orientation beneath central California from regional earthquake travel times, J. Geophys. Res., in press.

Papageorgiou, A. S. and K. Aki (1983a) A specific barrier model for the quantitative description of inhomogeneous faulting and the prediction of strong ground motion. I. Description of the model, Bull. Seism. Soc. Am., 73: 693-722.

Papageorgiou, A. S. and K. Aki (1983b) A specific barrier model for the quantitative description of inhomogeneous faulting and the prediction of strong ground motion. II. Applications of the model, Bull. Seism. Soc. Am., 73: 953-978.

Patton, H. J. (1983) L_g excitation and propagation in the western United States, preprint for the Fifth Annual DARPA/AFOSR Symposium, May.

Poupinet, G., W. L. Ellsworth, and J. Frechet (1984) Monitoring velocity variations in the crust using earthquake doublets: An application to the Calaveras Fault, California, J. Geophys. Res., 89: 5719-5732.

Pulli, J. J. and K. Aki (1981) Attenuation of seismic waves in the lithosphere: comparison of active and stable areas, in Earthquakes and Earthquake Engineering: the Eastern U. S., J. E. Beavers, ed., Ann Arbor Science Publishers Inc., Ann Arbor, Michigan, 129-141.

Pulli, J. J. (1984) Attenuation of coda waves in New England, Bull. Seism. Soc. Am., 74: 1149-1166.

Rautian, T. G. and V. I. Khalturin (1978) The use of the coda for determination of the earthquake source spectrum, Bull. Seism. Soc. Am., 68: 923-948.

Rhea, S. (1984) Q determined from local earthquakes in the South Carolina coastal plain, Bull. Seism. Soc. Am., 74: 2257-2268.

Reiter, L. and M. E. Monfort (1977) Variations in initial pulse width as a function of anelastic properties and surface geology in Central California, Bull. Seism. Soc. Am., 67: 1319-1338.

Roecker, S. W., B. Tucker, J. King, and D. Hatzfeld (1982) Estimates of Q in Central Asia as a function of frequency and depth using the coda of locally recorded earthquakes, Bull. Seism. Soc. Am., 72: 129-149.

Rovelli, A. (1982) On the frequency dependence of Q in Friuli from short-period digital records, Bull. Seism. Soc. Am., 72: 2369-2372.

Roy, R. F., D. D. Blackwell, and E. R. Decker (1972) Continental heat flow, in The Nature of the Solid Earth, E. C. Robertson, ed., McGraw-Hill, NY.

Sato, H. (1977a) Energy propagation including scattering effects, single isotropic scattering approximation, J. Phys. Earth, 25: 27-41.

Sato, H. (1977b) Single isotropic scattering model including wave conversions; simple theoretical model of the short period body wave propagation, J. Phys. Earth, 25: 163-176.

Sato, H. (1978) Mean free path of S-waves under the Kanto district of Japan, J. Phys. Earth, 27: 185-198.

Sato, H. (1982b) Attenuation of S-waves in the lithosphere due to scattering by its random velocity structure, J. Geophys. Res., 87: 7779-7785.

Sato, H. (1982b) Coda wave excitation due to nonisotropic scattering and nonspherical source radiation, J. Geophys. Res., 87: 8665-8674.

Sato, H. (1984) Attenuation and envelope formation of three-component seismograms of small local earthquakes in randomly inhomogeneous lithosphere, J. Geophys. Res., 89: 1221-1241.

Sato, H. and S. Matsumura (1980) Q^{-1} value for S-waves (2-32 Hz) under the Kanto district in Japan (in Japanese), Zisin, 33: 541-543.

Singh, S. K., R. J. Apsel, J. Fried, and J. N. Brune (1982) Spectral attenuation of SH waves along the Imperial fault, Bull. Seism. Soc. Am., 72: 2003-2016.

Singh, S. K. and R. B. Herrmann (1983) Regionalization of crustal coda Q in the continental United States, J. Geophys. Res., 88: 527-538.

Smith, M. B. (1964) Map showing distribution and configuration of basement rocks in California, U.S.G.S. Oil and Gas Investigations map OM-215.

Stewart, S. W. (1968) Preliminary comparison of seismic travel times and inferred crustal structures adjacent to the San Andreas Fault in the Diablo and Gabilan Ranges of central California, in Proc. of Conf. on Geological Problems of the San Andreas Fault System, W. R. Dickinson and A. Granz, eds., Stanford Univ. Pub. Geol Sci. 11: 218-230.

Stewart, S. W. and M. E. O'Neill (1980) Calculation of the frequency response of the U.S.G.S. telemetered short-period seismic system, U.S.G.S. Open File Report 80-143.

Thomson, D. J. (1982) Spectrum estimation and harmonic analysis, Proc. IEEE, 70: 1055-1096.

Tsujiura, M. (1978) Spectral analysis of the coda waves from local earthquakes, Bull. Earthquake Res. Inst., Univ. Tokyo, 53: 1-48.

Tucker, B. E. and J. L. King (1984) Dependence of sediment-filled valley response on input amplitude and valley properties, Bull. Seism. Soc. Am., 74: 153-165.

Tucker, B. E., J. C. King, D. Hatzfeld, and I. L. Nersesov (1984) Observations of hard rock site effects, Bull. Seism. Soc. Am., 74: 121-136.

Walter, A. W. and W. D. Mooney (1982) Crustal structure of the Diablo and Gabilan Ranges, central California: a reinterpretation of existing data, Bull. Seism. Soc. Am, 72: 1567-1590.

Wesson, R. L., J. C. Roller, and W. H. K. Lee (1973) Time-term analysis and geologic interpretation of seismic travel time data from the Coast Ranges of Central California, Bull. Seism. Soc. Am., 63: 1447-1471.

Wu, R. S. (1982a) Mean field attenuation and amplitude atten-
uation due to wave scattering, Wave Motion, 4: 305-316.

Wu, R. S. (1982b) Attenuation of short period seismic waves
due to scattering, Geophys. Res. Lett., 9: 9-12.

Wu, R. S. (1984) Seismic wave scattering and the small scale
inhomogeneitites in the lithosphere, Ph.D. thesis,
M.I.T., Cambridge, MA.

Wyss, M. (1983) Precursory phenomena before large earth-
quakes, Proc. of the U. S.-Japan Symposium on Earthquake
Prediction, Tokyo, submitted.

Zandt, G. (1978) Study of the three-dimensional heterogeneity
beneath seismic arrays in Central California and Yellow-
stone, Wyoming, Ph.D. thesis, M.I.T., Cambridge, MA.

Appendix

A1   Moving Window Program Outline

1   Choose moving window parameters: sample width and increment for each band.

2   Choose event to process, read in event parameters (summary cards).

3   Station loop:

   A   Read in station parameters (phase cards)

   B   Plot seismogram

   C   Pick moving window limits, noise window, P arrival, comment

   D   Blow-up seismogram, repick P arrival

   E   Remove glitches:

      a   identify

      b   plot

      c   remove if necessary

   F   Re-display seismogram between moving window limits

   G   Frequency band loop:

      a   add power spectra vs. time to display

      b   display best fit to single scattering model

      c   enter quality 1, 2 or 3 (see text)

   H   Output

Comments: This scheme is slow and tedious as run on a VAX 780.   For operational ease, this program should be split into three parts: 1) pick the moving window limits, etc.; 2) run the moving window, which should be done after hours

or batch, requiring no operator input; and 3) display, quality assignment and final output. It is imperative that all data be looked at.

A2   Regression for Source, Path and Site Terms

Many results in this thesis are obtained using linear inverse theory. Inverse techniques are commonly employed by geophysicists; only the simplest methods are required here. In the following we will briefly outline the background theory, and show the normal equations for the site response calculation. A simple solution of the matrix of normal equations for the single scattering calculation (Chouet et al., 1978) will also be given.

A2.1   The generalized inverse

Equations 2.5 and 2.6 can each be put in the form:

$$d = Gm \tag{A2.1}$$

where d and m are the data and model vectors of lengths N and M respectively, while G is a real matrix of size NxM. Our goal is to obtain a particular solution m_p, given G and d:

$$m_p = G_p^{-1}d$$

To do this we follow Aki and Richards (1980) and ultimately Lanczos (1961).

First, a Hermitian matrix is constructed:

$$S = \begin{bmatrix} o & G \\ \tilde{G} & o \end{bmatrix}$$

where the $\sim$ indicates the complex conjugate transpose. A set of real eigenvalues λ_j and orthogonal eigenvectors x_j are guaranteed:

$$Sx_j = \lambda_j x_j; \quad j = 1, N + M$$

If the x_j are partitioned into u_j and v_j of lengths N and M, we can write:

$$Gv_j = \lambda_j u_j \qquad (A2.2)$$

$$\tilde{G}u_j = \lambda_j v_j \qquad (A2.3)$$

It follows that:

$$\tilde{G}Gv_j = \lambda_j^2 v_j$$

$$G\tilde{G}u_j = \lambda_j^2 u_j$$

Since both $\tilde{G}G$ and $G\tilde{G}$ are also Hermitian, the v_j and u_j <u>each</u> represent an orthogonal set of vectors. After normalization the orthogonality is expressed:

$$\tilde{U}U = U\tilde{U} = I$$

$$\tilde{V}V = V\tilde{V} = I$$

where the columns of U and V are the u_j and v_j, and I is the identity matrix. Define U_p and V_p as matrices with columns u_j and v_j such that $\lambda_j \neq 0$, U_0 and V_0 as matrices with columns u_j and v_j such that $\lambda_j = 0$, and Λ_p as a matrix with the non-zero λ_j along the diagonal, zero elsewhere. Using the

orthogonality of the eigenvector matrices, A2.2 and A2.3 can be combined to write:

$$G = U_p \Lambda_p \tilde{V}_p$$

This is an important decomposition since it suggests:

$$G_g^{-1} = V_p \Lambda_p^{-1} \tilde{U}_p$$

which is known as the generalized inverse.

Our problem is an over-determined one. This means that there are more data points than model parameters, and that the data cannot be modelled exactly; there will always be a residual vector left over. In other words, U_0 exists. Our problem is non-unique which means that V_0 also exists. It can be shown that in this case the particular solution

$$m_g = G_g^{-1}d$$

has the property that $|d - Gm_g|^2$ and $|m_g|^2$ are minimized. Thus our solution is the minimum of all possible least squares solutions. In order to ease the burden on the computer, we choose to solve the problem:

$$\tilde{G}Gm = \tilde{G}d$$

which is known as the system of normal equations. The solution is calculated via:

$$m_g = V_p \Lambda_p^{-2} \tilde{V}_p (\tilde{G}d)$$

It is also important to check the resolution and covariance associated with the regression. In our case, non-uniqueness implies that V_0 exists which means that

$$m_g \neq m$$

where m is the "true" solution. Instead

$$m_g = G_g^{-1} Gm = V_p \tilde{V}_p m$$

The quantity $V_p \tilde{V}_p$ relates the particular and true solutions and is called the resolution. The resolution is the identity when V_0 space does not exist, otherwise the resolution will indicate that an estimate is a weighted average over some portion of m.

The covariance is a measure of the solution error. An error in the data is propagated into the solution via

$$\Delta m_g = G_g^{-1} \Delta d$$

Forming the covariance, and assuming:

$$\langle \Delta d \; \tilde{\Delta d} \rangle = \sigma_d^2 \; I$$

implies:

$$\langle \Delta m_g \; \tilde{\Delta m}_g \rangle = \sigma_d^2 \; V_p \Lambda_p^{-2} \tilde{V}_p$$

A2.2 Normal equations

We use Equations 2.5 and 2.6 to solve for site and source terms. These equations can be expressed in the

form

$$Gm = d$$

where d and m represent the data and model vectors. The data vector is arranged so that station, source and time bin indices i, j, and k change in a systematic way; $d_I = 0$ if no data exists for $I = I(i,j,k)$. In the site calculation case (Equation 2.5) the I, J th element of G can be written:

$$[g]_{IJ} = w_1(I) \, w_2(J,j,k) \, (\delta_{Ji} - \frac{1}{N_{jk}})$$

where $w_1 = 0$ if $d_I = 0$, or $= 1$ otherwise; $w_2 = 0$ if $d_{I(J,j,k)} = 0$, or $= 1$ otherwise; δ is the Kronecker delta and N_{jk} is the number of stations measuring event j at lapse time k. The system of normal equations is given by

$$\tilde{G}Gm = \tilde{G}d$$

where $\sim$ indicates the transpose. The K, Lth element of $G\tilde{G}$ is as follows:

$$[\tilde{g}g]_{KL} = \sum_{I=1}^{n} g_{IK} \, g_{IL}$$

$$= \sum_{I=1}^{n} w_1(I)w_2(K,j,k)w_2(L,j,k) \cdot$$

$$[\delta_{ki} - \frac{1}{N_{jk}}] \, [\delta_{Li} - \frac{1}{N_{jk}}]$$

where n is the length of d. The i, j, k are fixed for each

I. Similarly the Kth element of $\tilde{G}d$ is:

$$[\tilde{g}d]_K = \sum_{I=1}^{n} w_1(I)w_2(K,j,k) \left[\delta_{Ki} - \frac{1}{N_{jk}}\right] d_I$$

The solution can now be obtained using the method described in section A2.1. Eigenvalues and eigenvectors are calculated using the IMSL singular value decomposition routine LSVDF. In our case, the resolution is as follows:

$$r_{ij} = \begin{cases} 1 - \dfrac{1}{N}, & i = j \\[2ex] -\dfrac{1}{N}, & i \neq j \end{cases}$$

since the particular solution represents the real solution minus its mean.

A2.3 Solution to Chouet single scattering problem

The extraction of Q_c and coda source factors from a number of coda decay curves is accomplished by inverting a sparse matrix whose only non-zero elements lie along the diagonal and symmetrically along the top row and left column (Chouet, 1976). This matrix can be solved without resorting to the usual matrix inversion subroutines, which makes the simultaneous inversion of an almost unlimited number of decay curves simple and fast. The solution was suggested by Gilles Garcia (1984, pers. comm.), and will be briefly described below.

The system of normal equations is written:

$$Ax = b$$

In this case the only non-zero elements of A are a_{ii}, $a_{1i} = a_{i1}$, $i = 1,n$. The first equation is:

$$b_1 = \sum_{j=1}^{n} a_{1j}x_j \qquad (A2.4)$$

Normal equations 2 through n give:

$$x_i = \frac{b_i - a_{1i}x_1}{a_{ii}} \qquad (A2.5)$$

Combining (A2.4) and (A2.5) gives:

$$x_1 = \frac{b_1 - \sum_{j=2}^{n} \frac{a_{1j}}{a_{jj}} b_j}{a_{11} - \sum_{j=2}^{n} \frac{a_{1j}^2}{a_{jj}}}$$

Now (A2.5) can be solved for the x_i.

To compute the standard errors of parameters $x_1,\ldots,x_n$ we must obtain the diagonal of the inverse of A. This is easily done by solving:

$$Ax = e_i$$

where e_i is the ith unit vector. The resulting x are the columns of A^{-1}.

$$a_{11}^{-1} = \frac{1}{a_{11} - \sum\limits_{j=2}^{n} \dfrac{a_{1i}^2}{a_{jj}}}$$

$$a_{ii}^{-1} = \frac{1}{a_{ii}} + \frac{a_{11}^{-1} \, a_{1i}^2}{a_{ii}^2} \qquad (i \neq 1)$$

The calculations of Q_c, coda source factors and standard errors can now be completed in the manner of Chouet (1976).

This solution is a special case of the inverse of a symmetric partitioned matrix. If

$$M = \begin{bmatrix} A & B \\ \tilde{B} & C \end{bmatrix}$$

is symmetric and the inverse exists, then:

$$M^{-1} = \begin{bmatrix} \alpha & \beta \\ \tilde{\beta} & \gamma \end{bmatrix}$$

where:

$$\gamma = (C - \tilde{B}A^{-1}B)^{-1}$$

$$\beta = -A^{-1}B\gamma$$

$$\alpha = A^{-1}(I - B\tilde{\beta})$$